NASA-CR-191378

A Very Efficient RCS Data Compression and Reconstruction Technique

N.Y. Tseng and W.D. Burnside

The Ohio State University

ElectroScience Laboratory

Department of Electrical Engineering
Columbus, Ohio 43212

Final Report, Volume IV, 722780-4
Grant No. NAG 2-542, Supp. No. 2
November 1992

University Affairs Branch
National Aeronautics and Space Administration
Ames Research Center 241-25
Moffett Field, CA 94035

NOTICES

When Government drawings, specifications, or other data are used for any purpose other than in connection with a definitely related Government procurement operation, the United States Government thereby incurs no responsibility nor any obligation whatsoever, and the fact that the Government may have formulated, furnished, or in any way supplied the said drawings, specifications, or other data, is not to be regarded by implication or otherwise as in any manner licensing the holder or any other person or corporation, or conveying any rights or permission to manufacture, use, or sell any patented invention that may in any way be related thereto.

50272-101

REPORT DOCUMENTATION PAGE	1. REPORT NO.	2.	3. Recipient's Accession No.

4. Title and Subtitle

A Very Efficient RCS Data Compression and Reconstruction Technique

5. Report Date
November 1992

6.

7. Author(s)
N.Y. Tseng and W.D. Burnside

8. Performing Org. Rept. No.
722780-4

9. Performing Organization Name and Address
The Ohio State University
ElectroScience Laboratory
1320 Kinnear Road
Columbus, OH 43212

10. Project/Task/Work Unit No.

11. Contract(C) or Grant(G) No.
(C)
(G) NAG 2-542, Supp. No. 2

12. Sponsoring Organization Name and Address
University Affairs Branch
NASA — Ames Research Center 241-25
Moffett Field, CA 94035

13. Report Type/Period Covered
Final Report, Vol. IV

14.

15. Supplementary Notes

16. Abstract (Limit: 200 words)

A very efficient compression and reconstruction scheme for RCS measurement data has been developed. The compression is done by isolating the scattering mechanisms on the target and recording their individual responses in the frequency and azimuth scans, respectively. The reconstruction, which is an inverse process of the compression, is granted by the sampling theorem. Two sets of data, the corner reflectors and the F-117 fighter model, have been processed and the results have been shown to be convincing. The compression ratio can be as large as several hundred, depending on the target's geometry and scattering characteristics.

17. Document Analysis a. Descriptors

DATA
IMAGING
STORAGE
SCATTERING
DATA COMPRESSION

b. Identifiers/Open-Ended Terms

c. COSATI Field/Group

18. Availability Statement	19. Security Class (This Report)	21. No. of Pages
A. Approved for public release; Distribution is unlimited.	Unclassified	111
	20. Security Class (This Page) Unclassified	22. Price

(See ANSI-Z39.18) *See Instructions on Reverse* OPTIONAL FORM 272 (4-77)
Department of Commerce

Contents

List of Figures

Chapter 1

Introduction

The real-world target response of a radar system often has rapid variations with frequency and scanning angle. As a result, one needs to sample quite densely in both frequency and angle to accurately represent the response. A compression technique is developed in this report that can be used to reduce this large amount of data. This technique is based on the concept of isolated scattering centers and Fourier analysis.

When a real-world target is illuminated by a microwave radar, the scattered field of the target tends to emanate from a few isolated spots, referred to as scattering centers, such as the corners, edges and discontinuities in the target's surface. Keller's geometrical theory of diffraction (GTD) [1] described the scattered field of a target in terms of various kinds of diffractions, and the diffraction coefficients of many simple geometries have been calculated. But a real-world target may have an arbitrary shape and these scattering centers can be widely spaced electrically, so the target's frequency response often varies rapidly and appears to be hard to analyze. In order to better understand a target's geometry and physical characteristics, it is important to be able to separate the different scattering mechanisms on the target.

A lot of researches have been done in the subject of mechanism extraction. For example, Ksienski [2] isolated two mechanisms in a matrix form in the frequency domain by using a least mean square error decomposition, and Dominek *et al.* [3]

used a time-gating approach to separate several scattering centers in an impulse response. Though the former presented his idea in the frequency domain and the latter did it in the time domain, both of their algorithms are dependent on the relative positional differences among the scattering centers.

It is noticed that after the extraction of these scattering mechanisms, the resulting individual responses are simple and smooth. Therefore, fewer data points are needed to represent the isolated scattering centers, which leads to the proposed goal of data compression. Moreover, this idea of data compression is extended to two dimensions in this research.

It is well known that radar cross section (RCS) measurement data can be used to generate a radar image (for example, see Mensa's book [4]), from which one can locate the scattering centers two-dimensionally. In this report a two-dimensional gating technique is then employed to separate these scattering centers in the image domain. In addition, a two-dimensional smoothing technique is also developed to separate these scattering centers directly in the spectral domain. After the separation, the resulting individual scattering centers' responses are smooth in both the frequency and angle dimensions, so one can sample these responses more loosely and a two-dimensional compressed database for the target under test can be formed. It will be shown that from this reduced database, one can reconstruct the originally measured data in both the frequency and angle scans. The compression ratio can be as large as several hundred.

Chapter 2 describes the one-dimensional target responses and the mechanism extraction methods, which in turn leads to the idea of data compression. Chapter 3 reviews the formulation of a radar image and extends the data compression scheme to two dimensions. Fourier analysis and the sampling theorem, which are the two basic tools in this research, are also reviewed. Chapter 4 displays the results of the data compression and reconstruction scheme of a simplified target composed of six corner reflectors. These results show that this algorithm works very well for

a near ideal case. Chapter 5 shows the results of applying the data compression and reconstruction scheme to a real-world target model and explores the problems facing this complicated, nonideal situation. Chapter 6 concludes this research and examines possible future studies related to this topic.

Chapter 2

One Dimensional Target Response and Mechanism Extraction

When an electrically large target is illuminated by a plane wave, the scattered fields are often modeled as if they come from several point scatterers, or scattering centers [3]. This model is helpful for analyzing a complicated real-world target because the physical properties of ideal point scatterers are simple and can be easily simulated.

An outline of this chapter is as follows. The one-dimensional frequency response of point scatterers is discussed in Section 2.1, followed by two approaches of mechanism extraction in Sections 2.2 and 2.3. Section 2.4 deals with the bandwidth of the frequency response and its effect on resolution. Section 2.5 describes the one-dimensional sampling theorem and its applications in terms of data compression and reconstruction.

2.1 Frequency Response of Ideal Point Scatterers

An ideal point scatterer can be viewed as an isotropic reradiating point source: the radar sends out an electromagnetic pulse, the pulse hits the point scatterer, the point scatterer reradiates isotropically and the radar detects the reradiation field (or the

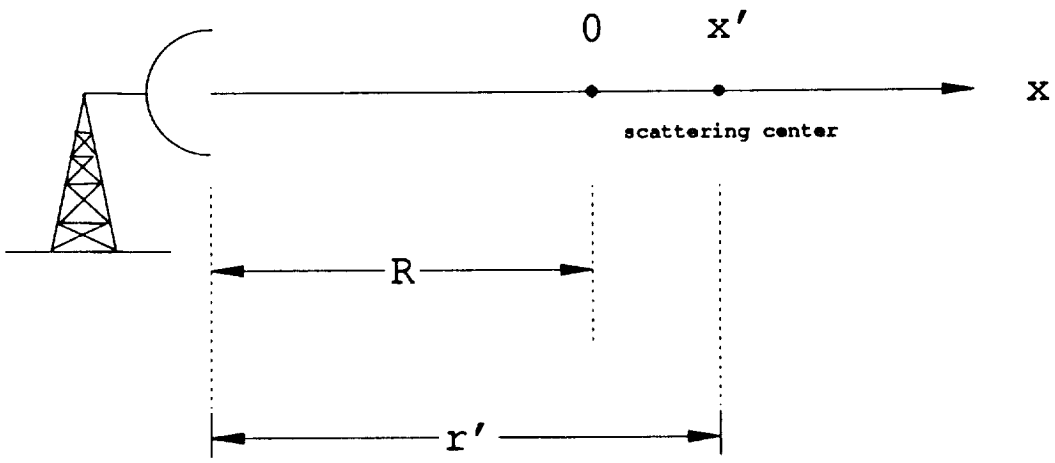

Figure 2.1: One dimensional target detection scheme.

backscattered field). The backscattered field of a point scatterer is given by

$$\bar{E} = \hat{e} A_o \frac{e^{-jk2r'}}{r'^2} \; ; \; r' \gg \lambda \tag{2.1}$$

where

$\bar{E}$ is the backscattered field

$\hat{e}$ is the unit vector of the backscattered field

r' is the distance from the radar to the point scatterer

k is the wave number, $k = \dfrac{2\pi f}{c}$

f is the frequency

c is the speed of light, and

λ is the wavelength.

For the one-dimensional (1-D) case shown in Figure 2.1, an ideal scattering center is located at $x = x'$ where $|x'| \ll R$, R is the distance from the radar to the target zone center. Then from Equation (2.1) and $r' = R + x'$, one obtains that

$$E = A_o \frac{e^{-jk2(R+x')}}{(R+x')^2} \approx A_o \left(\frac{e^{-j2\pi f \frac{2R}{c}}}{R^2}\right) e^{-j2\pi f \frac{2x'}{c}}. \tag{2.2}$$

For convenience, one can change the phase reference from the radar to the target zone center $x = 0$, then Equation (2.2) becomes

$$E \approx \frac{A_o}{R^2} e^{-j2\pi f \frac{2x'}{c}} \equiv B_o e^{-j2\pi f \frac{2x'}{c}}. \tag{2.3}$$

Equation (2.3) represents the 1-D frequency response of an ideal scattering center with the phase reference set at $x = 0$.

Frequency responses for an ideal scattering center located at different positions are shown in Figures 2.2, 2.3 and 2.4. From these figures one can see that the amplitude response of an ideal scattering center is constant, and the phase response is linear. Furthermore, if the scattering center is located at the origin (Figure 2.2), there is no phase variation. If the scattering center is moved away from the origin, a linear phase change occurs (see Figures 2.3 and 2.4). In other words, the slope of the phase response contains the information of how far from the origin the scattering center is shifted.

Next consider the response of two scattering centers located at $x' = -d/2$ and $x' = d/2$. The total field at the observation point $x = 0$, according to Equation (2.3), is

$$E = A_1 e^{j2\pi f \frac{d}{c}} + A_2 e^{-j2\pi f \frac{d}{c}} \tag{2.4}$$

where A_1 and A_2 are the magnitudes of the two scattering centers. From Figure 2.5 one can see that in this case, the amplitude response oscillates as does the phase response. To gain a better understanding of the oscillation in the amplitude response, one can rewrite Equation (2.4) as

$$E = A_1 e^{j2\pi f \frac{d}{c}} (1 + a e^{-j2\pi f \frac{2d}{c}}) \tag{2.5}$$

where $a = \frac{A_2}{A_1}$. Note that $1 + a e^{-j2\pi f \frac{2d}{c}}$ is a circle in the complex plane. It is centered at $(1, 0)$ and has a radius a, with $-2\pi f \frac{2d}{c}$ being the argument parameter. So the amplitude response of Equation (2.5) has maxima at $f = n\frac{c}{2d}$ and minima at $f = (n - \frac{1}{2})\frac{c}{2d}$ for $n = \pm 1, 2, 3...$, and is periodic with a period $\Delta f = \frac{c}{2d}$. Figure 2.5

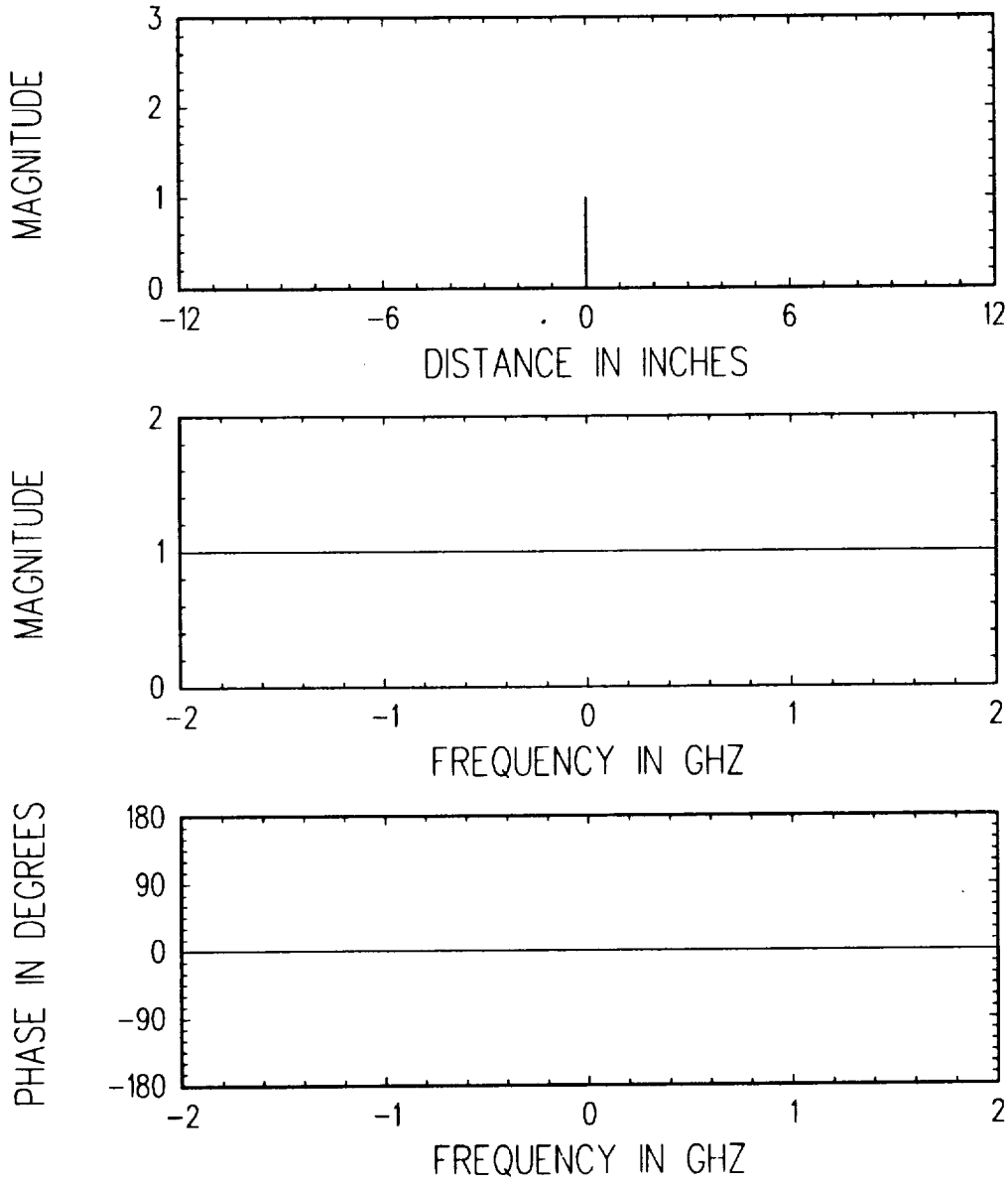

Figure 2.2: Frequency response of an ideal point source located at the origin.

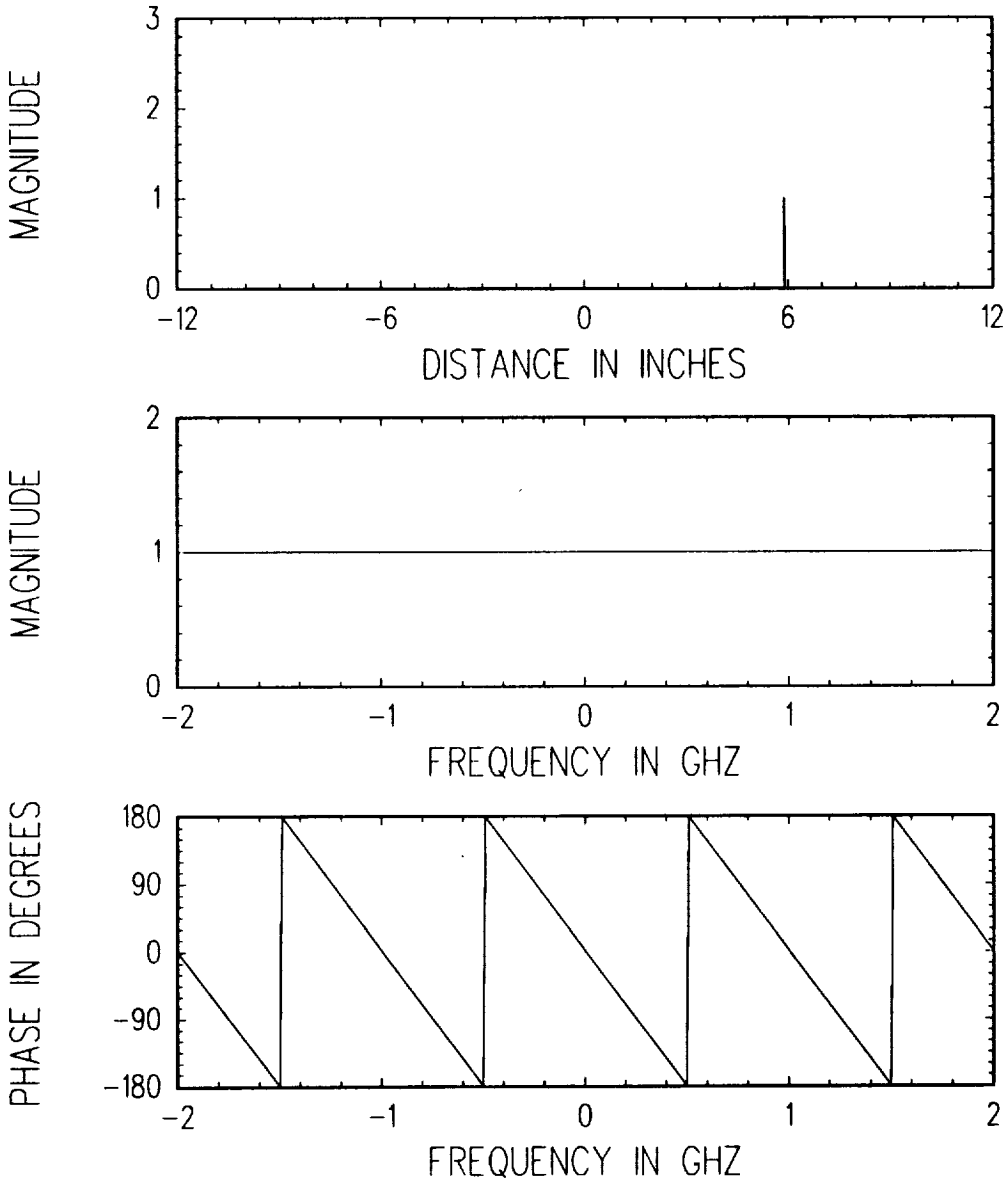

Figure 2.3: Frequency response of an ideal point source located at 5.9″.

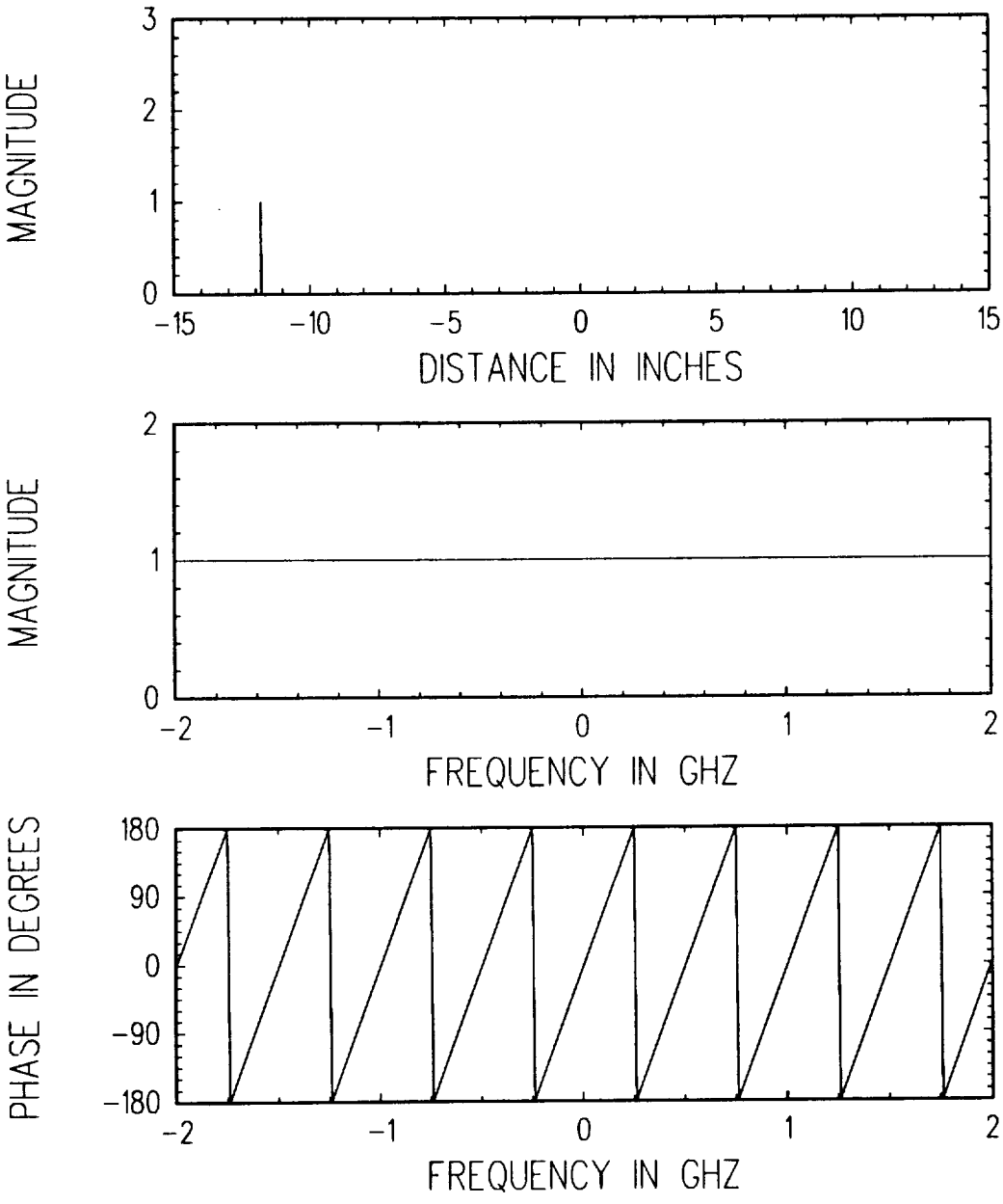

Figure 2.4: Frequency response of an ideal point source located at $-11.8''$.

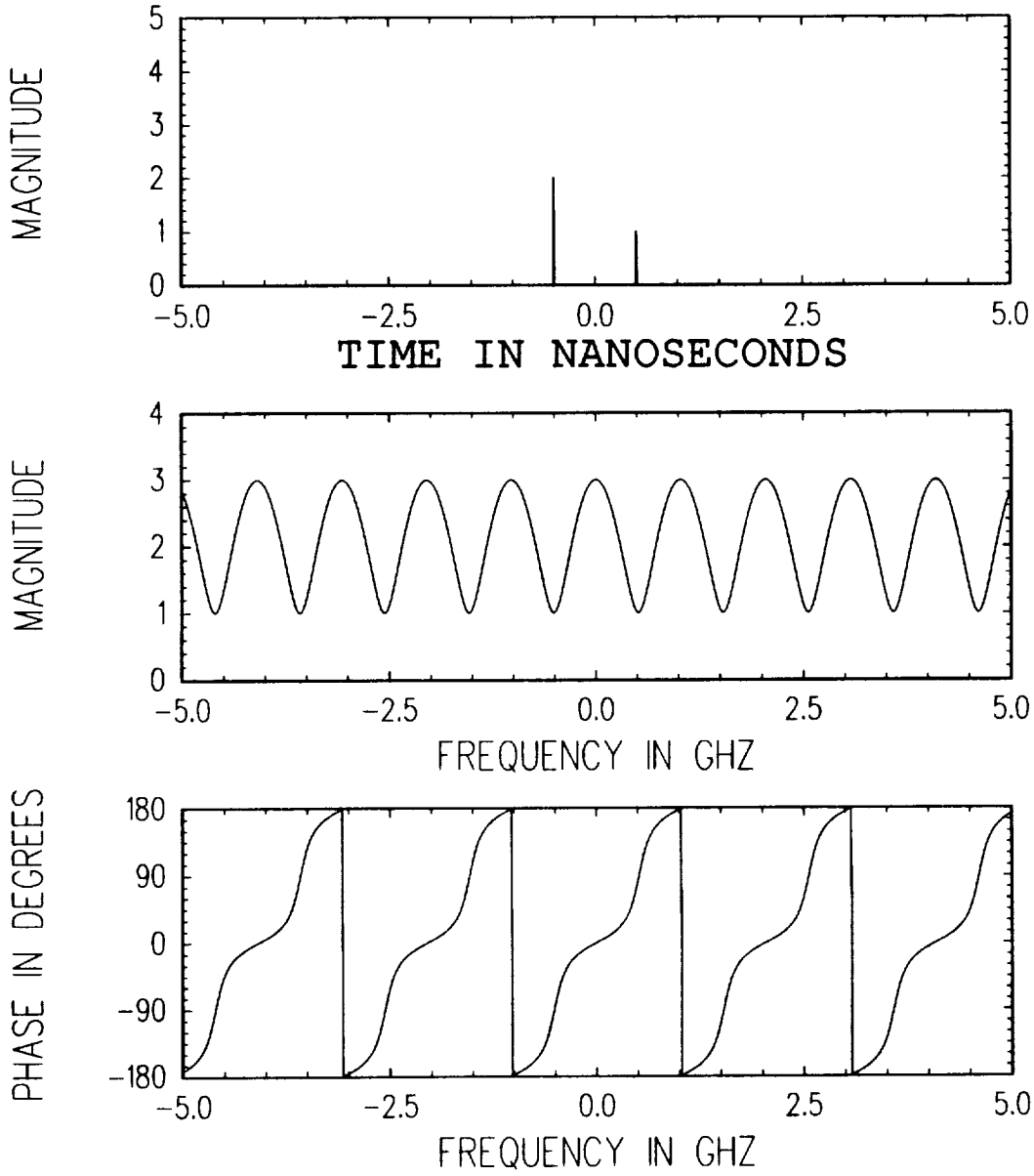

Figure 2.5: 1-D frequency response of two scattering centers.

showed the periodicity of Equation (2.5) when $\frac{d}{c} = 0.5$ nanoseconds (ns), A_1=2 and $a = 0.5$.

If there are more than two scattering centers, the frequency response can be obtained simply by superposition such that

$$E = \sum_{i=1}^{n} A_i e^{-j2\pi f \frac{2x_i'}{c}} \quad . \tag{2.6}$$

Similar to the two scattering centers case, rapid variations in both the amplitude and phase responses are expected due to interactions among these scattering centers.

In the above discussion the 1-D case of the "ideal" scattering center has been studied. An ideal scattering center is a fixed point scatterer, and it reradiates the incident plane wave isotropically. But in the real world, the scattering centers are located in a three dimensional space, and they may not be ideal. In other words, the terms A_i in Equation (2.6) are not necessarily constants; they can be functions of both the frequency and the incident angle of the plane wave. So for a real-world target composed of a finite set of scattering centers, the 1-D frequency response along the incident wave direction, or down range direction, is slightly modified as

$$E^s(f) = \sum_{i=1}^{n} E_i(f,\theta,\phi)|_{\theta=\theta_o,\phi=\phi_o} \cdot e^{-j2\pi f \frac{2x_i'}{c}} \tag{2.7}$$

where $E_i(f,\theta,\phi)$ is the individual response of the i-th scattering center and (θ,ϕ) represents the incident direction of the plane wave. Note that $E_i(f,\theta,\phi)$ represents the physical scattering property of the i-th scattering center. Though not necessarily a constant, the $E_i(f,\theta,\phi)$ should be slow-varying, or "smooth", in frequency for a given incident angle since its behavior should not be far from an ideal point scatterer.

One should note that Equation (2.7) is valid under two assumptions and requirements:

1. the target is electrically large; and

2. the target has a finite number of scattering centers.

The first assumption states that the target size has to be large with respect to the wavelength of the incident field such that a scattering mechanism on the target can really be treated as a point scatterer. Since a point scatterer is a line-of-sight scatterer, this assumption is not valid for higher order effects such as multiple reflections, creeping waves and edge waves in that they will not be correctly located.

The second assumption dictates that the scattering centers are discrete such that the total response can be written as a linear superposition of individual scattering center responses. If this assumption does not hold, then other models; e.g., the GTD model, should be employed to calculate the scattered fields. (For example, in the case where the incident wave normally hits a straight edge, the scattered field will not be the summation of individual scattering centers, but rather the integration of the contribution along the whole edge.)

In this research, it is assumed that Equation (2.7) represents a target's frequency response under the above two requirements.

2.2 One Dimensional Gating Technique for Mechanism Extraction

Figure 2.6 shows a typical 1-D target response measured in the OSU compact range. Two main reasons lead one to try to extract out individual scattering center responses from such a complicated response:

1. By extracting out the scattering centers, one can study the individual scattering mechanisms and gain a deeper insight into the geometry and physical characteristics of the target.

2. The frequency response of an individual scattering center is smoother and simpler than the frequency response of the entire target as mentioned before; hence, storing the former instead of the latter should be much space-saving if the number of scattering centers is not big.

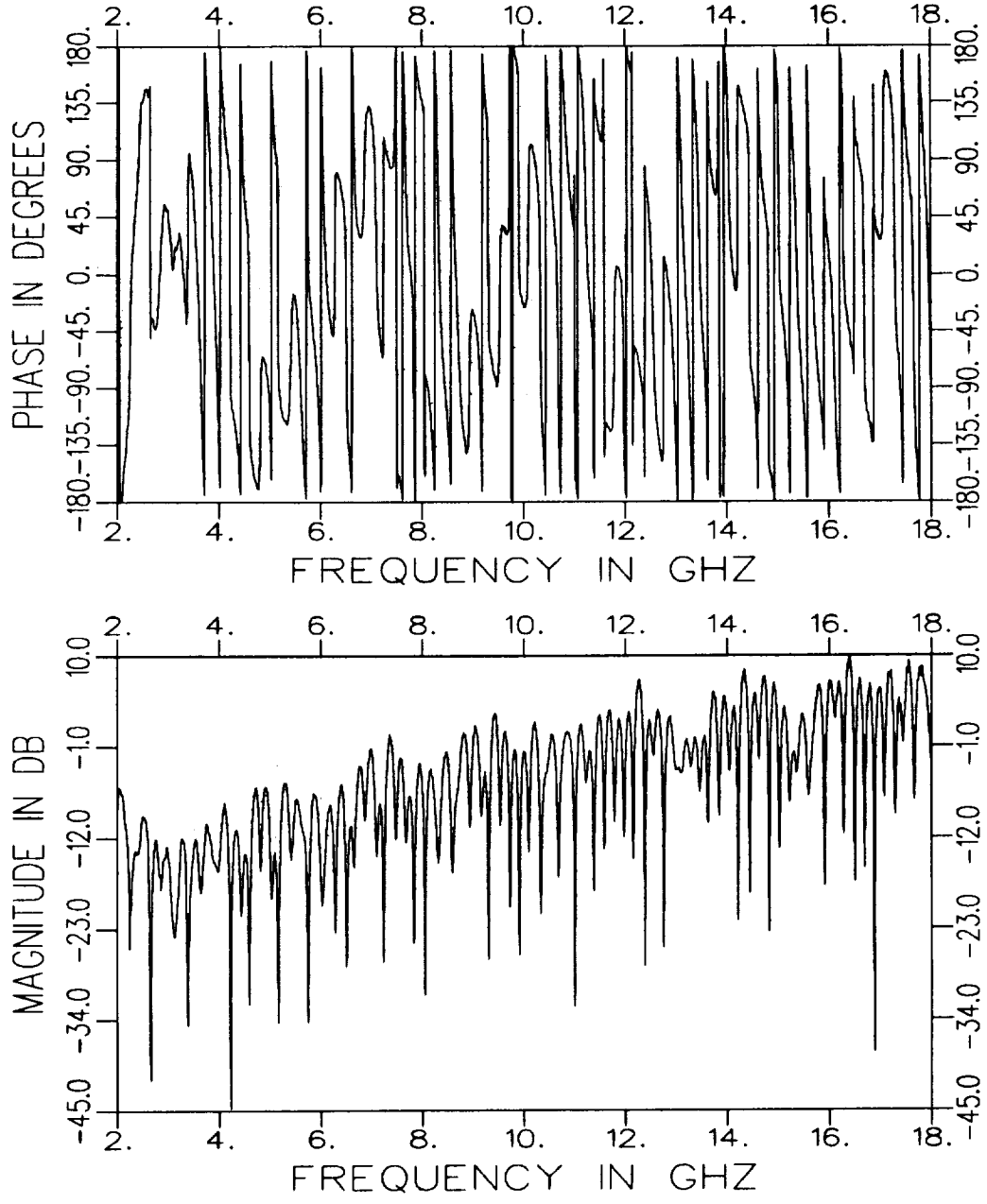

Figure 2.6: A typical 1-D target response.

The second reason is of special interest in this research because a smaller database can be conveniently carried around and installed in most computers for the target identification's purpose, and it can help identify a target more efficiently by saving the sorting time. With these motivations, the major concern now is how to extract out the individual scattering mechanisms.

As mentioned before, it is assumed that Equation (2.7) represents a target's frequency response. For a given incident direction (θ_o, ϕ_o), one can write the inverse Fourier transform of Equation (2.7) as

$$e^s(t) = \sum_{i=1}^{n} e_i(t - T_i) \tag{2.8}$$

where

$$\begin{aligned} T_i &\equiv \frac{2x_i'}{c}, \\ e^s(t) &= \mathcal{F}^{-1}[E^s(f)] \text{ and} \\ e_i(t) &= \mathcal{F}^{-1}[E_i(f)]. \end{aligned} \tag{2.9}$$

Throughout this report, $e^s(t)$ is called the time domain impulse response in the down range direction.

Because of the invertibility of the Fourier transform, frequency and time are dual domains. Namely, any linear operator carried out in one domain can be correspondingly carried out as a linear operation in the other domain. Therefore, the extraction of scattering centers can be performed in either domain. For example, Dominek *et al.* [3] suggested a time domain gating technique to separate individual scattering mechanisms. And this research will basically follow their approach.

The impulse response of the frequency domain data in Figure 2.6 is shown in Figure 2.7. Note that this impulse response checks well with Equation (2.8). It seems much easier to extract out individual scattering mechanisms in Figure 2.7 than in Figure 2.6 because a natural way to separate these "pulses", which represent the scattering centers, in Figure 2.7 is to use a proper "time gate". The steps are as follows:

1. Pinpoint the peak location of each scattering center in the impulse response.

2. Shift the scattering center of interest to the coordinate origin.

3. Apply a time gate to extract out that scattering center.

4. Repeat steps 2,3 until all the scattering centers are extracted.

The above procedure is called the time domain gating technique.

Various kinds of time gates and their properties have been discussed in [5]. For example, a 0.8 ns Hanning gate which has a waveform of

$$w(t) = 0.5 \cdot [1 + \cos(\pi \frac{t}{0.4})] \; ; \; -0.4 \text{ ns} < t < 0.4 \text{ ns} \tag{2.10}$$

has been used to extract the individual scattering centers given in Figure 2.7. The frequency responses of individual scattering centers after extraction are shown in Figures 2.8 and 2.9. Note that the resulting individual responses after extraction are smooth both in amplitude and phase, as was suggested in Section 2.1.

A potential drawback of gating is that when two or more scattering centers are too close in the down range direction such that they are coupled together in the impulse response, they cannot be completely separated by gating. However, since the scattering centers are located in a 3-D space, two scattering centers with close down range positions do not necessarily mean they cannot be separated in the cross range direction — the direction transverse to that of the down range. This fact motivates one to separate scattering mechanisms in two (or even three) dimensions, as will be discussed later in this report.

2.3 One Dimensional Smoothing Technique for Mechanism Extraction

The counterpart operation of gating in the time domain is convolution in the frequency domain:

$$\mathcal{F}[e^s(t) \cdot w(t)] = \int_{-\infty}^{\infty} E^s(f')W(f - f')df' \equiv E^s(f) * W(f) \tag{2.11}$$

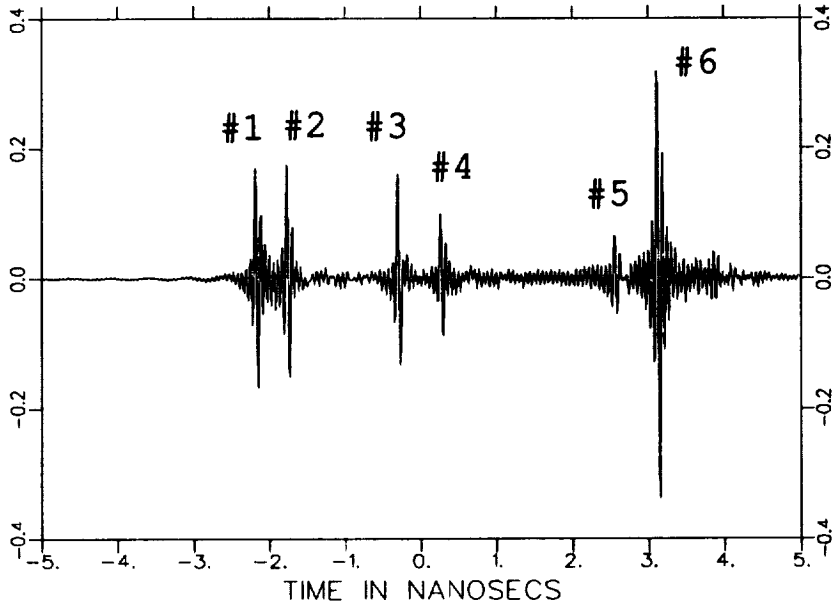

a) impulse response

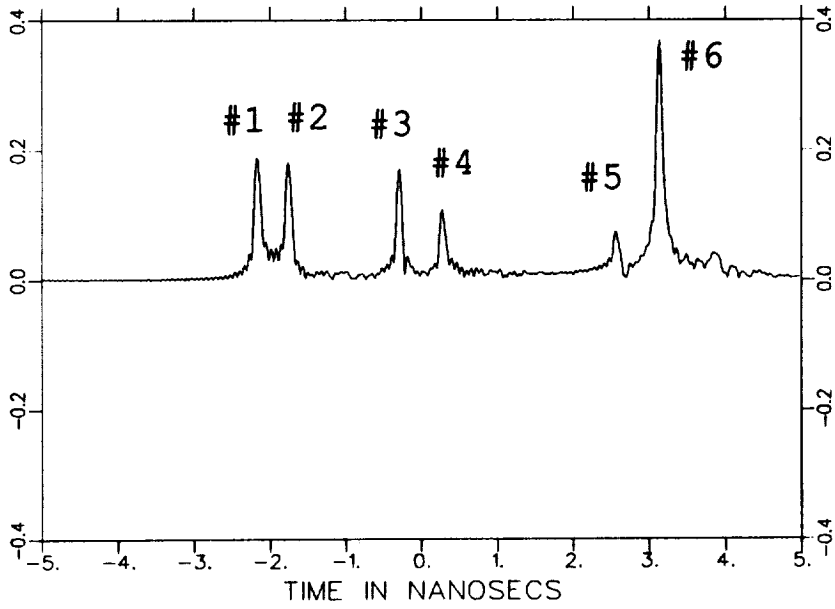

b) envelope of impulse response

Figure 2.7: Impulse response of the typical target.

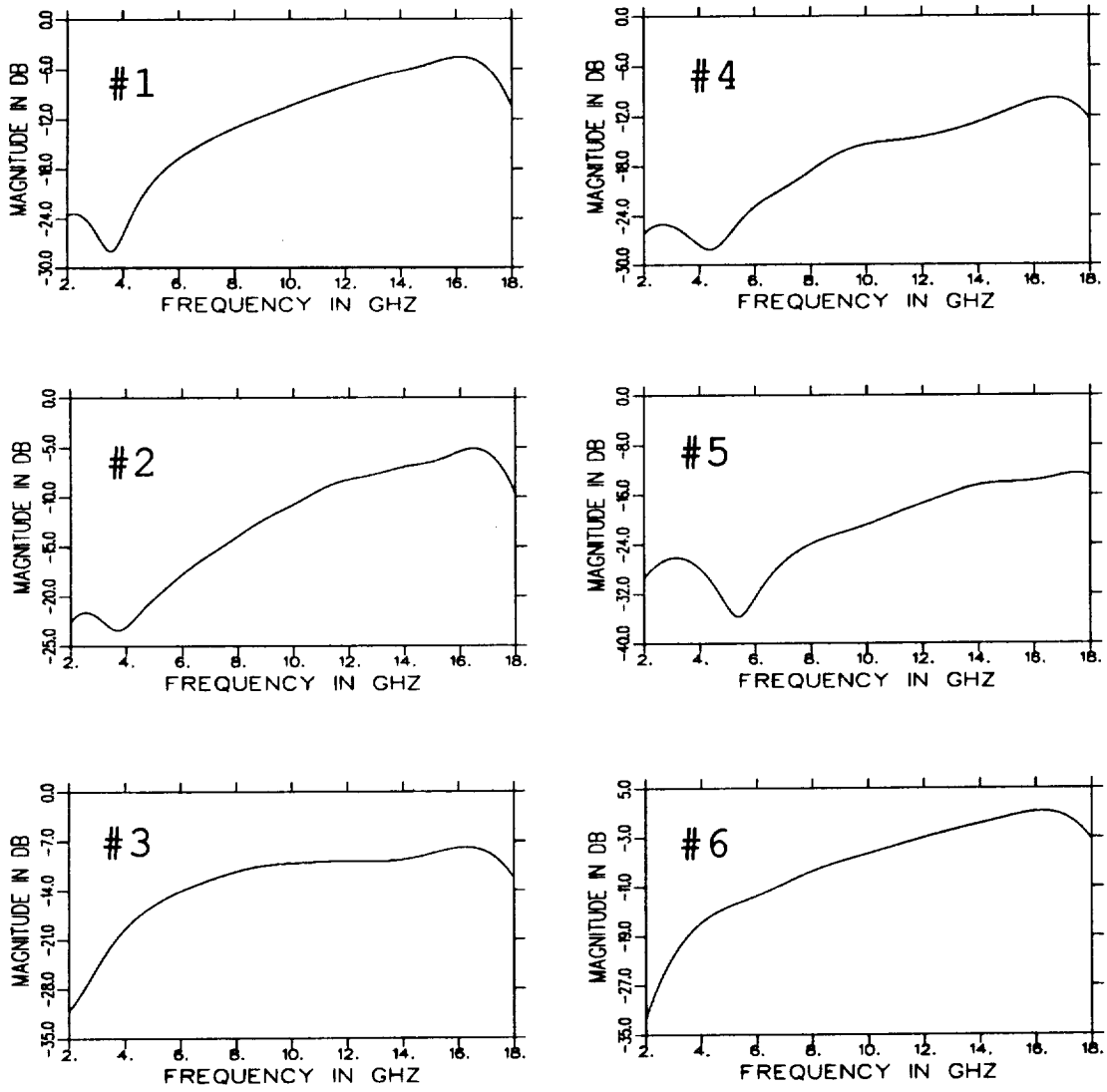

Figure 2.8: Amplitude responses of individual scattering centers on the typical target, obtained by gating.

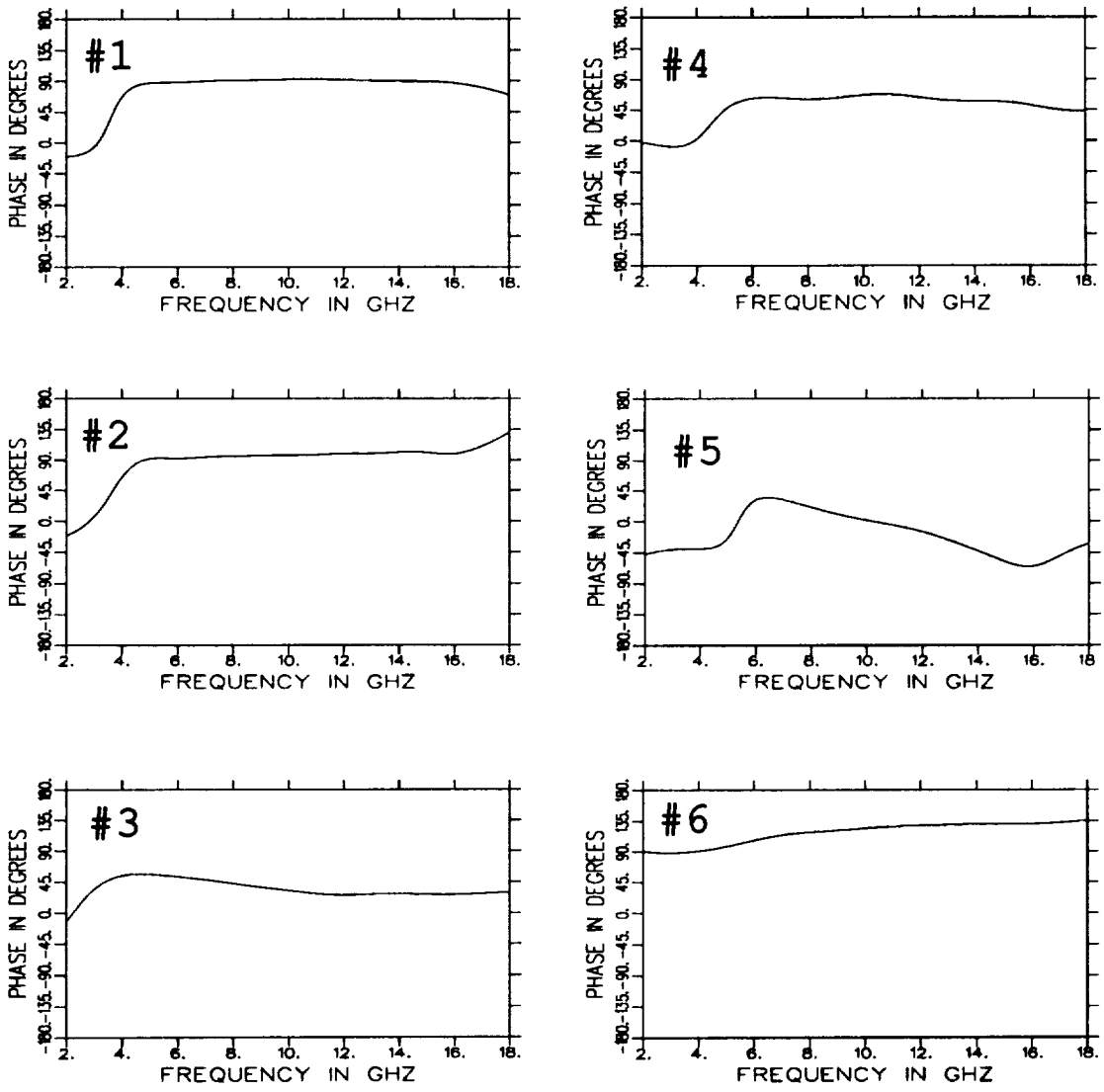

Figure 2.9: Phase responses of individual scattering centers on the typical target, obtained by gating.

where $w(t)$ is the time gate and $W(f)$ is its Fourier transform pair. Theoretically one can apply Equation (2.11) to separate individual scattering mechanisms in the frequency domain if the position of each scattering center is given, but this convolution is more computationally complicated than gating in the time domain because the integration in Equation (2.11) ranges over the whole frequency axis. Figure 2.10 plots the time-limited Hanning gate described in Equation (2.10). To make things easier, one should notice that in Figure 2.10, the frequency response of a Hanning gate is a lowpass function. The energy of this lowpass function concentrates around the mainbeam area (low frequency band) and dramatically decays over the sidelobes (high frequency band). So one can approximate the infinite-bandwidth frequency response of the Hanning gate by a truncated version obtained by neglecting the sidelobes outside, say, -30 dB; then, Equation (2.11) becomes

$$\mathcal{F}[e^s(t) \cdot w(t)] \approx \int_{f-f_w}^{f+f_w} E^s(f')W(f-f')df'. \tag{2.12}$$

Note that the right-hand side of the above expression is nothing but a weighted moving average, or a smoothing operation, in the frequency domain. As a result one can choose various kinds of bandlimited smoothing operators $W(f)$ in the frequency domain to execute mechanism extraction. This approach of separating scattering mechanisms in the frequency domain goes as follows:

1. Detect the down range position T_i of each scattering center in the impulse response.

2. Shift the scattering center of interest to the coordinate origin by multiplying the the term $e^{j2\pi fT_i}$ to the frequency response.

3. Smooth the frequency response by performing the integration in Equation (2.12).

4. Shift back the scattering center by multiplying the complex conjugate term in step 2 to the smoothed data and subtract this smoothed data from the pre-smoothed response.

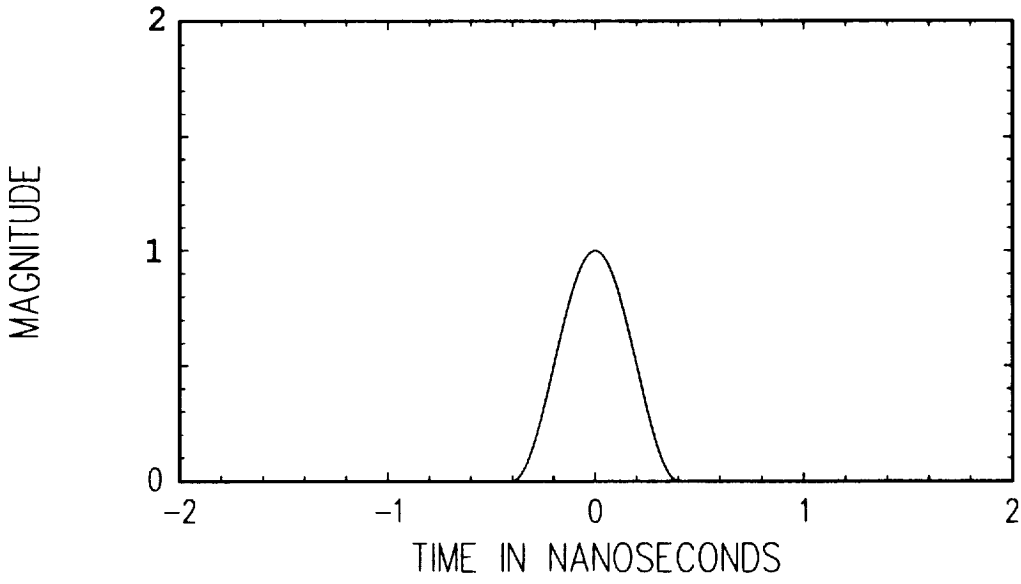

a) time response

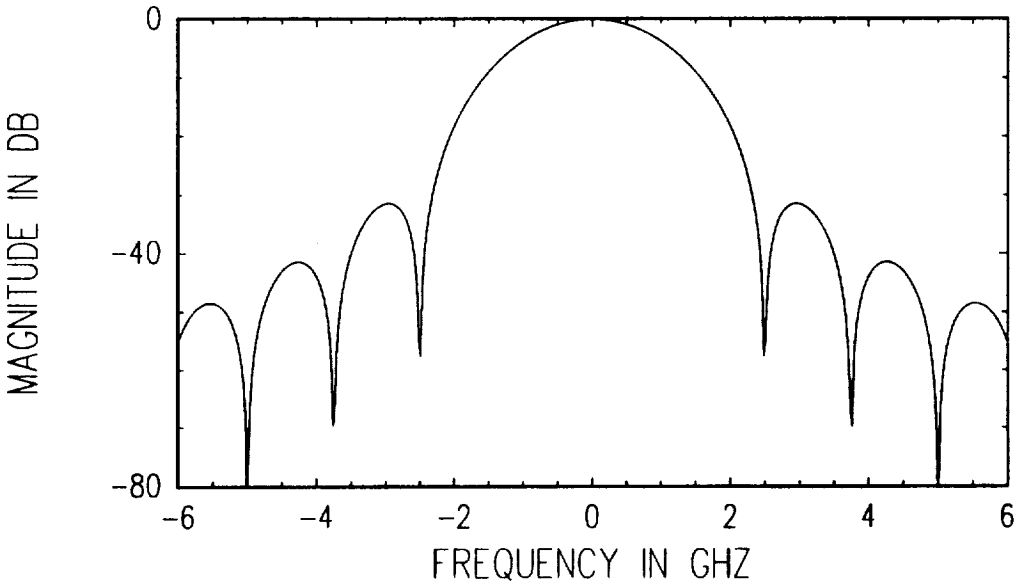

b) frequency response

Figure 2.10: Hanning gate.

5. Repeat steps 2 to 4 until all the scattering centers are extracted.

The above procedure is called the smoothing technique in the frequency domain.

Note that the accuracy of the mechanism extraction by smoothing is at the cost of the computation time; i.e., one can always achieve better separation by increasing the bandwidth f_w of the smoothing operator in Equation (2.12). Also note that smoothing can be interpreted as time-unlimited gating in the time domain; hence, when scattering centers are too close to separate by gating, nor can they be separated by smoothing.

Figures 2.11 and 2.12 show the six individual scattering center responses by applying the smoothing technique to the frequency response shown in Figure 2.6. The smoothing operator chosen here is:

$$W(f) = \frac{1}{A}[1 + \cos(\frac{\pi f}{2.5})] \; ; -2.5 < f < 2.5 \; , \; f \text{ in GHz} \tag{2.13}$$

where A is the normalization constant. The bandwidth ± 2.5 GHz is chosen because the first nulls of the frequency response of a 0.8 ns Hanning gate are at ± 2.5 GHz. These smoothing results compare well to Figures 2.8 and 2.9 which are obtained by time-gating.

2.4 Resolution and Bandwidth

In Section 2.2, it was shown that if two scattering centers are too close to each other, they cannot be separated by gating. But how close is too close? It is a question of resolution, and the resolution is mostly decided by the available bandwidth.

An ideal scattering center is represented by a Dirac Delta function in the time domain and its frequency response is nonzero over the whole spectrum. If one did have the ability to store data over the whole spectrum, two ideal scattering centers could always be separated in the time domain no matter how close they are. However, in the real world only a finite bandwidth is available due to equipment limitations. In our experiments only the frequency response from 2 GHz to 18 GHz has been

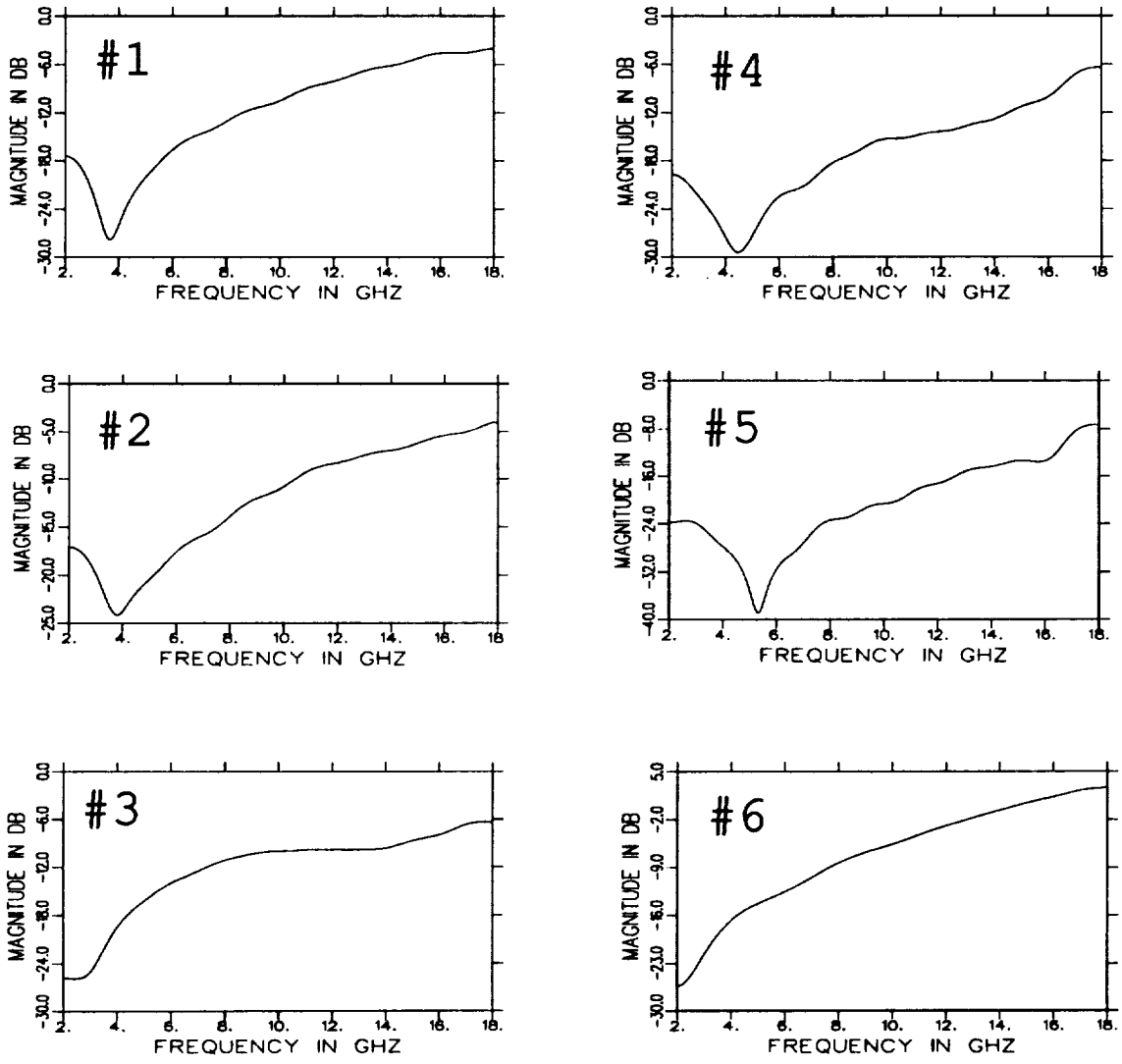

Figure 2.11: Amplitude responses of individual scattering centers on the typical target, obtained by smoothing.

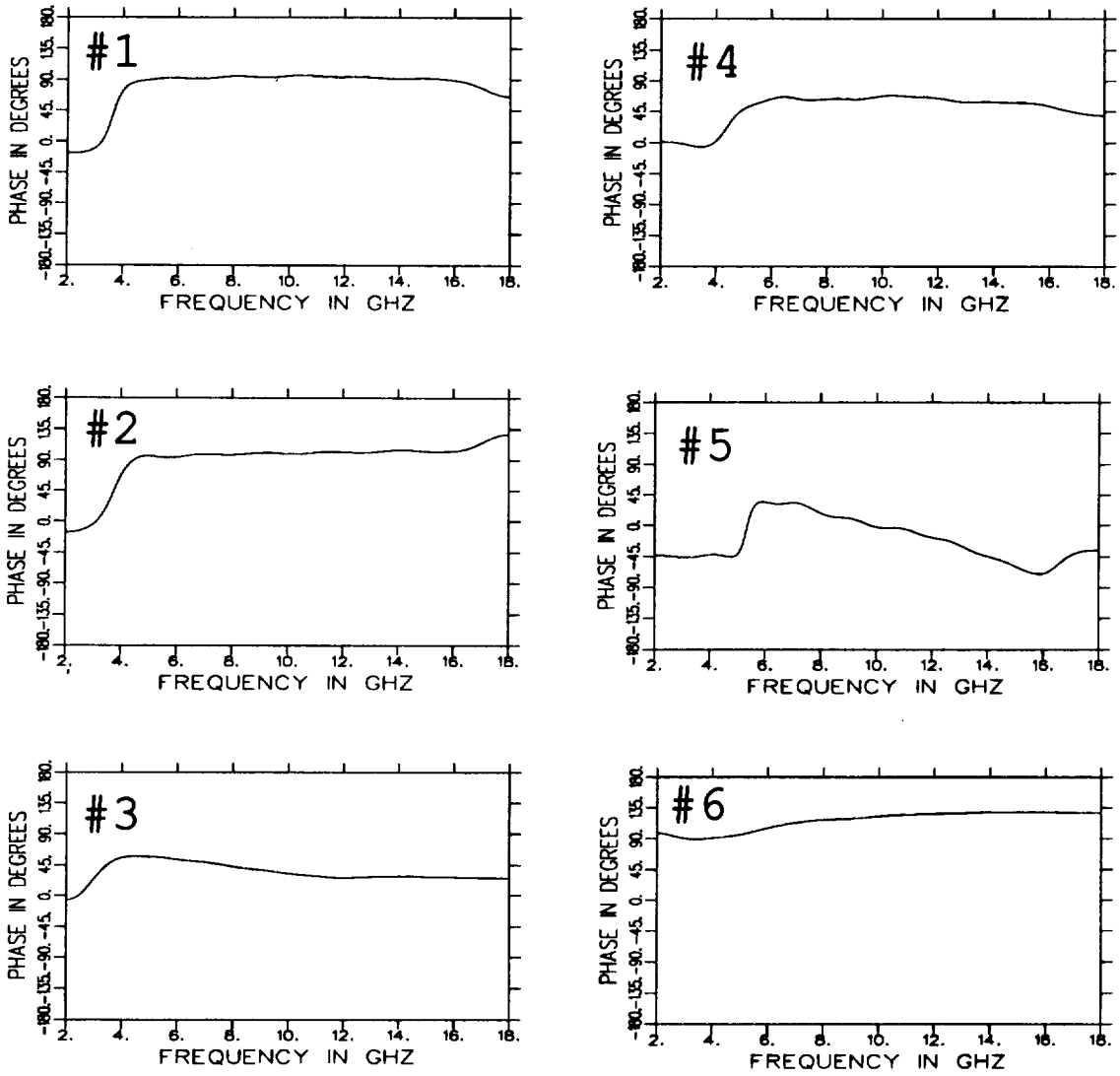

Figure 2.12: Phase responses of individual scattering centers on the typical target, obtained by smoothing.

measured. This is equivalent to applying an ideal bandpass filter to the infinite spectrum. Note that the inverse Fourier transform of an ideal filter with a unity passband for $-\frac{B}{2} < f < \frac{B}{2}$, is a sinc function:

$$h(t) = B\text{sinc}(Bt) \tag{2.14}$$

where

$$\text{sinc}(x) \equiv \frac{\sin \pi x}{\pi x}. \tag{2.15}$$

Therefore, the effect of a truncated bandwidth is equivalent to convolving a sinc function with the original impulse response in the time domain. Consequently, an ideal scattering center will look like a sinc function in the time domain after the bandwidth is truncated. This is shown in Figure 2.13. Since under the bandlimited condition ideal scattering centers become sinc-shaped pulses, the resolution, Δt_r, is defined as the width between the first zeros of the sinc pulse such that

$$\Delta t_r = \frac{2}{B} \text{ (ns)} \tag{2.16}$$

where B is the bandwidth. Note that the resolution is inversely proportional to the available bandwidth. In the case of a 16 GHz bandwidth, the resolution is about 0.125 ns (or 0.75 inches by Equation (2.9)).

Also note that the high sidelobes of the sinc function can give ambiguity to the number of scattering centers in a measurement. A traditional way to reduce the sidelobes of the sinc function is to apply a window function in the frequency domain to taper off the frequency response instead of using abrupt truncation. Here a Kaiser-Bessel window is chosen such that

$$W(f) = \frac{I_o\left[2\pi\sqrt{1-\left(\frac{f-f_o}{B/2}\right)^2}\right]}{I_o[2\pi]}, \; f_o - \frac{B}{2} < f < f_o + \frac{B}{2} \tag{2.17}$$

where $I_o(\cdot)$ is the zeroth-order modified Bessel function of the first kind, f_o is the central frequency of the frequency band one uses and B is the total bandwidth. Note

that an inverse window $\frac{1}{W(f)}$ should be applied at the end of processing to remove the effect of this window if one uses the gating technique to execute mechanism extraction.

2.5 One Dimensional Sampling Theorem and Its Applications to Data Compression and Reconstruction

Though a target's frequency response is continuous, it is often recorded in a discrete form in order to be stored in a computer. The data increment required to represent a continuous frequency response is dictated by the sampling theorem [6].

From the property of the Fourier transform, one knows that if a continuous frequency response is sampled at a step of f_{step} GHz, the effect of this sampling is to make the corresponding impulse response periodical every $\frac{1}{f_{step}}$ ns, or about $\frac{0.5}{f_{step}}$ feet. This property is shown in Figure 2.14. Therefore, if the target is larger than $\frac{0.5}{f_{step}}$ feet, the periodicity will cause overlapping, or aliasing, in the time domain. This would prevent the possible recovery of the original impulse response and is called an undersampling situation. Thus, in order to fully represent a continuous frequency response in a discrete form, the data increment has to be decided by the target size. In this research, a 10 MHz increment in the frequency domain is chosen, which corresponds to an aliasing distance (or wrap-around period) of 100 ns, or about 50 feet. Since the targets in our measurements are restricted within 8 feet, any target will be highly oversampled.

In Section 2.2, it was shown that the resulting frequency response of an individual scattering center is a smooth curve. For the purpose of data compression, one may hope to represent this smooth curve by just a few data points. Again this is guaranteed by the sampling theorem. In Figure 2.7, if a scattering center is extracted out by a 0.8 ns gate, then the scattering center's frequency response (see Figures 2.8 and 2.9) can be sampled at a step of $1/0.8 = 1.25$ GHz without introducing aliasing.

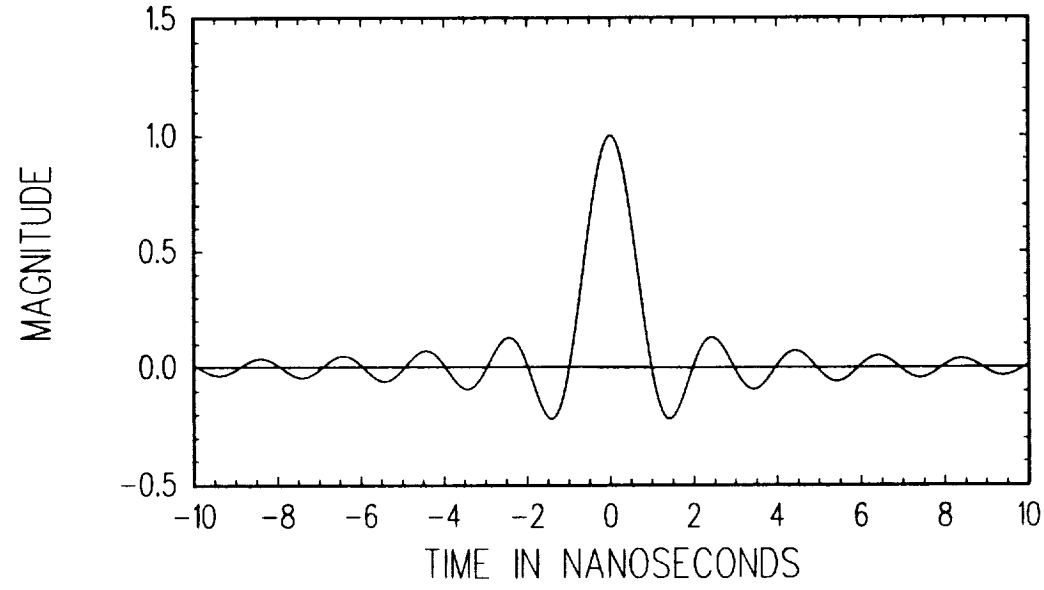

a) time response

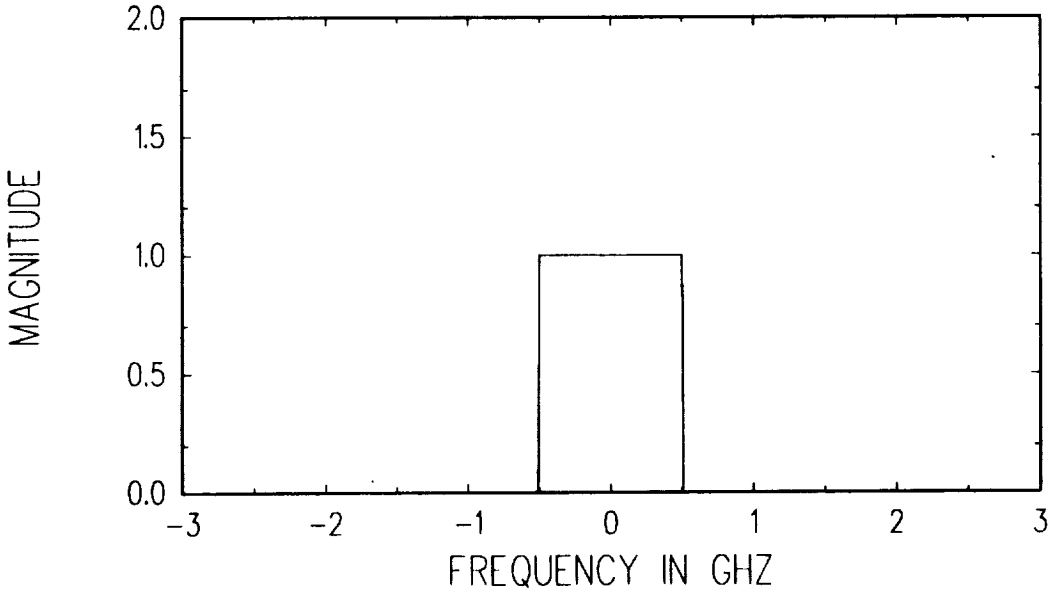

b) frequency response

Figure 2.13: Ideal lowpass filter.

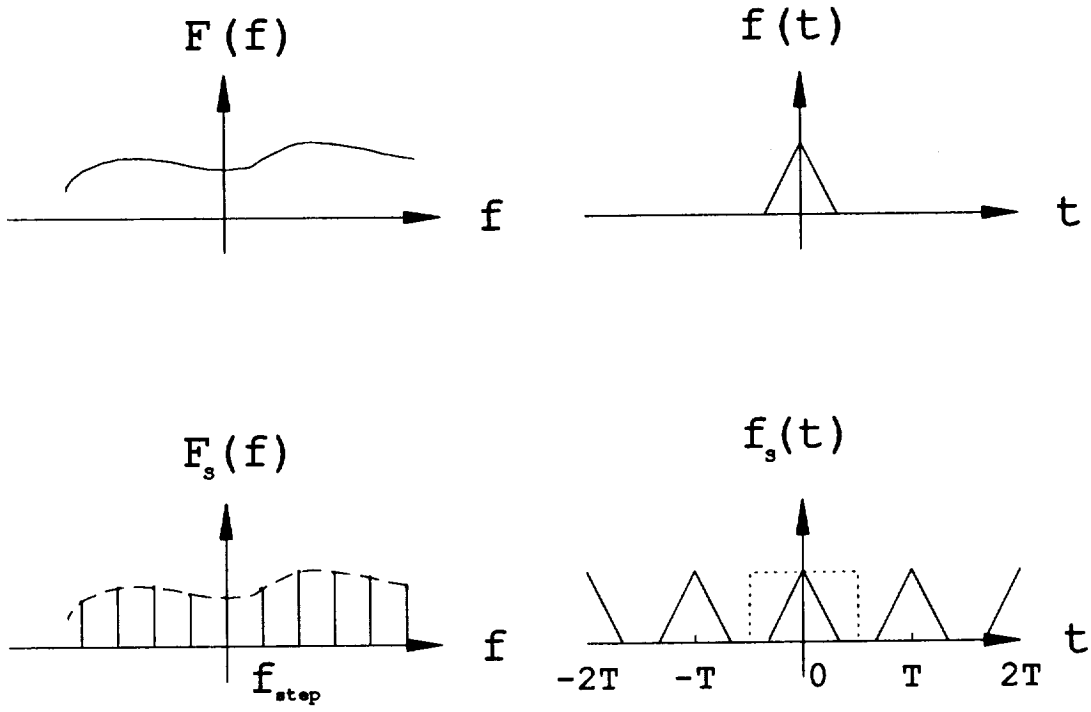

$$T = \frac{1}{f_{step}}$$

Figure 2.14: The effect of sampling.

In this research, the preliminary goal is to reduce the database from storing every 10 MHz to 1 GHz, which can be achieved as long as the gate width is less than 1 ns.

The reconstruction of the continuous response out of these sampled points can be done by applying a rectangular gate to the periodical impulse response in the time domain as shown in Figure 2.14. This could also be thought of as interpolating the sampled points by a sinc function directly in the frequency domain [6]. Figure 2.15 shows the latter approach.

Once one gets back the individual scattering center's frequency response, the original target's frequency response can be obtained by shifting back each scattering center to its down range position and then summing up all the individual scattering center responses. Figure 2.16 shows the reconstructed data of Figure 2.6. From Figure 2.16 one can see that the data compression-reconstruction scheme is promising for building a compact database of a complicated target.

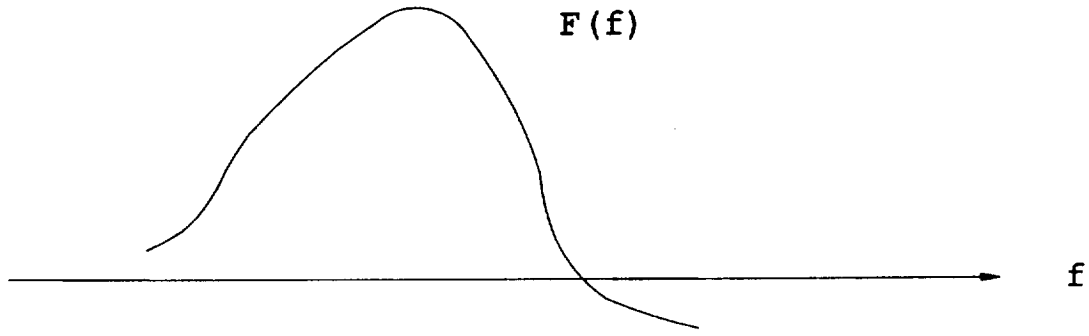

(a)

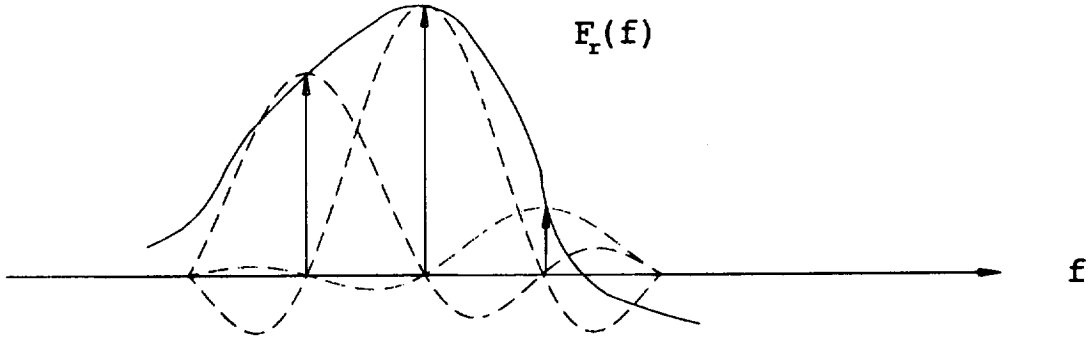

(b)

Figure 2.15: Sinc interpolation.

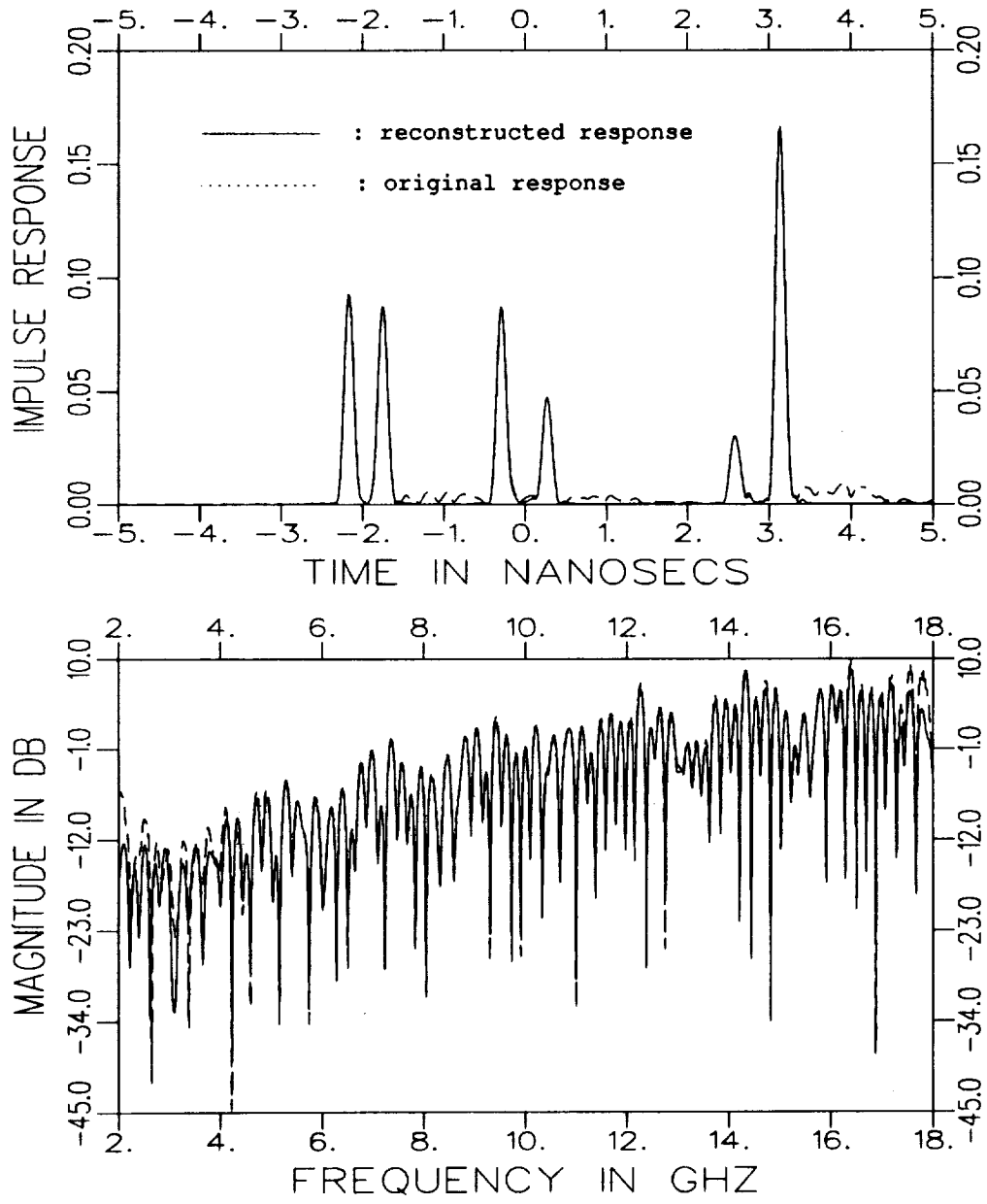

Figure 2.16: Comparison between the reconstructed and original responses for the typical target shown in Figure 2.6, obtained by 1-D gating.

Chapter 3

Two Dimensional Target Response and Mechanism Extraction

Early radar systems were designed to detect a target's range and speed, which is basically one-dimensional information. Recently more high resolution radar techniques have been developed to "see" and identify a target in two or three dimensions (for example, see [9]). Thus, "radar imaging" ensues.

A radar image can be represented by a two-dimensional (2-D) reflectivity function $u(x, y)$. This reflectivity function is related to the two-dimensional frequency response $U(f_x, f_y)$ by the 2-D Fourier transform. Some important properties and applications of the 2-D Fourier transform can be found in [7], [8] and many others. However, the computations needed to perform a 2-D Fourier transform are extensive even by using a 2-D Fast Fourier Transform (FFT) subroutine, and it is also inconvenient to collect the rectangular type data $U(f_x, f_y)$ if only one antenna is available. The above problems can be solved by using the Inverse Synthetic Aperture Radar (ISAR) technique. In short, polar type data $U(f, \theta)$, instead of the rectangular type $U(f_x, f_y)$, is collected from swept frequency and angle measurements in order to generate the 2-D radar image.

This ISAR technique is reviewed in Section 3.1. Section 3.2 examines the relation between the ISAR image and the available 2-D spectral domain data, including

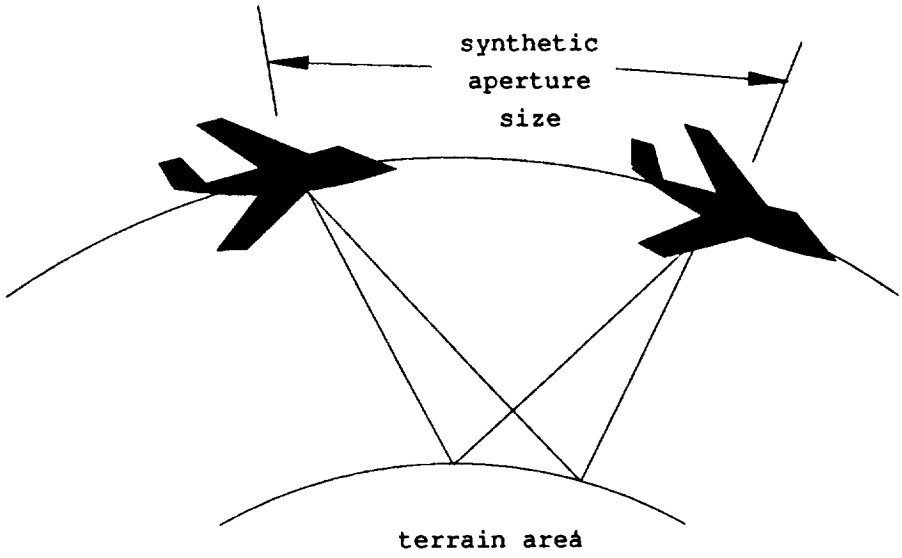

Figure 3.1: Spotlight SAR.

resolution and aliasing. Section 3.3 discusses the 2-D mechanism extraction methods, which are extensions of the 1-D case. The sampling theorem for 2-D signal processing is also explained. Section 3.4 is the core of this report, which displays the procedure of the 2-D data compression, the formulation of a reduced database and the reconstruction of the original data from the reduced database.

3.1 2-D ISAR Image Technique

ISAR draws its name from SAR: the Synthetic Aperture Radar. SAR is an airborne radar which illuminates a terrain area and records the reflected signal in order to generate a high resolution map of that terrain area. This technique was first demonstrated in early 50's [9]. Figure 3.1 illustrates how one kind of SARs works called the Spotlight SAR. Basically the Spotlight SAR collects data of a fixed target (e.g., a terrain area) from a rotating antenna. But the same data can be collected in an "inverse" way; i.e., from a fixed antenna illuminating a rotating target. This is

exactly the idea of ISAR. ISAR is easy to set up in a compact range facility [10]. Model target can be measured and a high resolution image can be obtained. This will be shown next.

Consider a radar image represented by a reflectivity function $u(x,y)$. Note that as discussed in Chapter 2, one has the following results:

$$t_x = \frac{2x}{c} \;\; ; \;\; t_y = \frac{2y}{c}$$

where x and y are units of length, t_x and t_y are units of time (round trip), and c is the speed of light. Consequently, one can freely change the scale from $u(x,y)$ to $u(t_x,t_y)$. The 2-D time domain function $u(t_x,t_y)$ can then be related to the 2-D spectral domain function $U(f_x,f_y)$ by the Fourier transform pairs:

$$u(t_x,t_y) = \int_{-\infty}^{\infty}\int_{-\infty}^{\infty} U(f_x,f_y)e^{j2\pi(t_x f_x + t_y f_y)}df_x df_y \tag{3.1}$$

and

$$U(f_x,f_y) = \int_{-\infty}^{\infty}\int_{-\infty}^{\infty} u(t_x,t_y)e^{-j2\pi(f_x t_x + f_y t_y)}dt_x dt_y. \tag{3.2}$$

Since

$$U(f,\phi) = U(f_x,f_y)|_{f_x = f\cos\phi, f_y = f\sin\phi},$$

one can substitute $f_x = f\cos\phi$, $f_y = f\sin\phi$ and $df_x df_y = f\,df\,d\phi$ into Equation (3.1) to obtain [8]

$$\begin{aligned} u(t_x,t_y) &= \int_0^{2\pi}\int_0^{\infty} U(f,\phi)e^{j2\pi f(t_x\cos\phi + t_y\sin\phi)} f\,df\,d\phi \\ &= \int_0^{\pi}\int_0^{\infty} U(f,\phi)e^{j2\pi f(t_x\cos\phi + t_y\sin\phi)} f\,df\,d\phi \\ &\quad + \int_{\pi}^{2\pi}\int_0^{\infty} U(f,\phi)e^{j2\pi f(t_x\cos\phi + t_y\sin\phi)} f\,df\,d\phi. \end{aligned} \tag{3.3}$$

Note that

$$\begin{aligned} \cos(\phi+\pi) &= -\cos\phi\,, \\ \sin(\phi+\pi) &= -\sin\phi\,, \text{ and} \\ U(f,\phi+\pi) &= U(-f,\phi). \end{aligned}$$

By substituting the above results into Equation (3.3), one finds that

$$u(t_x, t_y) = \int_0^{\pi} \int_{-\infty}^{\infty} U(f, \phi) e^{j2\pi f(t_x \cos\phi + t_y \sin\phi)} |f| df d\phi. \tag{3.4}$$

The radar image can thus be achieved by completing the integration in either Equation (3.1) or Equation (3.4).

Since the measured data is normally obtained in a polar form (i.e., swept frequency and swept angle), one needs a precise interpolation routine to change the polar form data to the rectangular form (see Figure 3.2) before performing the 2-D inverse Fourier transform in Equation (3.1). Interested readers can refer to [11] for this approach. On the other hand, one can use Equation (3.4) to construct an image with less effort. To show this, the Fourier Slice Theorem, which is extensively applied in Computer Tomography, should first be introduced [8].

In Figure 3.3, let $p_{\phi_o}(\tilde{t}_x)$ be the parallel projection of an image $u(t_x, t_y)$ onto the $\tilde{t}_x$ axis, which is the rotation of the t_x axis by ϕ_o. Then the Fourier Slice theorem says the 1-D Fourier transform of $p_{\phi_o}(\tilde{t}_x)$ is $U(f, \phi = \phi_o)$, a slice of the 2-D spectral response oriented at the same angle $\phi = \phi_o$.

The proof of the Fourier Slice theorem is straightforward. By definition,

$$p_{\phi_o}(\tilde{t}_x) = \int_{-\infty}^{\infty} u(\tilde{t}_x, \tilde{t}_y) d\tilde{t}_y. \tag{3.5}$$

Let $P_{\phi_o}(f)$ be the Fourier transform of $p_{\phi_o}(\tilde{t}_x)$, then

$$\begin{aligned} P_{\phi_o}(f) &= \int_{-\infty}^{\infty} p_{\phi_o}(\tilde{t}_x) e^{-j2\pi f \tilde{t}_x} d\tilde{t}_x \\ &= \int_{-\infty}^{\infty} \int_{-\infty}^{\infty} u(\tilde{t}_x, \tilde{t}_y) e^{-j2\pi f \tilde{t}_x} d\tilde{t}_x d\tilde{t}_y \end{aligned}$$

Note that for a rotation of a coordinate system by angle ϕ_o,

$$\tilde{t}_x = t_x \cos\phi_o + t_y \sin\phi_o \tag{3.6}$$

$$\tilde{t}_y = -t_x \sin\phi_o + t_y \cos\phi_o, \tag{3.7}$$

so

$$P_{\phi_o}(f) = \int_{-\infty}^{\infty} \int_{-\infty}^{\infty} u(t_x, t_y) e^{-j2\pi f(t_x \cos\phi_o + t_y \sin\phi_o)} dt_x dt_y. \tag{3.8}$$

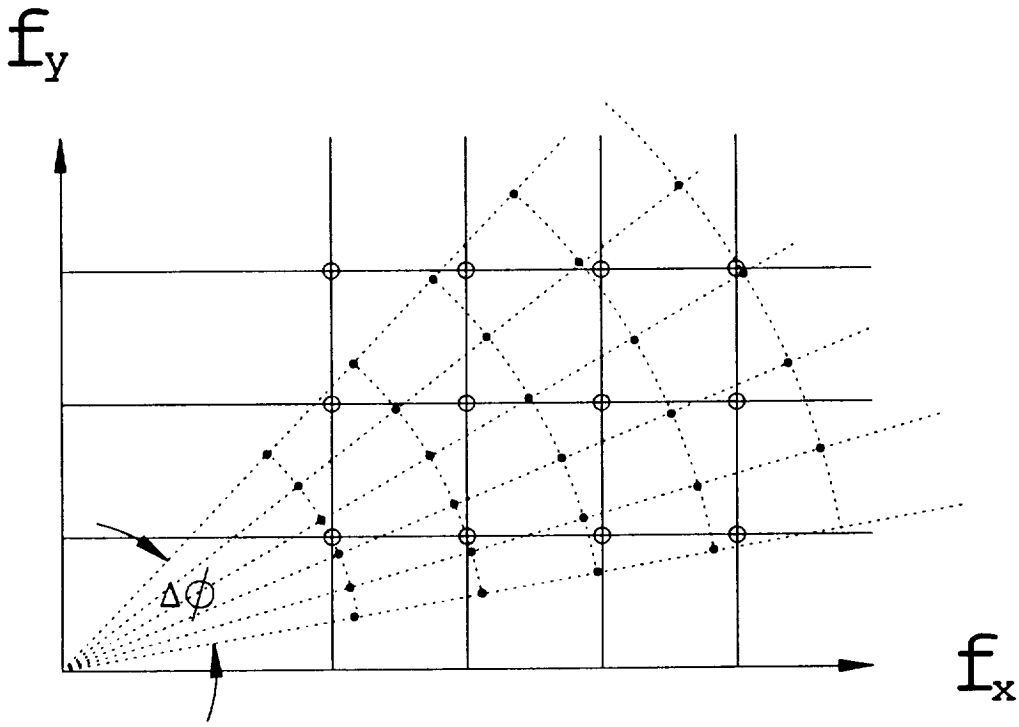

Figure 3.2: Polar and rectangular grid formats.

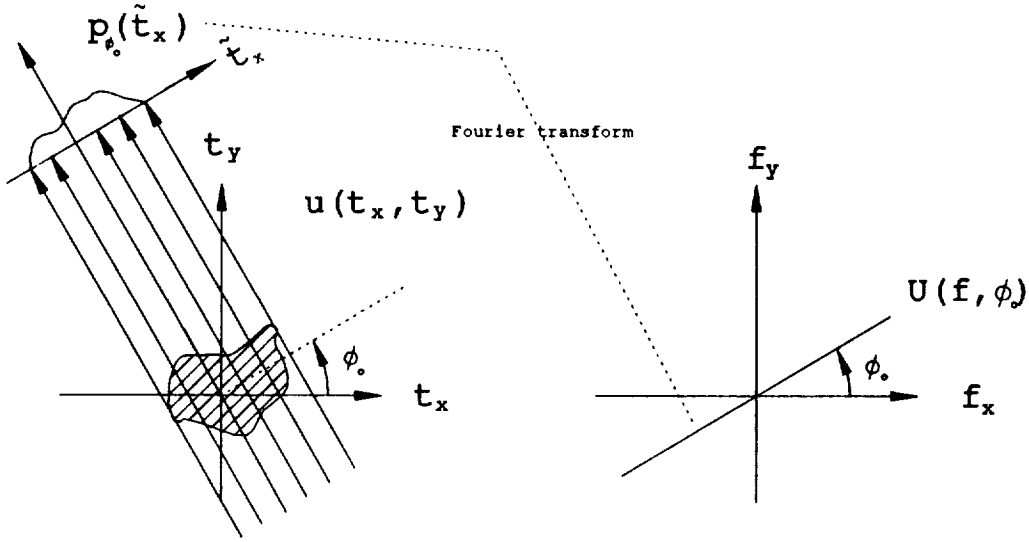

Figure 3.3: The Fourier Slice (or Fourier Projection) Theorem.

Comparing Equation (3.8) to Equation (3.2), one knows that $P_{\phi_o}(f) = U(f, \phi_o)$, proved.

According to the Fourier Slice theorem, the 1-D inverse Fourier transform of $U(f, \phi_o)$ is a "projection" of the 2-D image. And one can define a "filtered projection" function I_ϕ such that

$$I_\phi(\tilde{t}_x) = \int_{-\infty}^{\infty} U(f, \phi)|f| e^{j2\pi f \tilde{t}_x} df. \tag{3.9}$$

Note that $I_\phi(\tilde{t}_x)$ is the 1-D inverse Fourier transform of a filtered slice of $U(f, \phi)$, with the filter coefficients being $|f|$, hence it is called a "filtered projection" function.

With the help of this function, Equation (3.4) can be rewritten to obtain

$$u(t_x, t_y) = \int_0^{\pi} I_\phi(\tilde{t}_x) d\phi|_{\tilde{t}_x = t_x \cos\phi + t_y \sin\phi}. \tag{3.10}$$

Equation (3.10) demands each filtered projection to be "backprojected" onto the (t_x, t_y) plane and then to be summed up over the angle variable to generate the

image $u(t_x, t_y)$. The above procedure is called the filtered backprojection algorithm and an image thus generated is called an ISAR image throughout this report. The following is a summary of the steps to generate an ISAR image [8]:

1. Measure the swept frequency data $U(f, \phi)$ at angle ϕ.
2. Filter the data by $|f|$ and then take the 1-D inverse Fourier transform (IFT).
3. Backproject the 1-D IFT result onto the whole (t_x, t_y) image plane in the orientation of ϕ.
4. Repeat steps 1-3 for each look angle and sum up each backprojection in the image plane to generate the ISAR image.

The filtered backprojection algorithm also needs interpolation, not in the spectral domain but in the image domain, when it is constructing an ISAR image. It turns out that the interpolation scheme in the image domain is much easier than what is needed by the 2-D IFT algorithm in the spectral domain [8]. Here a linear interpolation is used and a typical ISAR image is shown in magnitude in Figure 3.4.

3.2 Resolution in 2-D Image Domain and Effect of Discrete Data Increments

To obtain an ISAR image as shown in the previous section, one needs data of all 360° look angles. But in practical cases, scattering centers are not isotropic; i.e., their scattered fields may change versus the illuminating angle. Besides, for a complicated target some parts may be shadowed by other parts when it is illuminated by an electromagnetic plane wave. These factors will make the 360° ISAR a complex image. To take these factors into account, Equation (3.10) is modified as

$$u_{\phi_o}(t_x, t_y) = \int_{\phi_o - \psi}^{\phi_o + \psi} I_\phi(\tilde{t}_x) d\phi \tag{3.11}$$

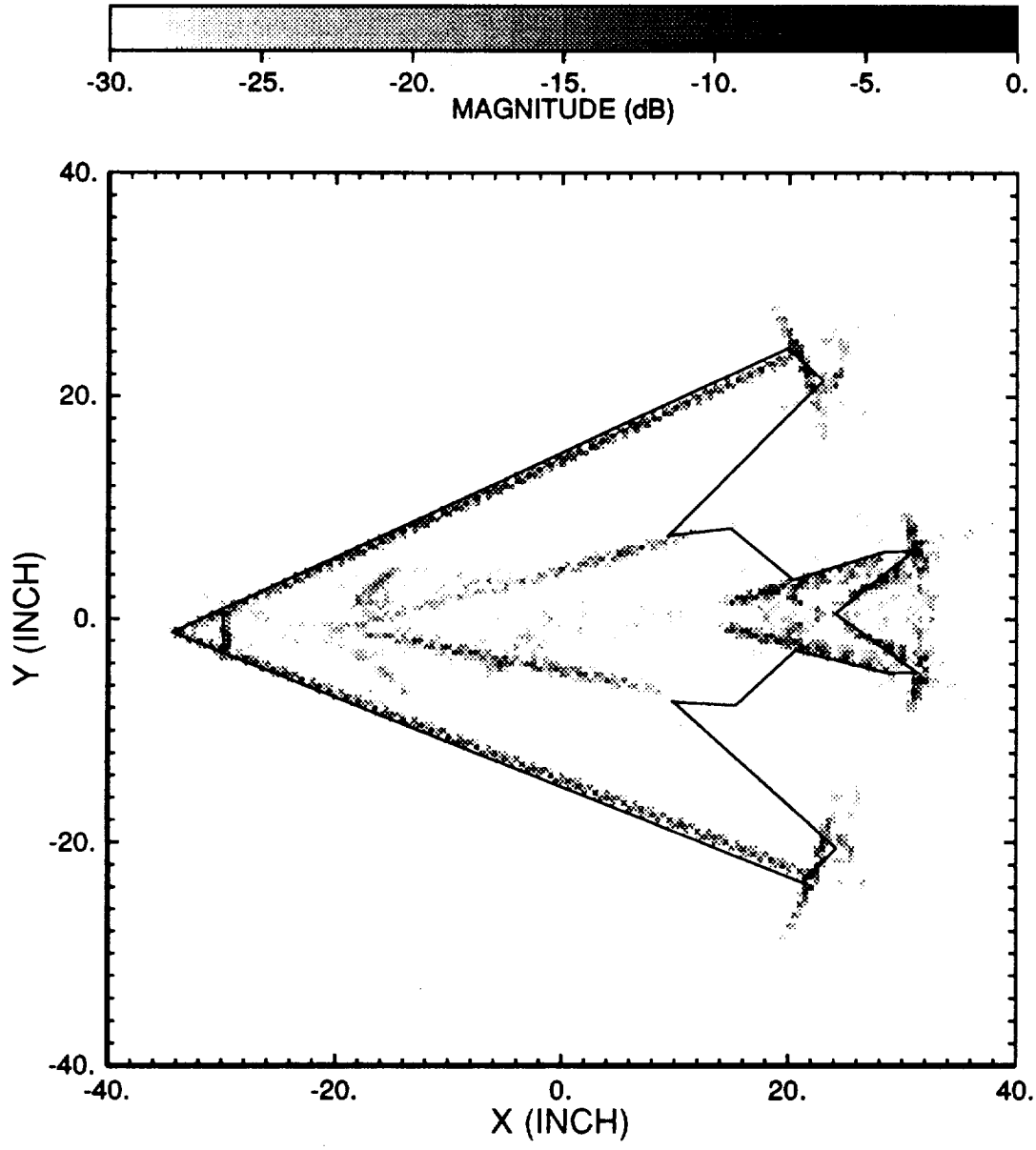

Figure 3.4: ISAR image of a fighter model.

in order to generate a "local" ISAR image for a desired look angle $\phi = \phi_o$. Here ψ is empirically set to be 10°. Note that by doing this one can actually make $u_{\phi_o}(t_x, t_y)$ a real image by arbitrarily satisfying the conjugate symmetry condition in the spectral domain.

In addition to the limited aspect angles, only a finite bandwidth is available. Thus, the data used to generate a local ISAR image is measured and stored within a small region of the whole 2-D spectral domain. To guarantee the target is fully represented, again one needs to investigate the effect of data truncation and the discrete data increments.

Assume $\phi_o = 0°$ in Equation (3.11) for convenience. For this particular look angle, t_x is the down range axis and t_y is the cross range axis. Remember that for the 1-D case shown in Chapter 2, the frequency bandwidth gives the time domain resolution, and the target size dictates the discrete data increment required to fully represent the target response. The same criterion holds between the 2-D (f_x, f_y) spectral domain and the 2-D (t_x, t_y) spatial domain. Namely, the available bandwidth in f_x gives the resolution along the t_x direction of the image; and the target's size along the t_x direction dictates the data increment required in the f_x axis. Similar for f_y and t_y.

Though here polar form data (f, ϕ) is measured instead of (f_x, f_y), when the angle span is small (say, $\pm 10°$) and the frequency is bandlimited, the rectangular type data can be approximated by the polar type data. In this case, $f_x = f \cos\phi \approx f$ and $f_y = f \sin\phi \approx f \cdot \phi$. So the down range resolution is primarily dictated by the bandwidth of f. In our measurements, the frequency band ranges from 2 GHz to 18 GHz for a total bandwidth of 16 GHz, so the down range resolution is about 0.75 inches as discussed in Chapter 2. On the other hand, the cross range resolution depends on both f and ϕ since $f_y \approx f \cdot \phi$. Note that the span of ϕ is $\pm 10°$, so f_y has a bandwidth of 0.7 GHz when $f = 2$ GHz; and 6.3 GHz when $f = 18$ GHz, which varies by a factor of 9. In other words, the bandwidth of f_y is not a constant. Since

in this case no direct relation can be used to decide the resolution in cross range, it is done by letting two scattering centers of equal strength move toward each other along the t_y axis until their positions become distorted. The cross range resolution thus achieved is approximately 3 inches under the $\pm 10°$ angle span condition.

Note that if the whole spectral domain data is available, the 2-D spatial response of an ideal point scatterer is a Dirac Delta function. But when the spectral domain data are abruptly truncated, the spatial domain Delta function begins to distort into a 2-D sinc function. The high sidelobes of the 2-D sinc function will deteriorate the quality of the ISAR image. The traditional way to deal with this problem is to apply a 2-D tapering window in the spectral domain to avoid abrupt truncation. Note that an inverse window should be used to compensate this effect after one gets back from the image domain to the spectral domain.

The discrete spectral data increments have to be chosen such that they can avoid aliasing in both the down and cross range directions of the ISAR image. As mentioned before, for a small angular data region in the spectral domain, the ISAR image's down range is closely related to f. So a 10 MHz frequency data increment corresponds to a 100 ns, or about 50 feet wrap-around period in the down range axis, which oversamples a target with a down range size of 8 feet. In the ISAR image's cross range direction, the spectral data increment $\Delta f_y \approx f\Delta\phi \propto f$, so one should consider the highest frequency case which has the smallest wrap-around period in cross range. At $f = 18$ GHz, if one uses an angle step of 0.1°, it is about an f_y increment of $18 \cdot \frac{0.1}{180} \cdot \pi = 0.031$ GHz, or roughly 30 MHz. This means the least wrap-around period is about 33 ns, or 16.5 feet in cross range, then a target with a cross range size of 8 feet is also oversampled.

Though the above chosen data increments (10 MHz, 0.1°) can fully represent the target in the spectral domain given the oversampling condition, the data amount thus achieved may be too large to save. For example, if one uses a bandwidth of 16 GHz to complete an ISAR measurement of a 360° circular illumination, one needs

to store $3600 \times 1601 = 5,763,600$ complex data points. So the challenge is how to reduce the data amount while still being able to preserve all the information contained in the measurements. Hence, 2-D mechanism extraction methods and data compression scheme will be explored in the next two sections.

3.3 2-D Mechanism Extraction

From the discussion of the Fourier Slice Theorem in Section 3.1, one knows that when a target is illuminated from a certain look angle, the 1-D frequency response is just a Fourier transform of $p_{\phi 0}(\tilde{t}_x)$ — the projection of the reflectivity function $u(t_x, t_y)$ onto the down range $\tilde{t}_x$ axis. Therefore, scattering centers of similar down ranges but different cross ranges, when projected onto the down range, may overlap and become impossible to separate using 1-D mechanism extraction techniques. This problem can be solved by extending the 1-D techniques to the 2-D case.

Figure 3.5 shows the spatial domain envelopes of six corner reflectors at the look angle $\phi = 180°$ obtained using the ISAR technique. From Figure 3.5 one can see that a 2-D gating technique is a straightforward method to isolate scattering centers in the spatial domain. To be specific, first Figure 3.5 is used to detect the peak location of each scattering center. Then a rectangularly-based uniform gate (which is a 2-D spatial gate with unity passband) is positioned to the scattering centers one at a time to extract each of them. The extracted area is then shifted to the coordinate origin and projected onto the down range axis. The final step is to take the 1-D Fourier transform of the projection to get each scattering center's frequency response for that look angle.

A 2-D smoothing technique can also be derived. As one knows, the equivalent operation of gating in the spatial domain is the 2-D convolution in the spectral domain such that

$$\mathcal{F}[u(t_x, t_y) \cdot g(t_x, t_y)] = \int_{-\infty}^{\infty} \int_{-\infty}^{\infty} U(f_x', f_y') G(f_x - f_x', f_y - f_y') df_x' df_y'$$

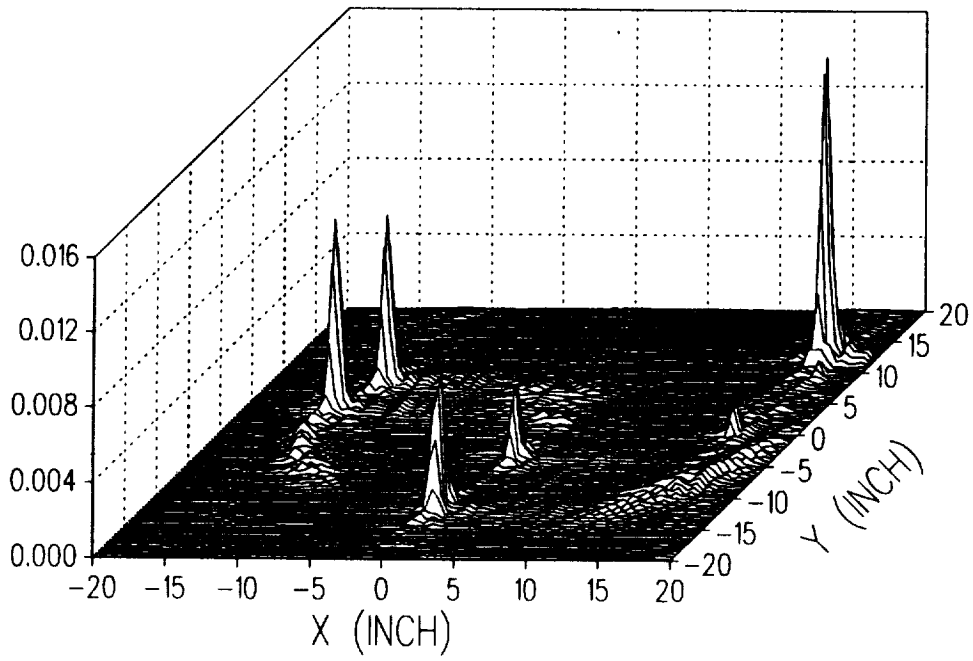

Figure 3.5: 2-D envelope response of the six corner reflectors at $\phi = 180°$.

$$\equiv \quad U(f_x, f_y) * G(f_x, f_y). \tag{3.12}$$

For a small angular region, the 2-D rectangular-type convolution can be approximated by a 2-D smoothing process along the frequency and angle scans, respectively. After the smoothing for one scattering center, the smoothed response is subtracted from the total spectral response, and the procedure continues until all scattering centers are extracted out.

The advantage of 2-D smoothing over 2-D gating is that smoothing operates directly on the spectral domain data, so it avoids the need to use windows and gates back and forth in both the spatial and spectral domains. The disadvantage is that smoothing takes longer time than gating to process the data. But basically these two techniques represent the same idea of mechanism extraction.

3.4 2-D Data Compression and Reconstruction

After the 2-D mechanism extraction by either gating or smoothing, the individual spectral response of a scattering center shifted to the origin should be smooth over the whole spectral domain because there are no interactions with other scattering centers and there is no propagation phase. The smoothness of individual scattering center's 2-D spectral response is what one can take advantage of when it comes to 2-D data compression. For example, one may expect to represent the smooth frequency response for a certain look angle by just a few data points, while in the angle domain one may also expect to represent the scattering center's angle response by just a few angles. By doing this one can reduce the data amount a lot. Let's assume there are in average 30 scattering centers making up a real-world target, since one originally measures the target every 10 MHz over a 16 GHz bandwidth and every 0.1° over 360° rotation, there will be 5,763,600 data points as calculated before. If one can extract out these 30 scattering centers and sample each scattering center's frequency response every 1 GHz and azimuth response every 5° and thus form a "reduced" database, then the number of data points needed to be stored will reduce to $30 \times 17 \times 72 = 36,720$, which is 150 times less than the originally measured data amount.

Though the above calculation seems attractive, a big concern is that whether or not one can reconstruct the original signal from the reduced database in real time. For example, in a target identification application, a moving target could come in from any look angle on a radar operating in different frequency bands; one must be able to generate the frequency response of a certain look angle or the azimuth response at a certain frequency from the reduced database in order to compare the incoming target signal with the stored information. From the 1-D experience in the previous chapter, one would expect to achieve this goal again by the sampling theorem.

In the 1-D case, the sampling theorem guarantees the recovery of a time-limited frequency domain signal from its sampled points. The reconstruction is done by either using a rectangular time gate in the time domain or a sinc interpolation in the frequency domain. The same concept can be extended to the 2-D case where the time-limit $\tilde{T}_x$ along the down range $\tilde{t}_x$ axis decides the sampling period in $\tilde{f}_x$ and the time-limit $\tilde{T}_y$ along the cross range $\tilde{t}_y$ axis decides the sampling period in $\tilde{f}_y$. To be specific, the 2-D sampling theorem states that a 2-D time-limited frequency domain function $U(\tilde{f}_x, \tilde{f}_y)$ can be completely recovered from the discrete spectral samples whose separation is given by [7]

$$\Delta \tilde{f}_x \leq \frac{1}{\tilde{T}_x}$$

and

$$\Delta \tilde{f}_y \leq \frac{1}{\tilde{T}_y}.$$

The recovery is then done by either using a rectangularly-based uniform gate in the 2-D spatial domain or a 2-D sinc interpolation in the spectral domain.

Note that in general one cannot apply the 2-D sampling theorem on the polar format (f, ϕ) data because there is no separable relation between f and the down range, and between ϕ and the cross range. But again for a small angular region and a truncated bandwidth, one can use the polar-type data to approximate the rectangular-type data and hence one can sample a scattering center's spectral response by just a few frequencies and angles after it is extracted out.

After one obtains the reduced database, the reconstruction procedure operates as follows:

1. Recover the frequency response of each scattering center at recorded angles by the sinc interpolation.

2. If the look angle to be reconstructed is not a recorded angle, linearly interpolate the response for each scattering center at the desired look angle using the data of the two neighboring recorded angles.

3. Shift back the proper down range position for each scattering center and sum up all the individual responses.

The above procedure can be used to get a frequency response of a desired look angle, or an azimuth response of a certain frequency, or the response at a desired look angle for a given frequency. And if the number of scattering centers is small, the reconstruction can be done very fast. The details and the results of this 2-D data compression and reconstruction scheme will be shown in the next two chapters.

Chapter 4

Data Compression and Reconstruction for a Simple Target: The Six Corner Reflectors Case

The basic ISAR imaging concepts, separation of individual scattering centers and data compression techniques have been explained in the previous chapter. In this chapter, a simple target composed of six corner reflectors is used to demonstrate the details of the 2-D data compression procedure and to evaluate the capability of the data reconstruction algorithm.

4.1 Measurement of a Simplified Target: Six Corner Reflectors

A simplified target composed of six corner reflectors is chosen to test the feasibility of the data compression-reconstruction algorithm in this chapter. The corner reflectors are chosen because they simulate point scatterers very well, provided that they are not very large electrically. Though corner reflectors are not isotropic scattering centers, the frequency and angle dependence of their backscattered fields can be calculated from their geometries.

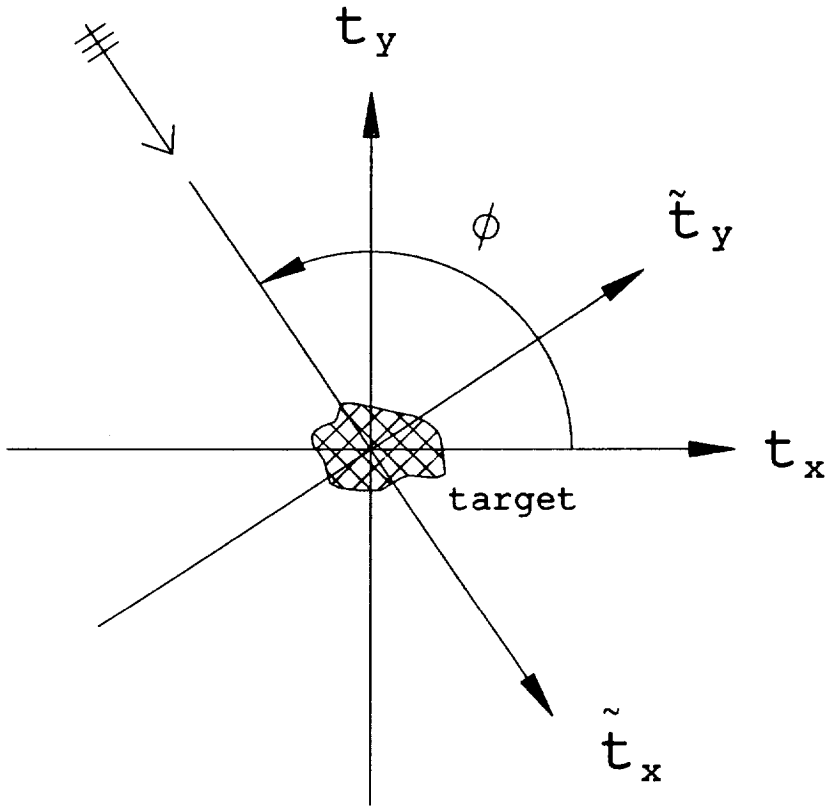

Figure 4.1: Target coordinate systems.

Table 4.1: Positions and sizes of the six corner reflectors.

No.	x (inch)	y (inch)	side length
# 1	-13.6	3.9	3″
# 2	-11.8	7.9	3″
# 3	0.5	-11.4	$3\frac{1}{2}$″
# 4	2.1	-3.8	$2\frac{1}{8}$″
# 5	15.7	0.0	$1\frac{3}{4}$″
# 6	17.1	12.1	$4\frac{1}{4}$″

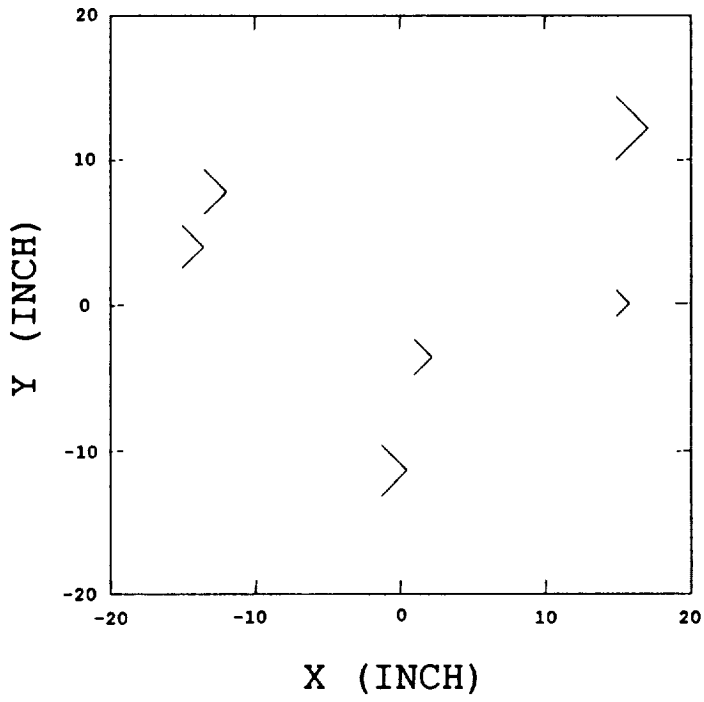

Figure 4.2: Top view of the six corner reflectors.

As shown in Figure 4.1, the (t_x, t_y) coordinate system is a fixed coordinate system with respect to the target, with the origin defined at the center of rotation. The $(\tilde{t}_x, \tilde{t}_y)$ coordinate system, which is rotating, indicates the down range and cross range of the incident wave direction, respectively. Figure 4.2 and Table 4.1 define the locations of these six corner reflectors.

The backscattered fields from the six corner reflectors were measured every 0.25° from $\phi = 160°$ to $\phi = 200°$. For each angle a frequency response from 2 GHz to 18 GHz was stored at an increment of 10 MHz. Thus, there are 1601 data points for each angle file. These discrete data increments (10 MHz, 0.25°) are both oversampling, hence they can fully represent the continuous target response in the 2-D spectral domain.

When an ISAR image centered at a certain look angle $\phi = \phi_o$ is formed, the azimuth data from $\phi_o - 10°$ to $\phi_o + 10°$ is used. This 20° angle span gives roughly a cross range resolution of 3 inches as discussed in Chapter 3. For each look angle, the available bandwidth of the frequency scan is 16 GHz, hence the down range resolution is about 0.75 inches as shown in Chapter 3, too. To avoid the abrupt truncations in both the azimuth and frequency scans, a Kaiser-Bessel window is applied to both the 20° azimuth span and the frequency data.

To execute the filtered backprojection algorithm to form an ISAR image, each frequency data array is multiplied by $|f|$ first. Then an 8192 point Inverse Fast Fourier Transform (IFFT) subroutine is used to transform the filtered 1601 frequency points to the time domain. Lastly, the time domain array is backprojected onto a 2-D ISAR image plane which is large enough to cover the whole target zone. Note that one can freely set the grid size in the ISAR image, but the smallest grid step is dictated by the IFFT subroutine. To be specific, since the frequency increment is 10MHz, correspondingly in the time domain the wrap-around period is 100 ns. The 8192 time domain array thus has an increment of 0.0122 ns, or 0.07 inches. This is the smallest grid representation of the ISAR image. Figures 4.3 to 4.5 show ISAR

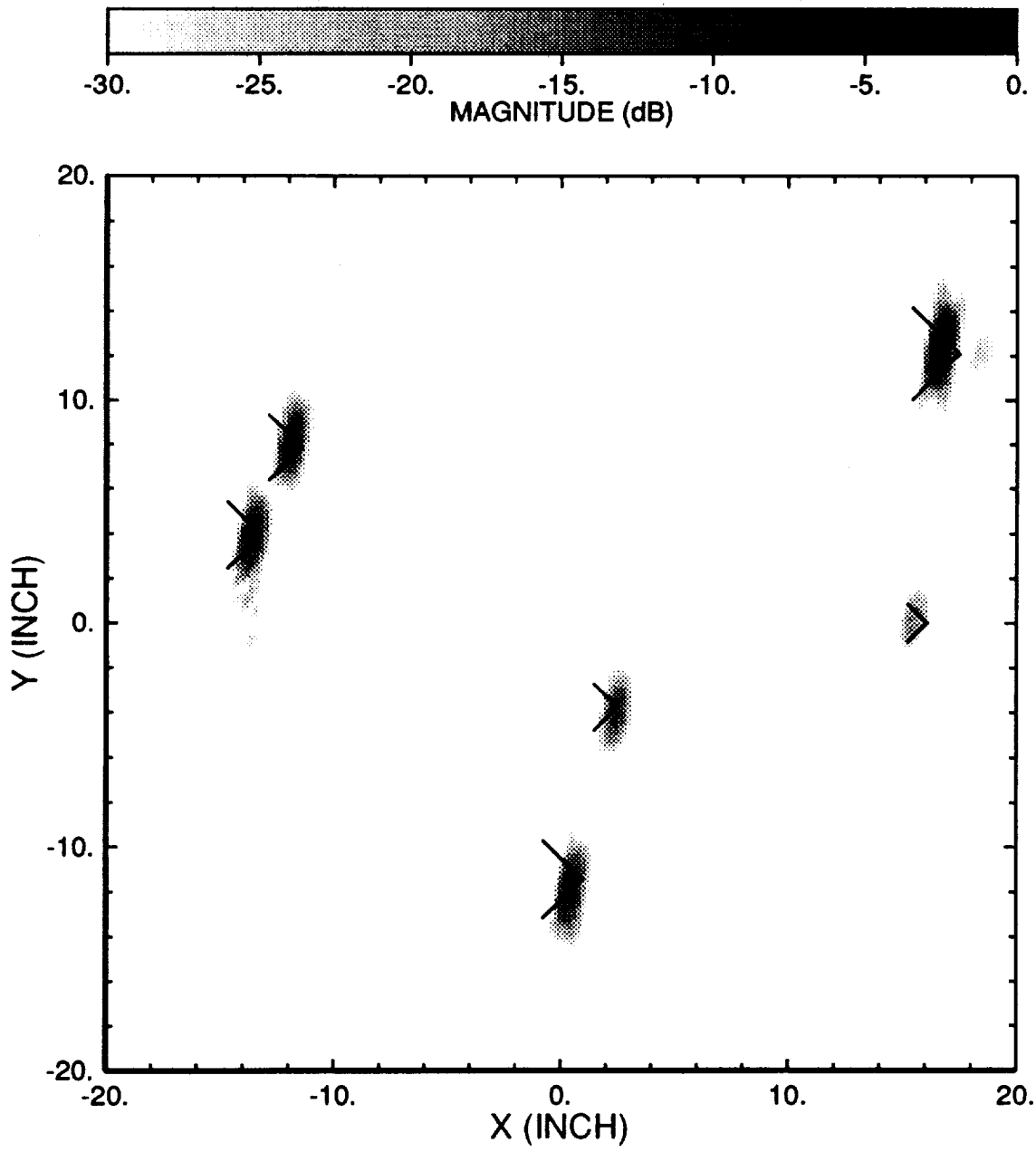

Figure 4.3: ISAR image of six corner reflectors for a central look angle of 170°.

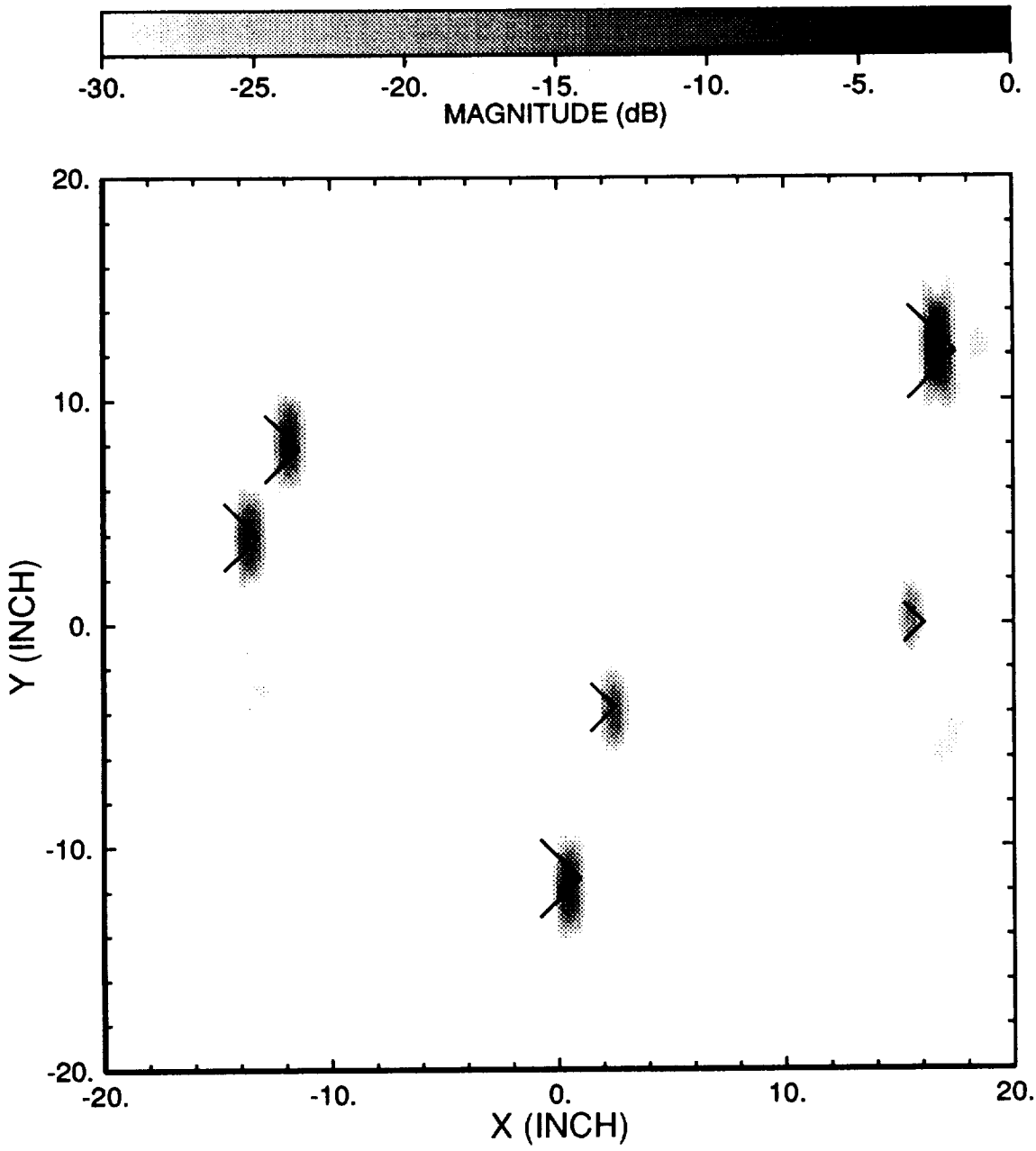

Figure 4.4: ISAR image of six corner reflectors for a central look angle of 180°.

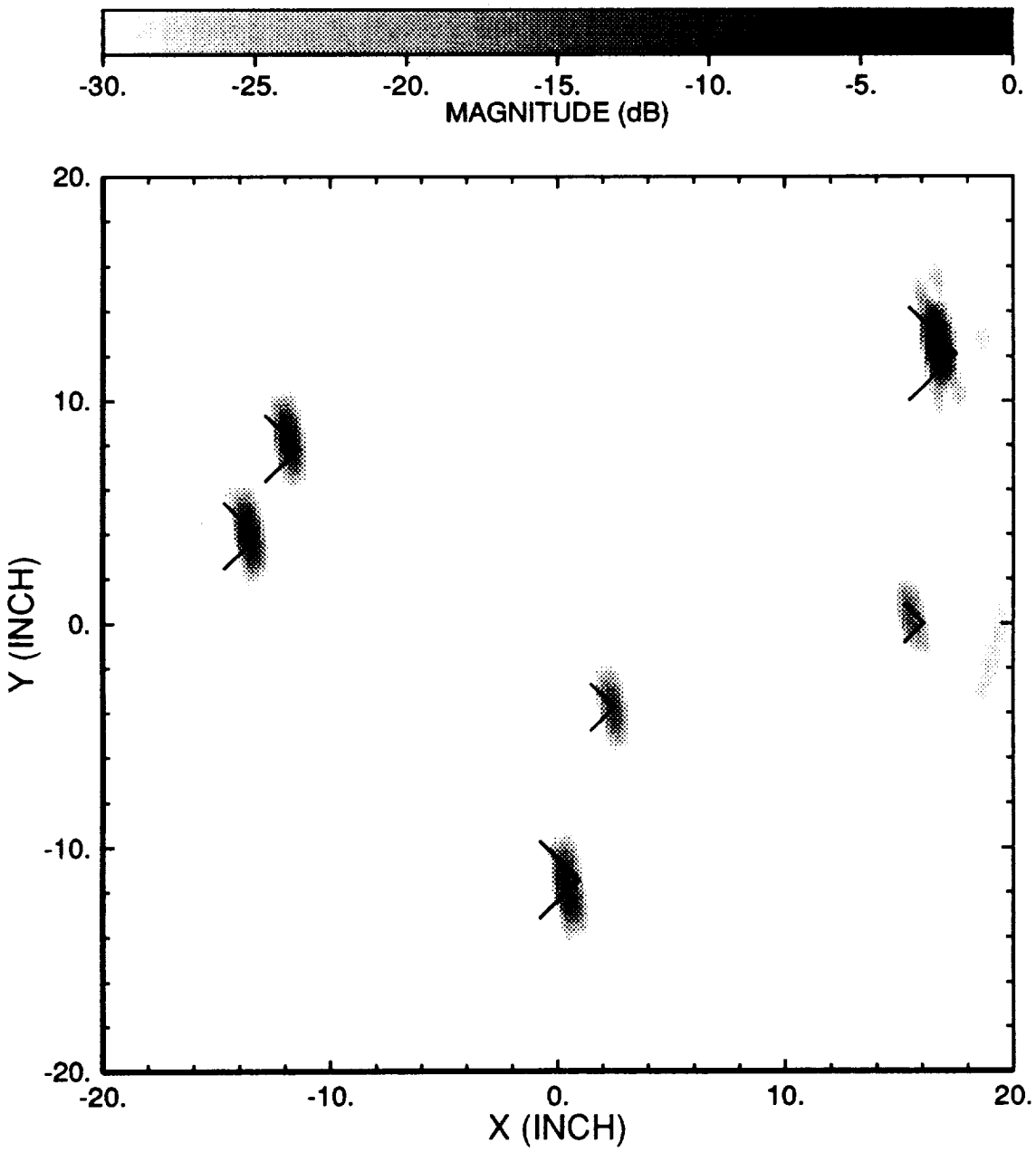

Figure 4.5: ISAR image of six corner reflectors for a central look angle of 190°.

images of the six corner reflectors for three different look angles. Note that:

- All the corner reflectors are correctly located.
- The energy of each corner reflector spreads out more in the cross range direction because the average bandwidth of $\tilde{f}_y$ is much smaller than that of $\tilde{f}_x$.

4.2 Compression and Reconstruction of Frequency Scan Data

To separate individual scattering centers in the image domain, a 6 inches down range by 4 inches cross range (i.e., about 1 ns by 0.67 ns) uniform gate is positioned at each scattering center to gate it out and shift it to the origin. According to the Fourier Slice Theorem, the projection of an ISAR image onto the down range axis is the impulse response along the central look angle. So one can take the projection of each extracted scattering center (i.e., add up the extracted subimage along the cross range direction), and then take the 1-D Fourier transform of the projection to get an individual scattering center's frequency response at the central look angle. Figures 4.6–4.7 show the individual frequency responses for each of the six corner reflectors thus obtained. Note that both the amplitude and phase responses are smooth.

Now there are six smooth frequency responses after separating out the six corner reflectors in the ISAR image. Since each frequency response is time-limited within 1 ns imposed by the down range gate width, the sampling theorem guarantees that one can sample the smooth frequency response at 1 GHz rate without loss of information. For a frequency bandwidth of 16 GHz, this means only 17 data points need to be recorded for each corner reflector's frequency response. If compared to the original frequency data array of 1601 points, the frequency scan data has thus been compressed by a factor of $\frac{1601}{6 \cdot 17} = 16$.

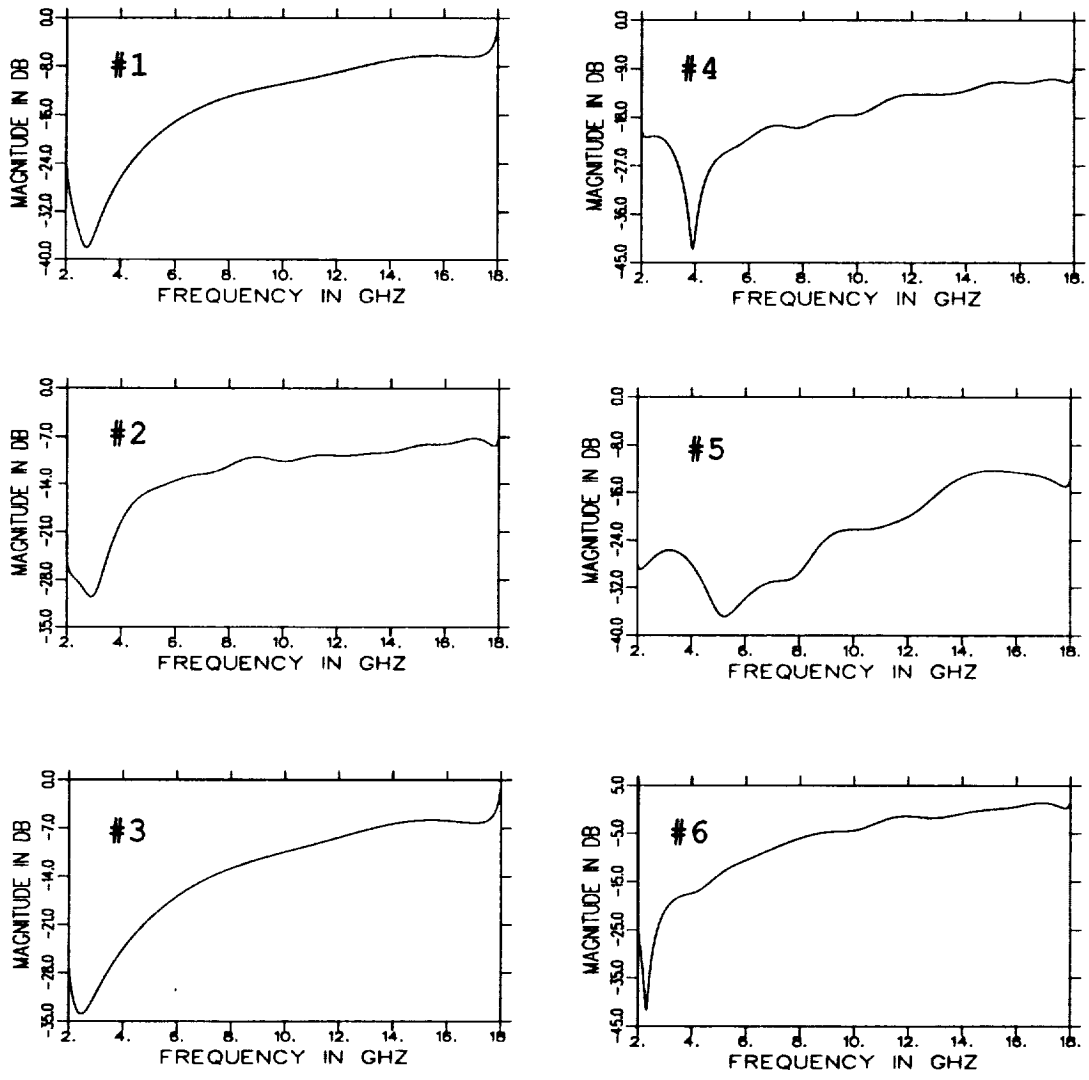

Figure 4.6: Individual amplitude responses for each corner reflector at 180°, obtained by 2-D gating.

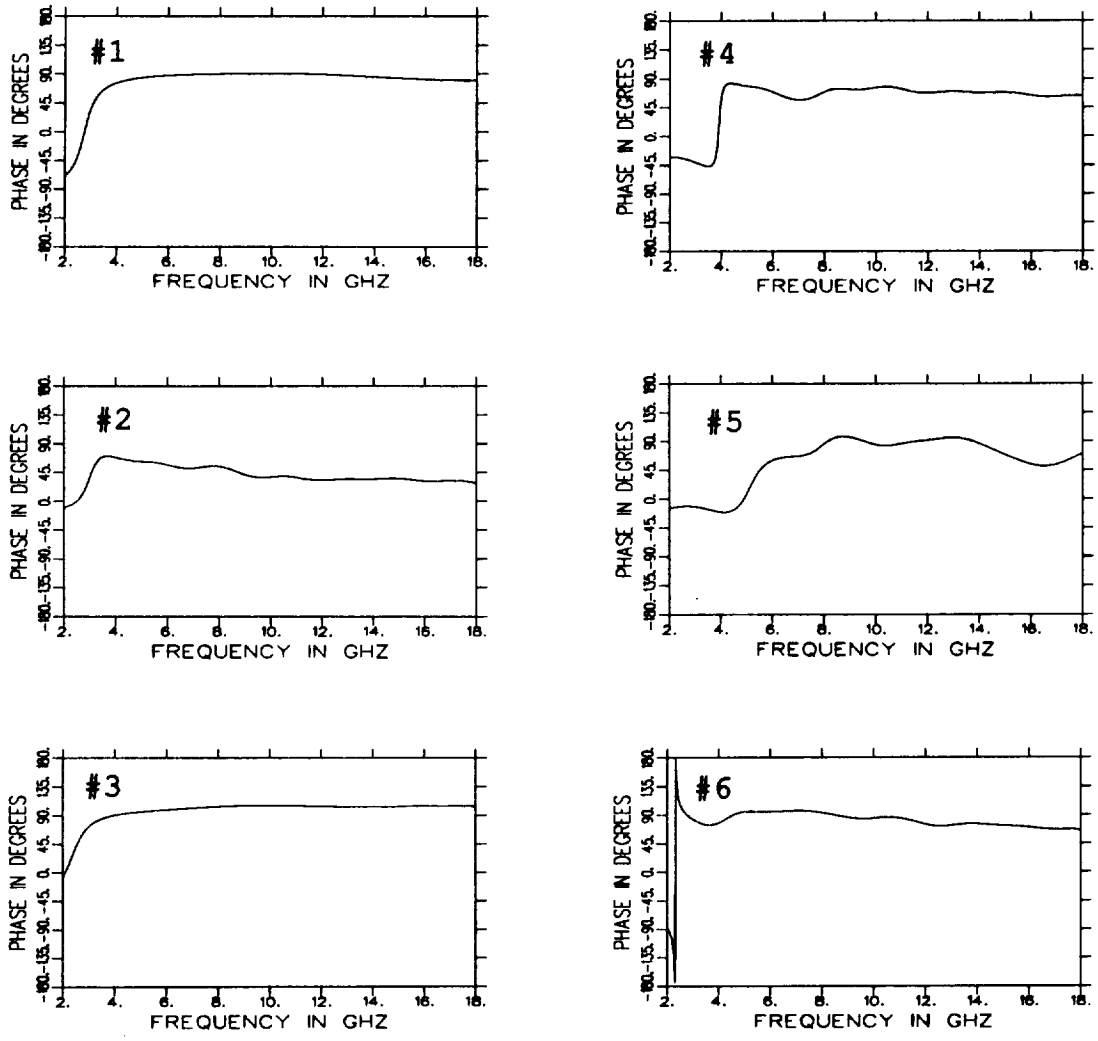

Figure 4.7: Individual phase responses for each corner reflector at 180°, obtained by 2-D gating.

The sampling theorem also provides how to reconstruct the smooth individual frequency response out of the 17 data points; namely, a sinc interpolation in the frequency domain. The frequency scan reconstruction is done in the following order:

1. Recover the six smooth frequency responses out of their own 17 sampled data points by the sinc interpolating function $\frac{\sin(\pi f)}{\pi f}$, with f in GHz.

2. Move the phase reference of each corner reflector back to its proper down range position $\tilde{t}_{x_i}$ by multiplying the term $e^{-j2\pi f \tilde{t}_{x_i}}$ to each frequency response.

3. Add up the six corner reflectors' frequency responses to reconstruct the original data.

Note that the criterion 1 ns down range gate width is based on the observation and calculation that for a frequency band of 2-18 GHz, the scattering center's impulse response is within 1 ns. But this criterion also limits this algorithm to further separating two scattering centers if they are as close as a ns. This problem may show up in a real-world target case and will be regarded as a grouping problem.

4.3 Compression and Reconstruction of Azimuth Scan Data

After the separation of individual corner reflectors, one would like to loosely sample the 2-D spectral response $U_i(f, \phi)$ of each corner reflector not only in the frequency scan but also in azimuth. For a small angular region, the sampling rate for a smooth azimuth response at any given frequency can be calculated by the time-limit imposed by the cross range gate width in the spatial domain. But since the frequency ranges from 2 GHz to 18 GHz, one must satisfy the sampling criterion for the highest frequency case. The gate width in cross range is 0.67 ns, which demands a sampling rate of 1.5 GHz along $\tilde{f}_y$. Note that $1.5 = \Delta\tilde{f}_y = f \cdot \sin(\Delta\phi) \approx f \cdot \Delta\phi$. For $f = 18$ GHz, $\Delta\phi$ is about 5°. So for an azimuth scan, one can sample the smooth

angle response of an individual scattering center every 5° based on the 4 inch cross range gate width. If compared to the original 0.25° data increment, this gives a compression factor of 20 in the angle domain.

Now suppose one has already got ISAR images at every 5°, extracted out individual corner reflectors in each ISAR image and obtained a reduced database. If this reduced database were in a rectangular grid, the ideal reconstruction procedure along the $\tilde{f}_y$ direction would still be a sinc interpolation. But sinc interpolation, which needs as many data points as possible to exactly recover the original response, is not proper for the polar-type angle reconstruction case because the time-limit in the cross range and the sampling rate in the angle domain relation does not hold if it is no longer a small angular region. Thus, one has to simplify the interpolation scheme in the angle domain. For the time being a linear interpolation is used. If linear interpolation is not working well, higher order interpolation schemes like a parabolic fit shall be considered.

There are two questions associated with angle reconstruction. The first is, given two reduced datasets; e.g., $\phi = 175°$ and $\phi = 180°$, can one recover the frequency response for some look angle in between, say, the one at $\phi = 177°$? The second is, for a fixed frequency, can one reconstruct the azimuth scan data between any recorded angles? In fact, the first case is just a special case of the second one, so here the study will concentrate on the second case.

Assume the scattering centers are stationary, that is, the positions detected in the $\phi = 175°$ ISAR image and $\phi = 180°$ ISAR image for the same scattering center are identical with respect to the fixed coordinate system (t_x, t_y). Then the propagation phase of each corner reflector at any look angle can be easily calculated. To reconstruct the azimuth response for a fixed frequency, one just needs to linearly interpolate a corner reflector's azimuth response out of the two datasets, put back the calculated propagation phase term, and sum up all six corner reflectors' contributions at each look angle between $\phi = 175°$ and $\phi = 180°$.

But in reality, the scattering centers are not necessarily stationary. For example, a corner reflector is not exactly a point scatterer, so the peak position of a corner reflector's spatial response changes slightly with look angle during the 5° azimuth scan. Besides, ISAR itself will introduce positional shifts depending on what kind of window one applies to the frequency and angle data and how large an angle span one uses to generate the ISAR image. Though these positional shifts are expected to be small, they cannot be neglected, especially in the higher frequency case because the error in the propagation phase term $e^{-j2\pi f \hat{t}_{x_i}}$ is proportional to frequency. For example, even with a positional shift of 0.1 inch (or 0.017 ns) in the down range, the phase error will still be 107° at 17 GHz.

To take this nonstationary case into account, consider the situation shown in Figure 4.8. In this figure, suppose the 175° ISAR image indicates that a scattering center is at point A and the 180° ISAR image shows that it has shifted to a nearby point B. It is reasonable to assume that for small look angle changes, the scattering center moves linearly from point A to point B. Thus, one can still calculate the propagation phase term for any look angle in between. However, this approach increases the complexity of the reconstruction process by the need to "match" the scattering centers in the two ISAR images; i.e., one has to compare the positions in the two images to decide which scattering center in dataset $\phi = 175°$ corresponds to the one in dataset $\phi = 180°$, for example.

Now assume a scattering center has a complex magnitude of A_1 and peak position (t_{x1}, t_{y1}) obtained from the $\phi = 175°$ ISAR image. The same scattering center has a complex magnitude A_2 and peak position (t_{x2}, t_{y2}) from the $\phi = 180°$ ISAR image. To estimate the azimuth response for a given frequency at, say, $\phi = 177°$, the linear interpolation scheme mentioned before will give the following results:

$$E_{i,177°} = (0.6A_1 + 0.4A_2)e^{-j2\pi f(0.6t_{d1}+0.4t_{d2})} \tag{4.1}$$

where t_{d1} and t_{d2} are the down range positions at $\phi = 177°$ calculated from the $\phi = 175°$ and $\phi = 180°$ data, respectively. Note that in the stationary case, $t_{d1} =$

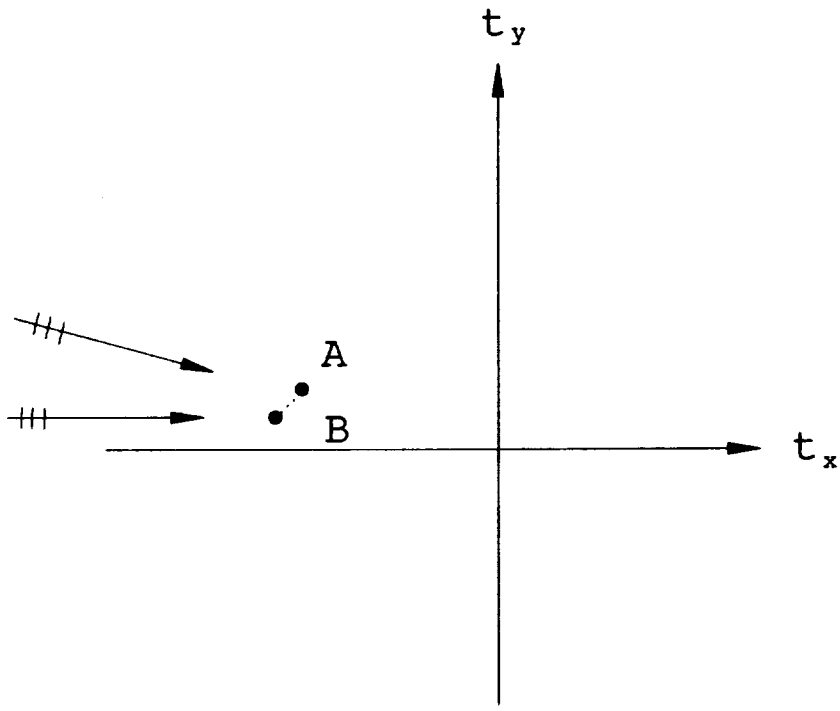

Figure 4.8: Positional shift of a scattering center between two look angles.

$t_{d2} = t_d$, and hence Equation (4.1) becomes

$$E_{i,177^\circ} = 0.6A_1 e^{-j2\pi f t_d} + 0.4A_2 e^{-j2\pi f t_d}. \tag{4.2}$$

As for the nonstationary case, the following approximation can be made for a small look angle changes (say, 5°):

$$t_d \equiv 0.6t_{d1} + 0.4t_{d2} \approx t_{d1} \approx t_{d2}.$$

Substituting the above approximate results into Equation (4.2), one obtains that

$$E_{i,177^\circ} \approx 0.6A_1 e^{-j2\pi f t_{d1}} + 0.4A_2 e^{-j2\pi f t_{d2}}. \tag{4.3}$$

Expression (4.3) is a good approximation of Equation (4.1) if the positional change of a scattering center between two 5° apart look angles is small; and it avoids the necessity to match scattering centers between the two look angles. But if the change is not small, Expression (4.3) indicates there will be two scattering centers in the down range instead of one, in which case the frequency response will begin to oscillate as shown in Chapter 2. This might be a potential problem of this approximation. However, one can always make the positional shifts smaller by reducing the azimuth sampling step. In the corner reflector case, Expression (4.3) seems to work well as will be shown next.

Figures 4.9 through 4.12 show the reconstructed frequency responses for the six corner reflectors at 176°, 177°, 178° and 179°, which are recovered from the 175° and 180° reduced datasets by Expression (4.3). Note that the reconstructed data is very close to the original one. Figures 4.13 through 4.16 show the reconstructed azimuth responses for the six corner reflectors at 4 (low frequency band), 10, 15.5 (medium frequency band) and 17 GHz (high frequency band). The errors are greater than those in the reconstructed frequency responses, because they are cumulated through the frequency reconstruction process. But the overall performance is very satisfactory.

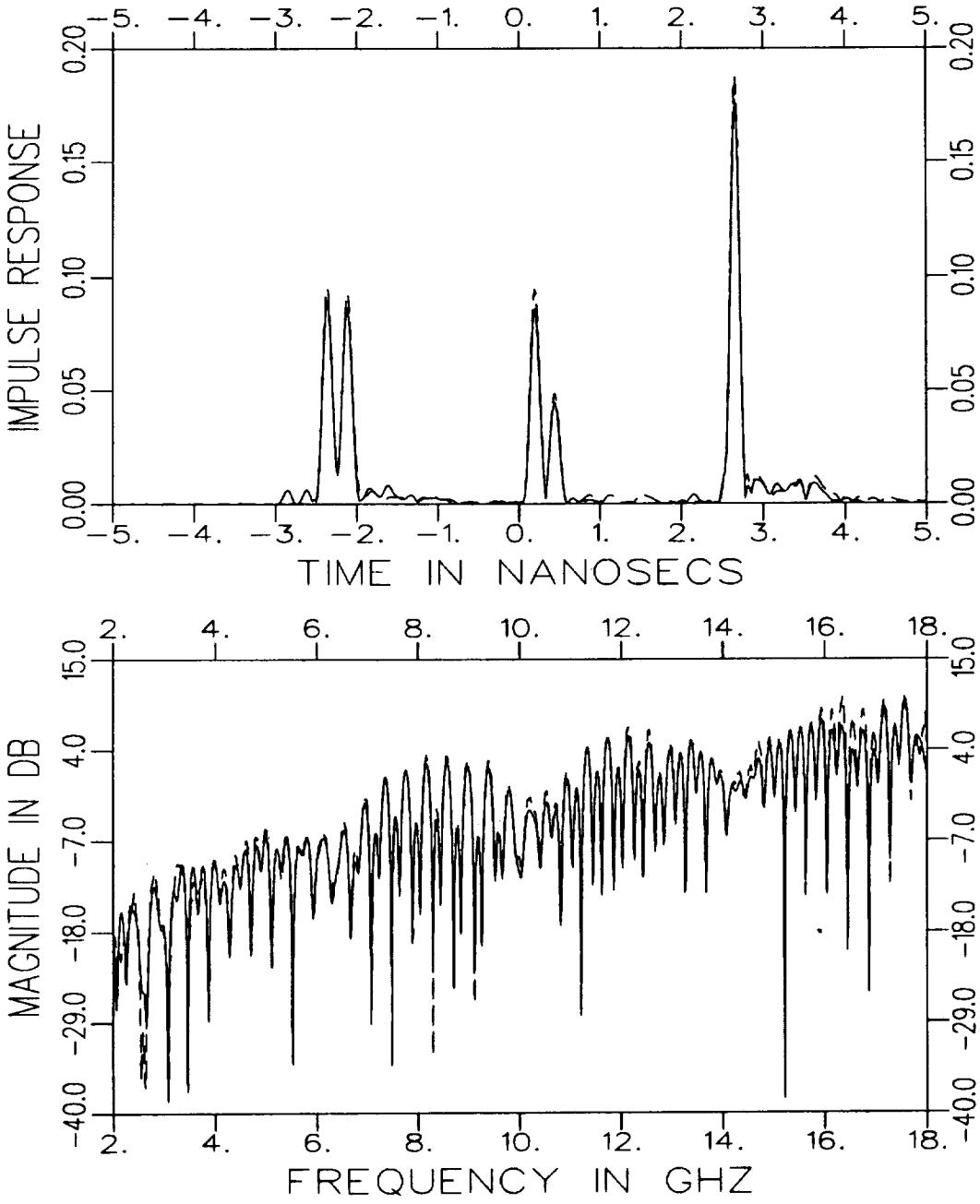

Figure 4.9: Comparison between the reconstructed (solid line) and original (dotted line) frequency responses at 176° for six corner reflectors, obtained by gating.

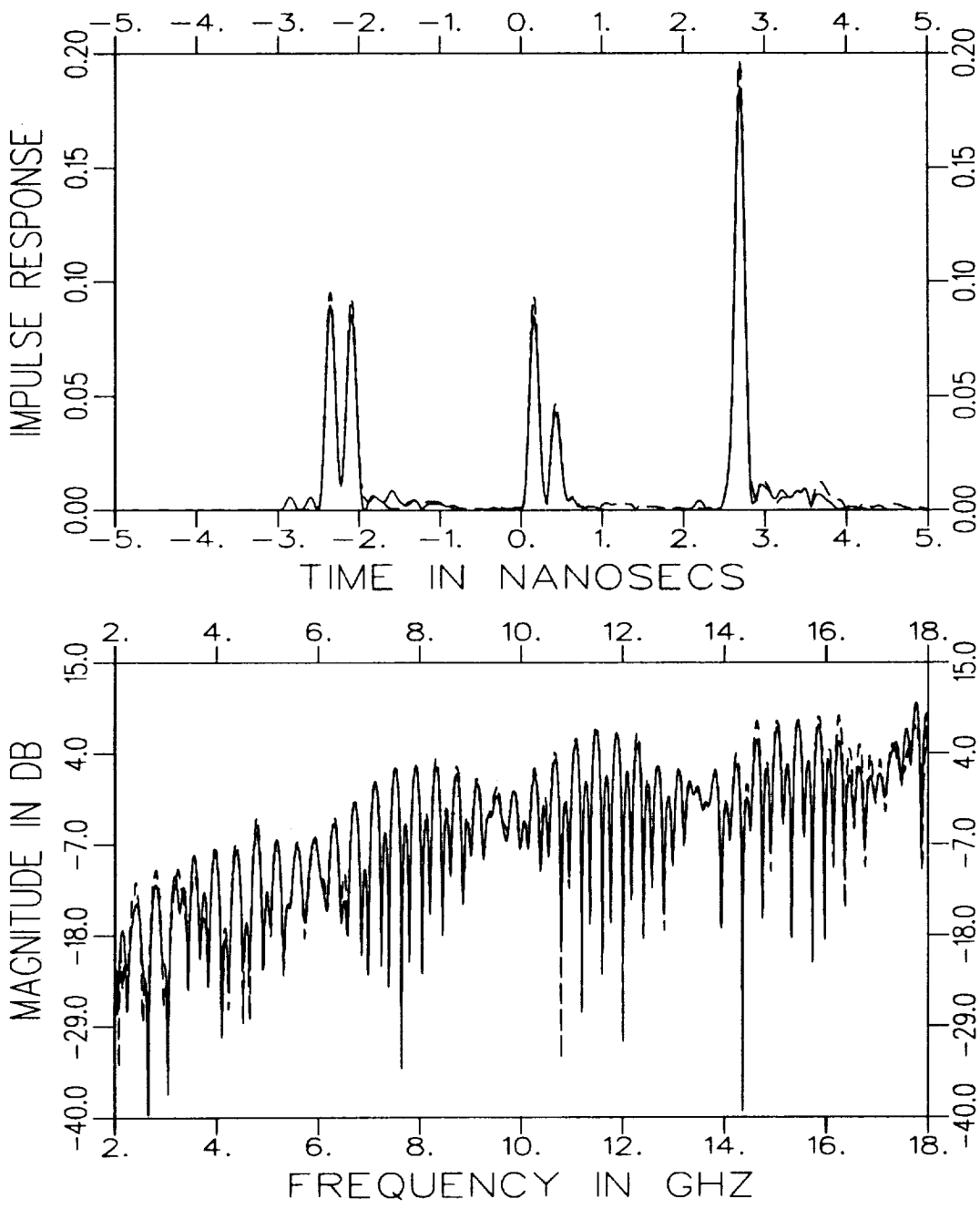

Figure 4.10: Comparison between the reconstructed (solid line) and original (dotted line) frequency responses at 177° for six corner reflectors, obtained by gating.

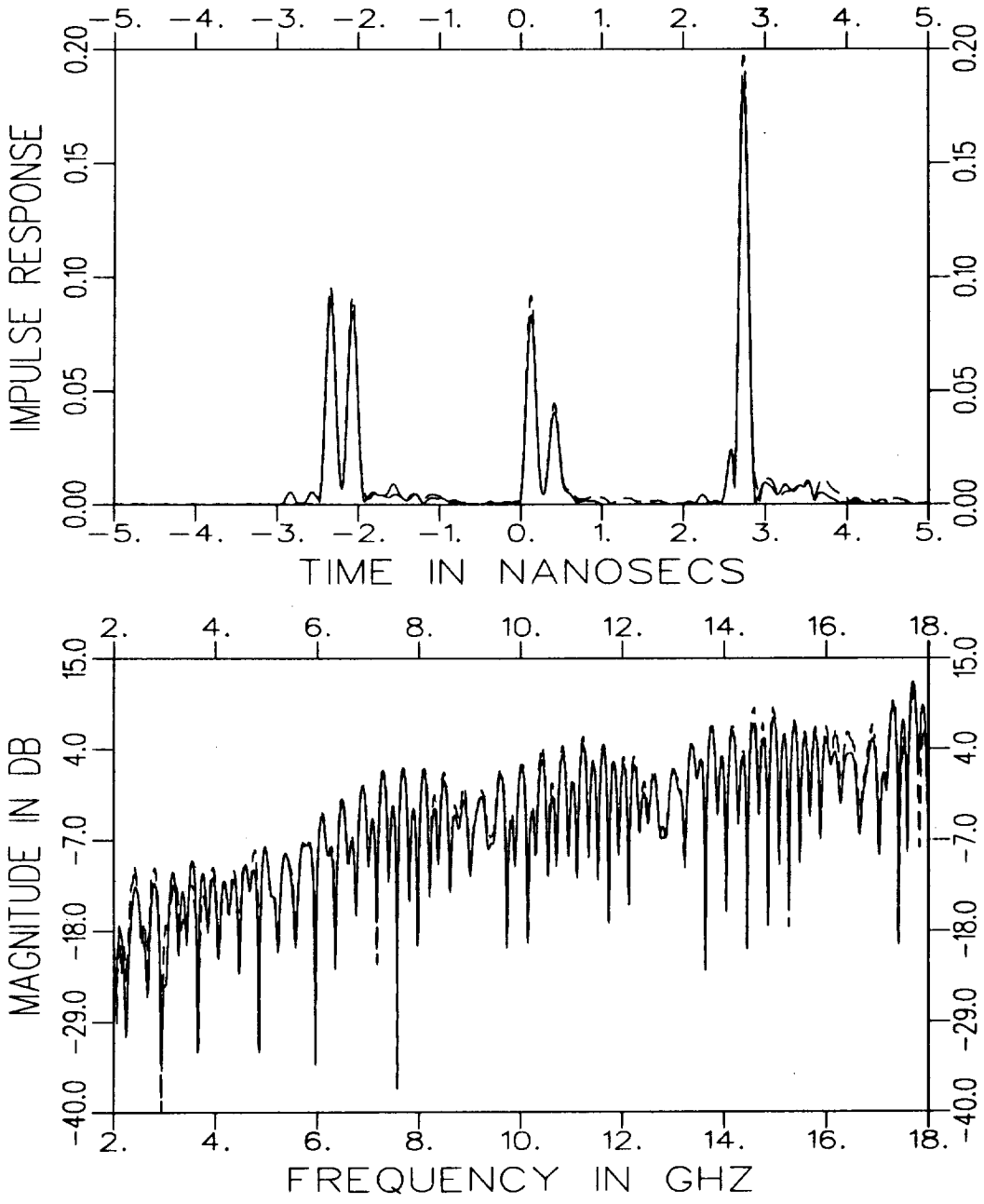

Figure 4.11: Comparison between the reconstructed (solid line) and original (dotted line) frequency responses at 178° for six corner reflectors, obtained by gating.

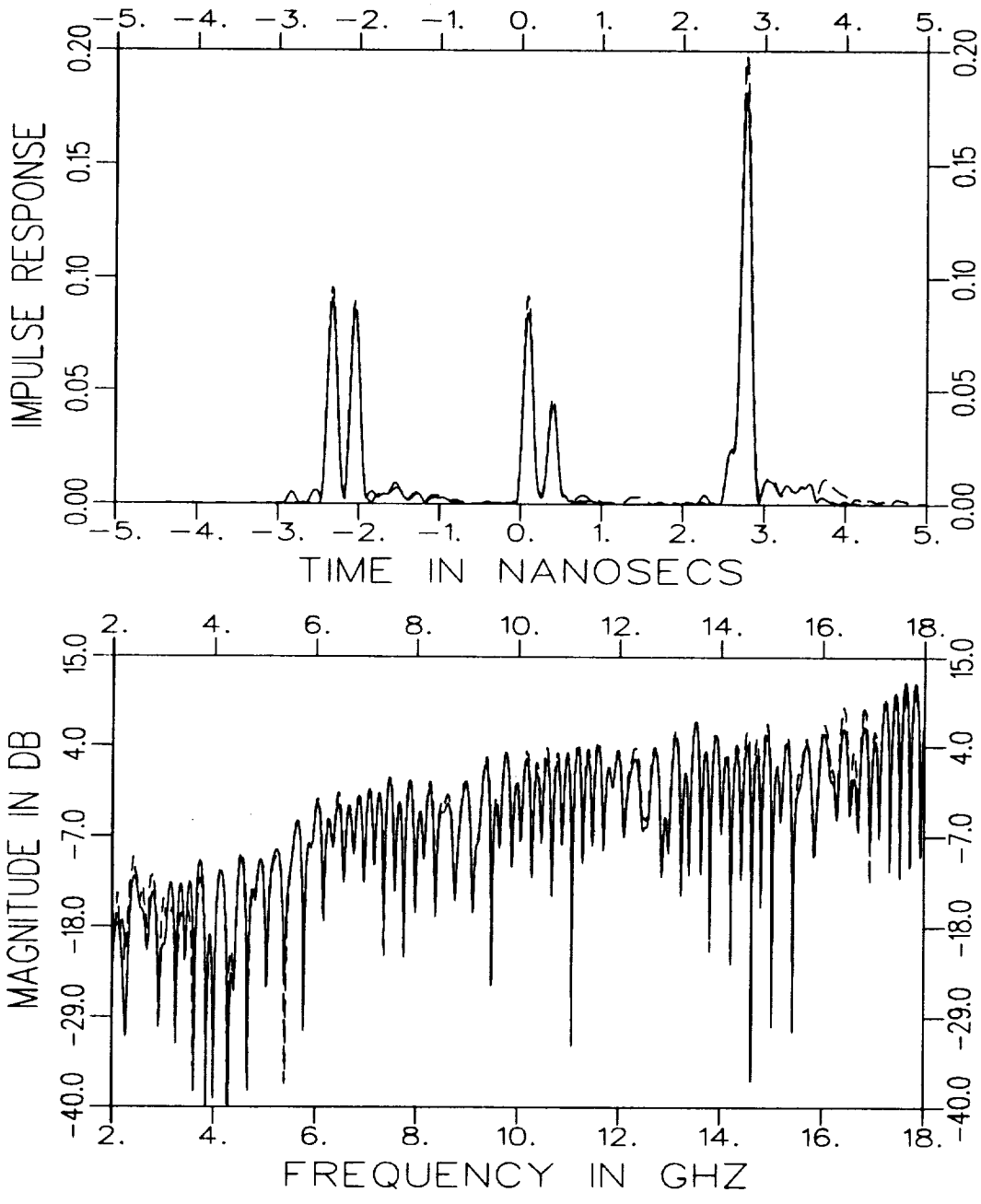

Figure 4.12: Comparison between the reconstructed (solid line) and original (dotted line) frequency responses at 179° for six corner reflectors, obtained by gating.

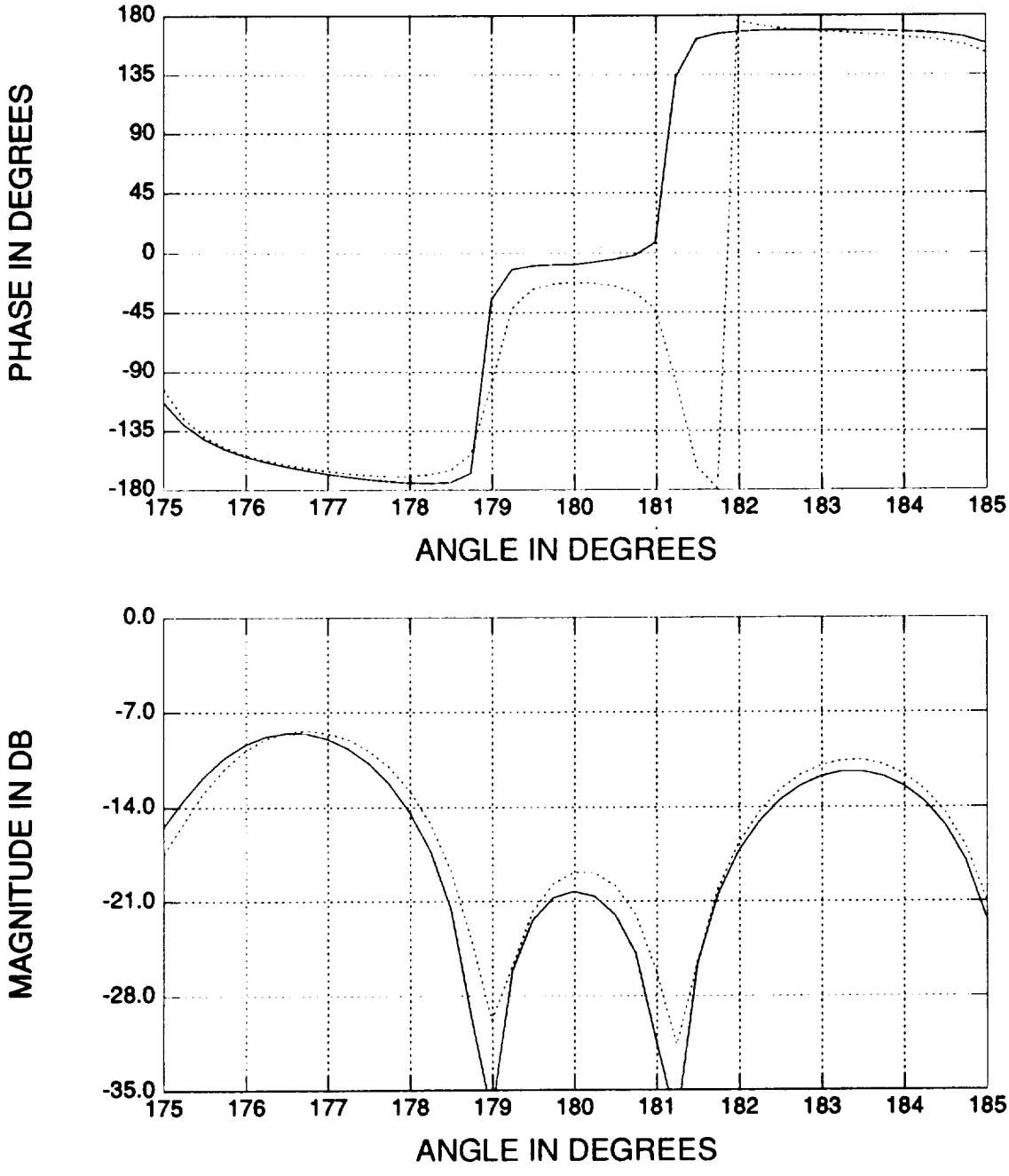

Figure 4.13: Comparison between the reconstructed (sold line) and original (dotted line) azimuth response at 4 GHz for six corner reflectors, obtained by gating.

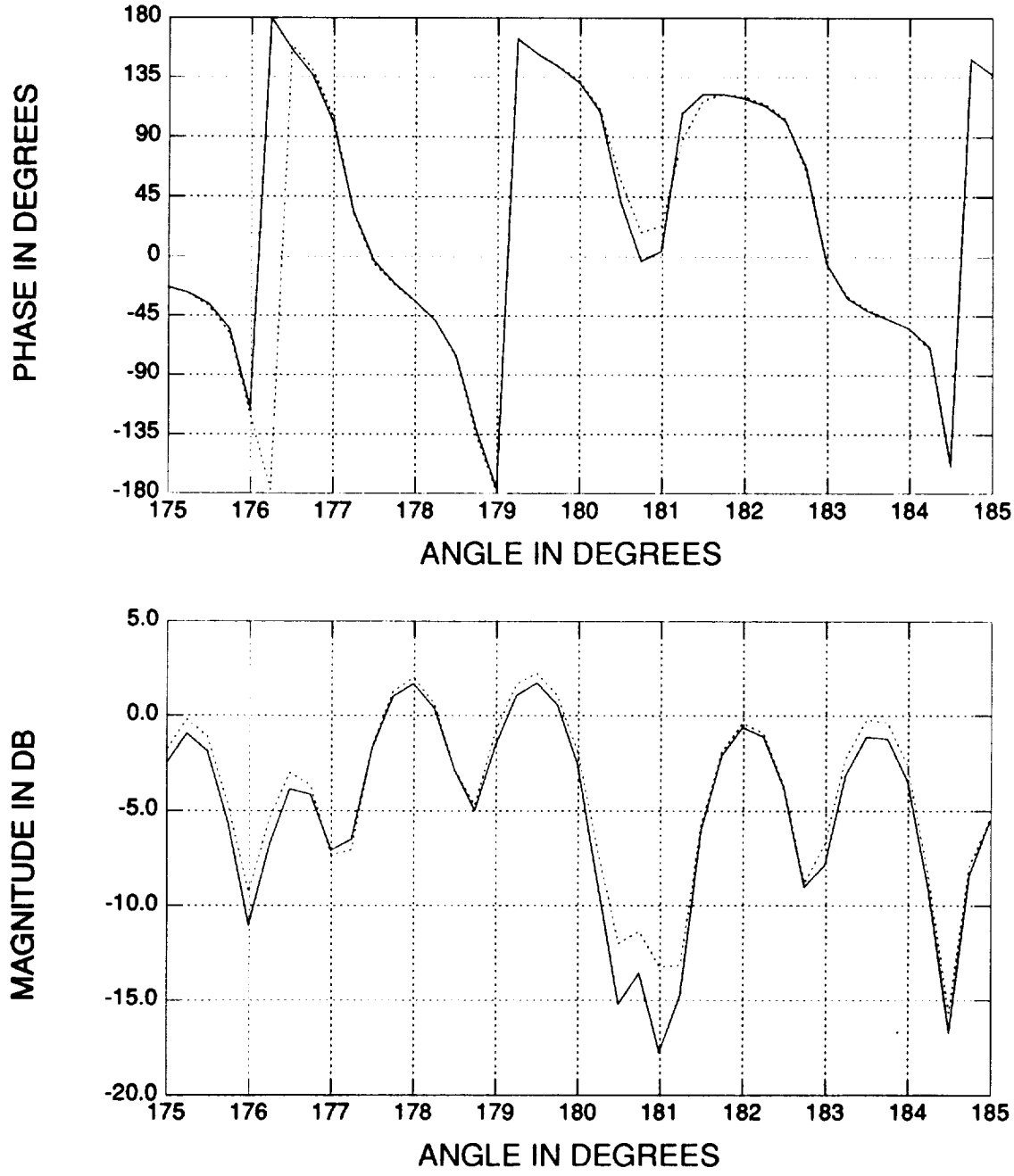

Figure 4.14: Comparison between the reconstructed (sold line) and original (dotted line) azimuth response at 10 GHz for six corner reflectors, obtained by gating.

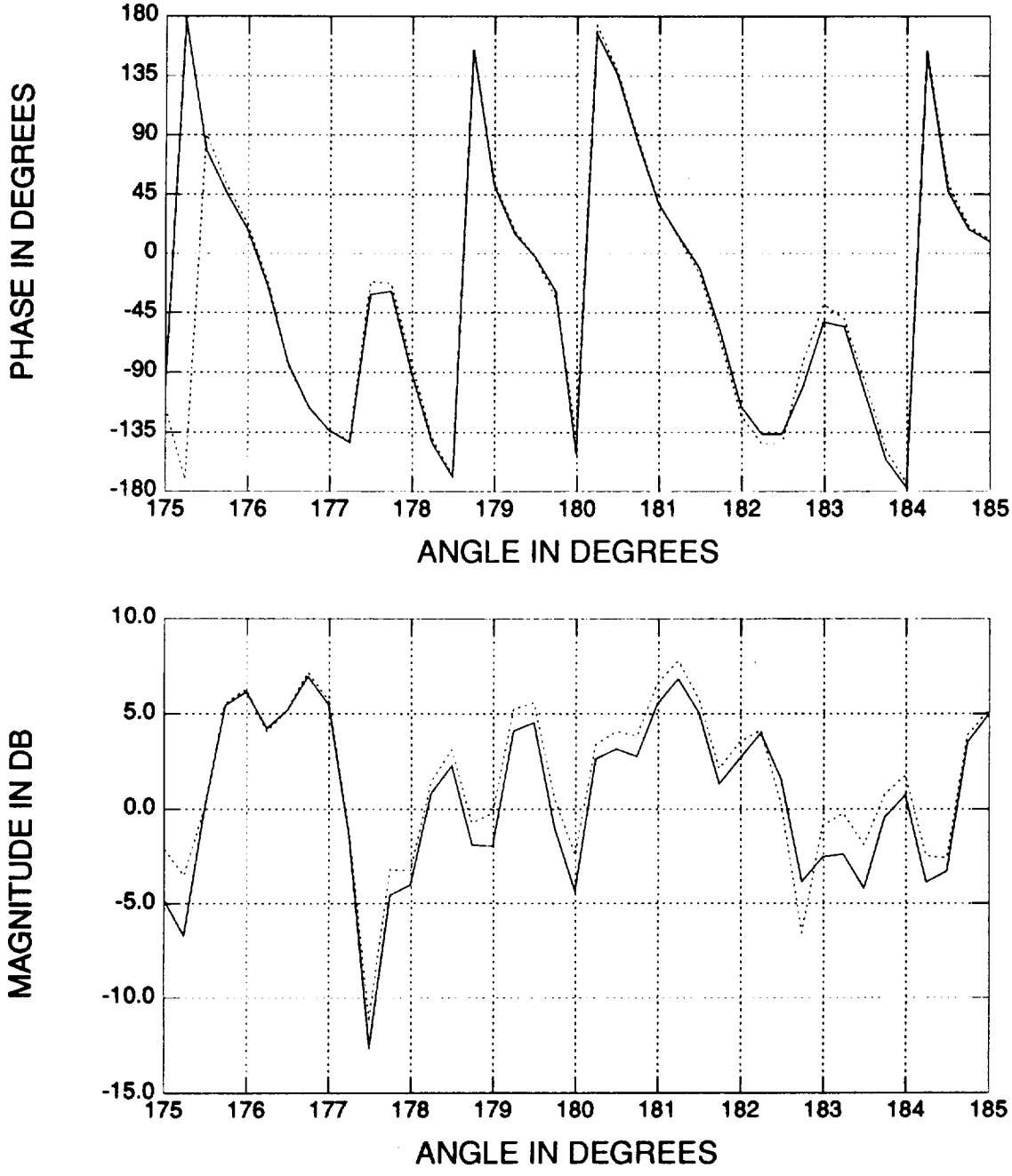

Figure 4.15: Comparison between the reconstructed (sold line) and original (dotted line) azimuth response at 15.5 GHz for six corner reflectors, obtained by gating.

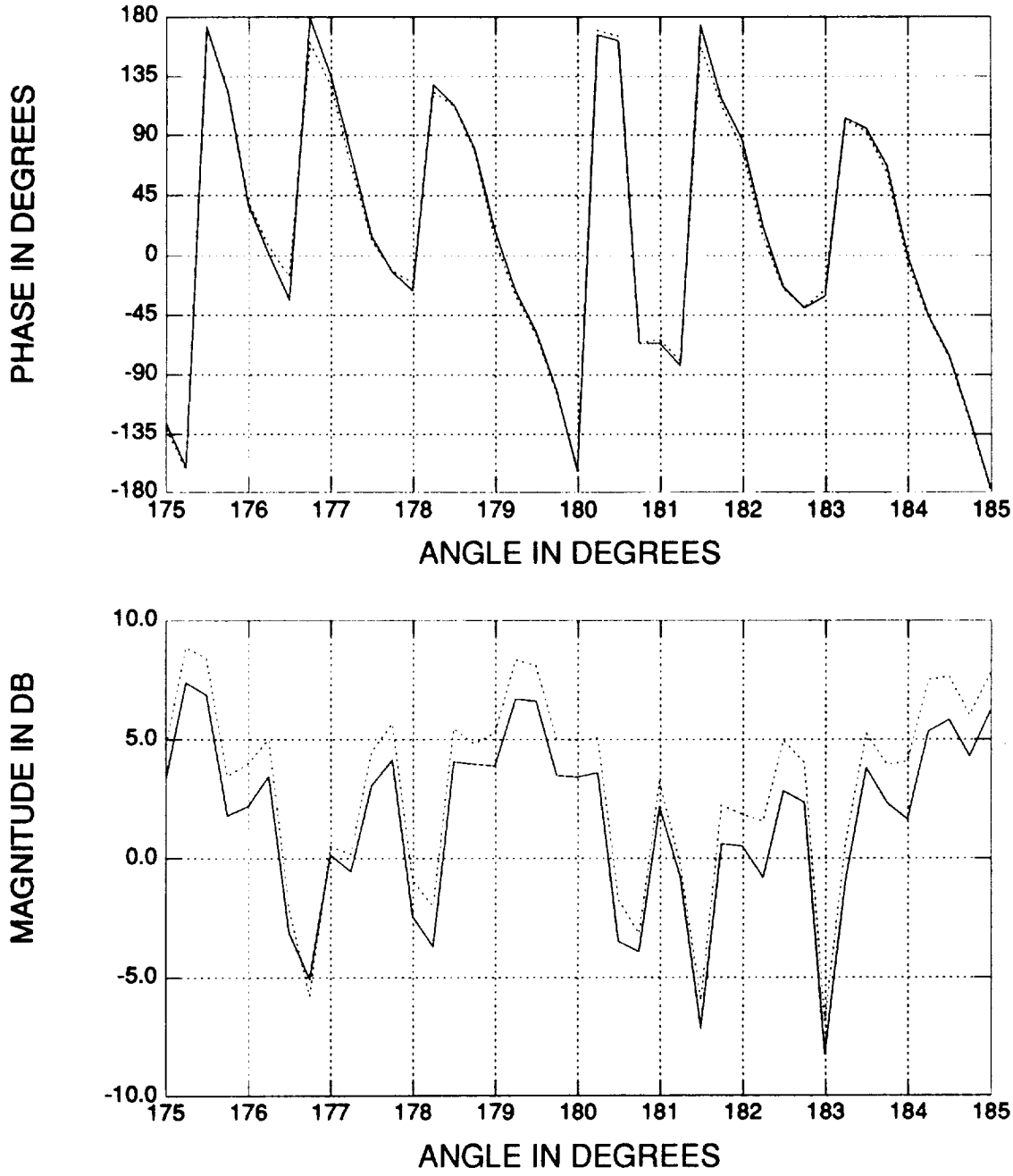

Figure 4.16: Comparison between the reconstructed (sold line) and original (dotted line) azimuth response at 17 GHz for six corner reflectors, obtained by gating.

4.4 2-D Smoothing versus Gating

As shown in Chapter 3, the separation of scattering mechanisms can also be executed in the 2-D spectral domain by a smoothing operation, which is the dual operation of gating in the image domain. According to the 2-D Fourier transform, a rectangular-based uniform gate in the image domain corresponds to a 2-D sinc function in the spectral domain. To avoid the infinite response of the 2-D sinc function, one can design other finite smoothing operators. Here the 2-D smoothing operator is designed specifically for the frequency data and the azimuth data. For the frequency data, a finite-duration cosine smoothing function is chosen. It is defined as

$$W(f) = \cos(80^\circ \cdot f) \tag{4.4}$$

where -1 GHz $\leq f \leq$ 1 GHz. Figure 4.17 compares the sinc and this cosine smoothing functions in both the frequency and time (down range) domains. The cosine function is chosen because in the time domain it has a corresponding gate width of 1 ns or so, yet has relatively low sidelobes.

As for the smoothing operator in the azimuth scan, since there is no direct relation between the cross range gate width and the angle variable, empirically one can use the average frequency (say, 10 GHz) as an estimate. Note that a 2 GHz cosine smoothing function along $\tilde{f}_x$ direction corresponds to a 1 ns down range gate width, so a 3 GHz cosine smoothing function along the $\tilde{f}_y$ direction corresponds to a 0.67 ns cross range gate width such that

$$3 = \tilde{f}_y \approx f \cdot \Delta\phi = 10 \cdot \Delta\phi \Rightarrow \Delta\phi = 17^\circ. \tag{4.5}$$

Therefore along the azimuth direction a $\pm 8.5^\circ$ cosine smoothing operator is used.

Note that a 2-D smoothing operator thus defined will not be a symmetric gate in the 2-D spatial domain. Furthermore, the corresponding gate widths, especially in cross range, cannot be explicitly computed. Also note that when one uses the 2-D smoothing operator on a finite spectral data region, the border area will not

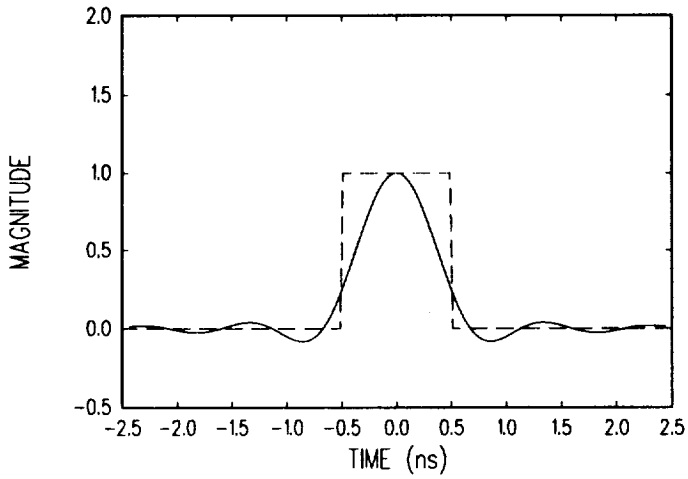

a) time response

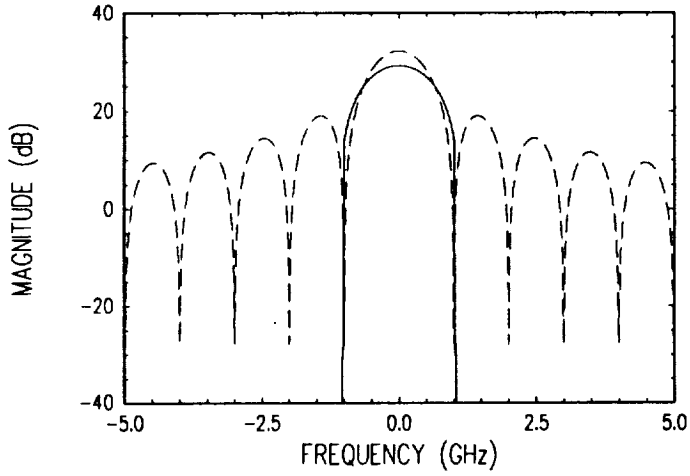

b) frequency response

Figure 4.17: Comparison between the sinc (dash line) and cosine (solid line) smoothing functions.

have enough data to be smoothed. One simple solution is to mirror-reflect the border area data, which is employed in this report. Better solutions involve linear prediction and spectral estimation methods which are beyond the discussion here. Moreover, *a priori* knowledge of the positions of scattering centers is required before smoothing.

The 2-D smoothing algorithm can be summarized as follows:

1. Estimate the peak locations $(\tilde{t}_{x_i}, \tilde{t}_{y_i})$ of all the scattering centers in the ISAR image.

2. Move the i-th scattering center to the origin by multiplying the term $e^{j2\pi f[\tilde{t}_{x_i}\cos(\phi-\phi_0)+\tilde{t}_{y_i}\sin(\phi-\phi_0)]}$ to the 2-D spectral data.

3. Apply the smoothing operator to smooth the spectral domain data in the frequency and angle scans, respectively.

4. Subtract the smoothed data from the pre-smoothed data.

5. Move the phase center back by multiplying the complex conjugate term of the one in step 2.

6. Continue from step 2 for the next scattering center.

Note that for a scattering center shifted to the origin, its 2-D spectral response should be smooth, so step 3 can be simplified by smoothing only a few selected data points instead of every data point, and then using a interpolation routine to generate all the other smoothed results in between. In this study, the spectral data is smoothed every 1 GHz and 1°. By doing so, one can significantly reduce the computations needed to perform the 2-D smoothing operation.

Also note that in step 2, it is recommended that one should perform the smoothing operation of the scattering centers in a magnitude order since the larger scattering centers have much stronger contribution than smaller ones. It is only reasonable to subtract out the larger one first especially when two or more scattering centers are close to each other.

Figures 4.18 and 4.19 show the 2-D smoothing results for the six corner reflectors. Comparing these to Figures 4.6 and 4.7, one should notice that the smoothing results are very similar to the gating ones. After the smoothing and extraction of the individual scattering centers, the reconstruction process remains the same.

Overall, the data compression and reconstruction algorithm works well for the six corner reflectors case considering the huge database reduction it provides.

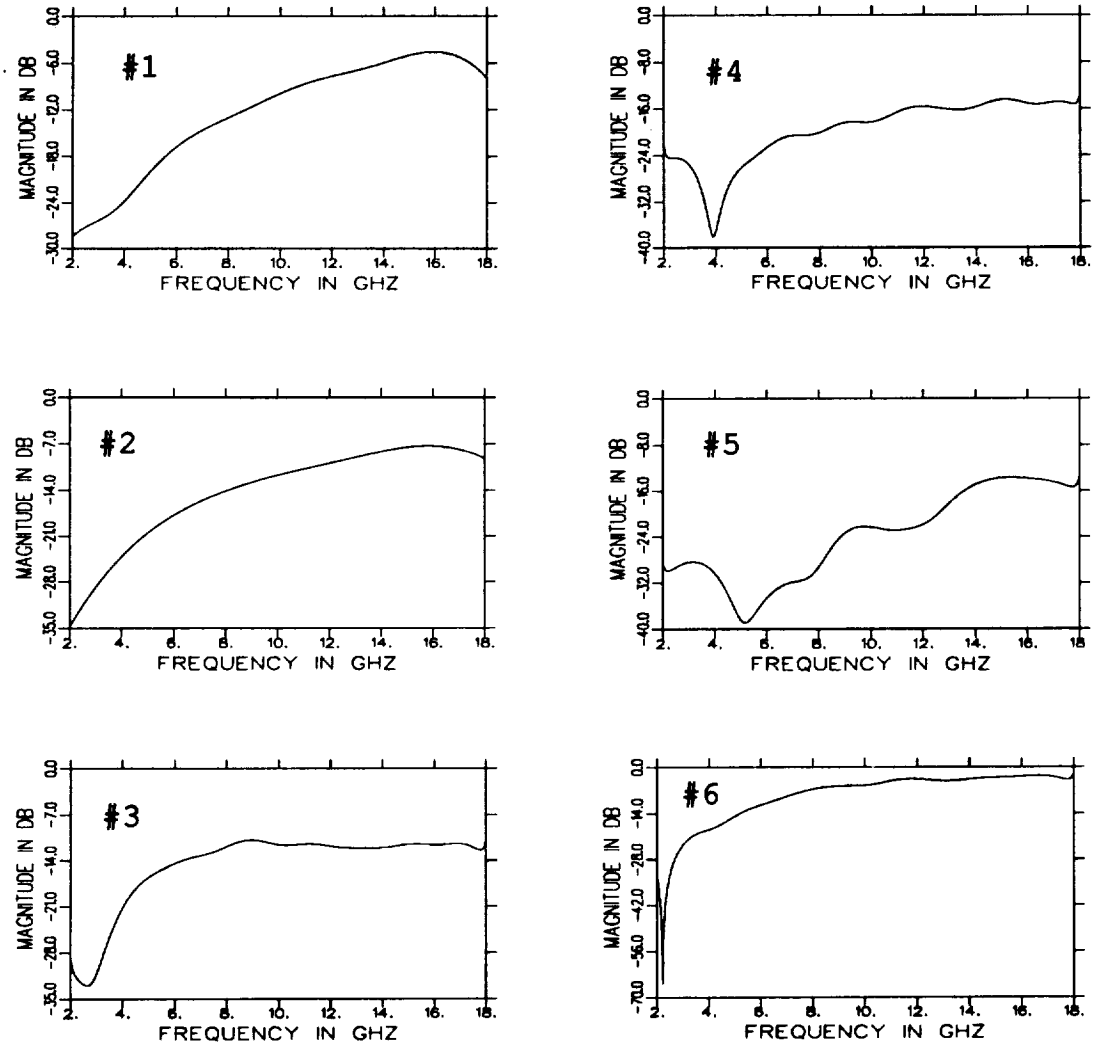

Figure 4.18: Individual amplitude responses for each corner reflector at 180°, obtained by 2-D smoothing.

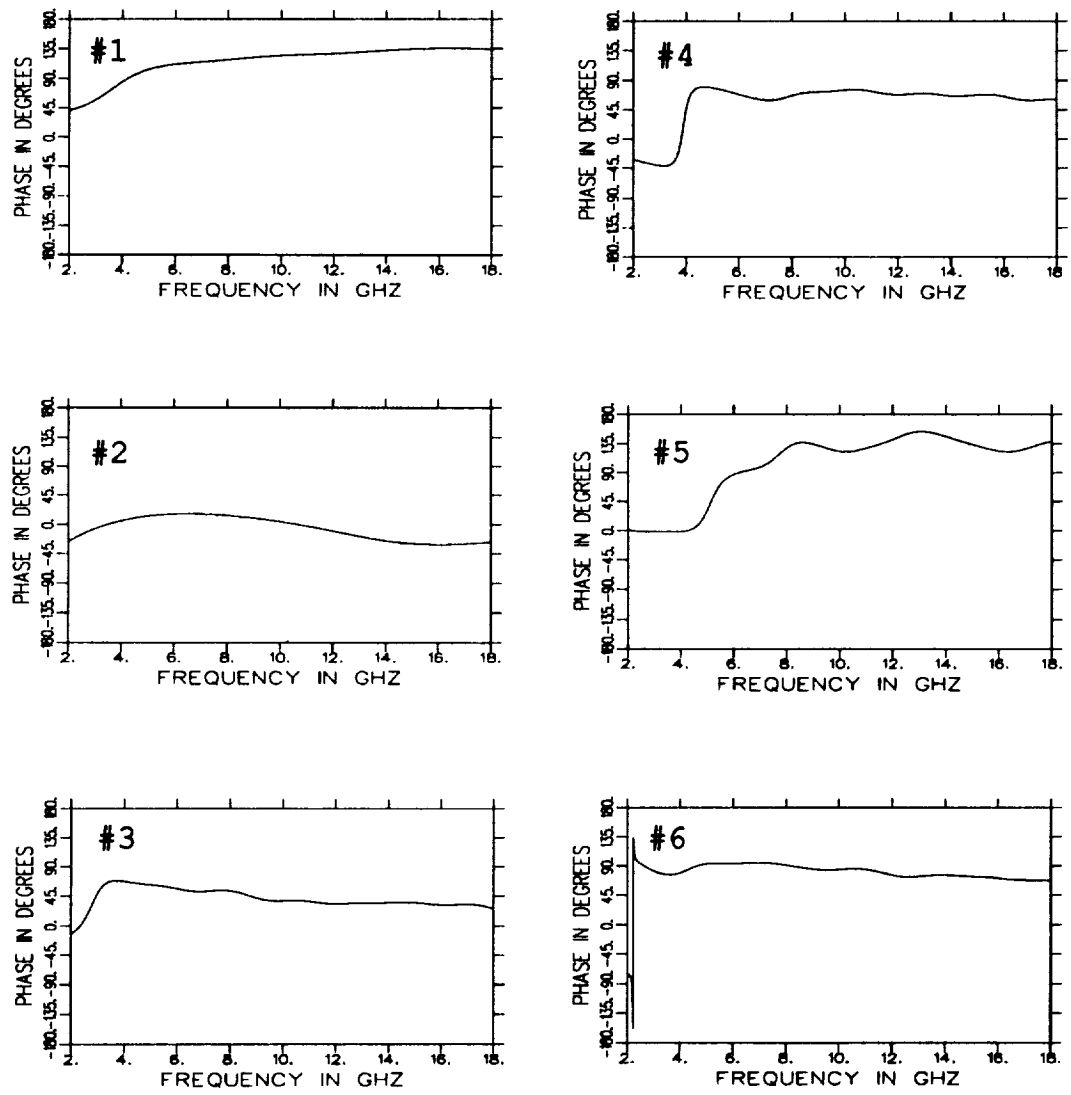

Figure 4.19: Individual phase responses for each corner reflector at 180°, obtained by 2-D smoothing.

Chapter 5

Data Compression and Reconstruction for a Complicated Target: The F-117 Fighter Model Case

Real-world targets are much more complicated than just a few corner reflectors. One has no clear idea where the scattering centers are and hence will find it difficult to set a threshold to define a scattering center. In addition, the magnitudes and number of scattering centers may vary dramatically from one look angle to the next, and these scattering centers may cluster together depending on the target's shape. In this chapter, an F-117 fighter model is used to test the data compression and reconstruction algorithm. It turns out that this algorithm works well for this fighter model in most cases. Even for a special case, such as the straight edge scattering from the plane wings, one can still manage to represent the edge by several "pseudo" scattering centers and obtain very good results. This special case will be shown in Section 5.4.

5.1 Setup for the F-117 Fighter Model Measurement

Figure 5.1 shows the physical scale of the F-117 fighter model used in this report. The model is made of aluminum sheets. It is about $5\frac{1}{2}$ feet long and 4 feet wide. The front tip to the rotation center is 35 inches; i.e., this target falls within a circular zone with a diameter of 6 feet, or 12 ns. When the front tip of the plane is aligning toward the radar direction, it is called the reference position, and this reference angle is defined as $\phi = 180°$.

The frequency response of the F-117 model was measured from 2 GHz to 18 GHz at an increment of 10 MHz. Since the target size is less than 12 ns, which is well within the aliasing period of 100 ns, no aliasing will occur in the down range direction. The azimuth scan was measured from $\phi = 90°$ to $\phi = 270°$ at a step of 0.1°. This azimuth increment gives an aliasing period of 32 ns at the highest frequency (18 GHz), which is also oversampled.

The ISAR image around a certain look angle is formed by a $\pm 10°$ angle span. Kaiser-Bessel window is used on both the frequency and azimuth data. In an ISAR image, since there is no absolute criterion to define a scattering center, a pulse whose peak value is the local maximum of the surrounding 1 inch radial area and is larger than -20 dB of the absolute maximum peak value is chosen to be a qualified scattering center. Figures 5.2 through 5.6 show the ISAR images of the F-117 model at $\phi = 115°$, 170°, 180°, 190° and 245°. Note that around the reference angle, the scattering centers are accurately located at the front tip, wing ends, tail and the pedestal mount. Also note that when the target rotates to $\phi = 115°$ or $\phi = 245°$, the incident wave is normal to the wing leading edge, and the broadside effect dominates. The scattering in these two angles definitely cannot be classified as a point scattering case, and hence it will be discussed separately later.

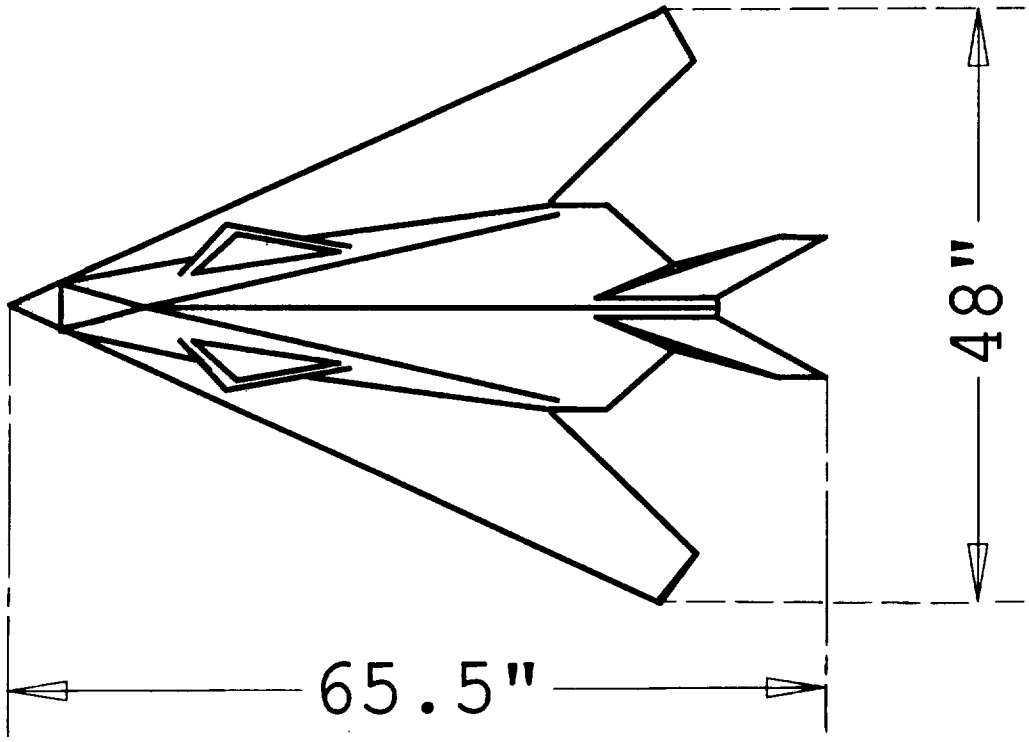

Figure 5.1: The F-117 fighter model.

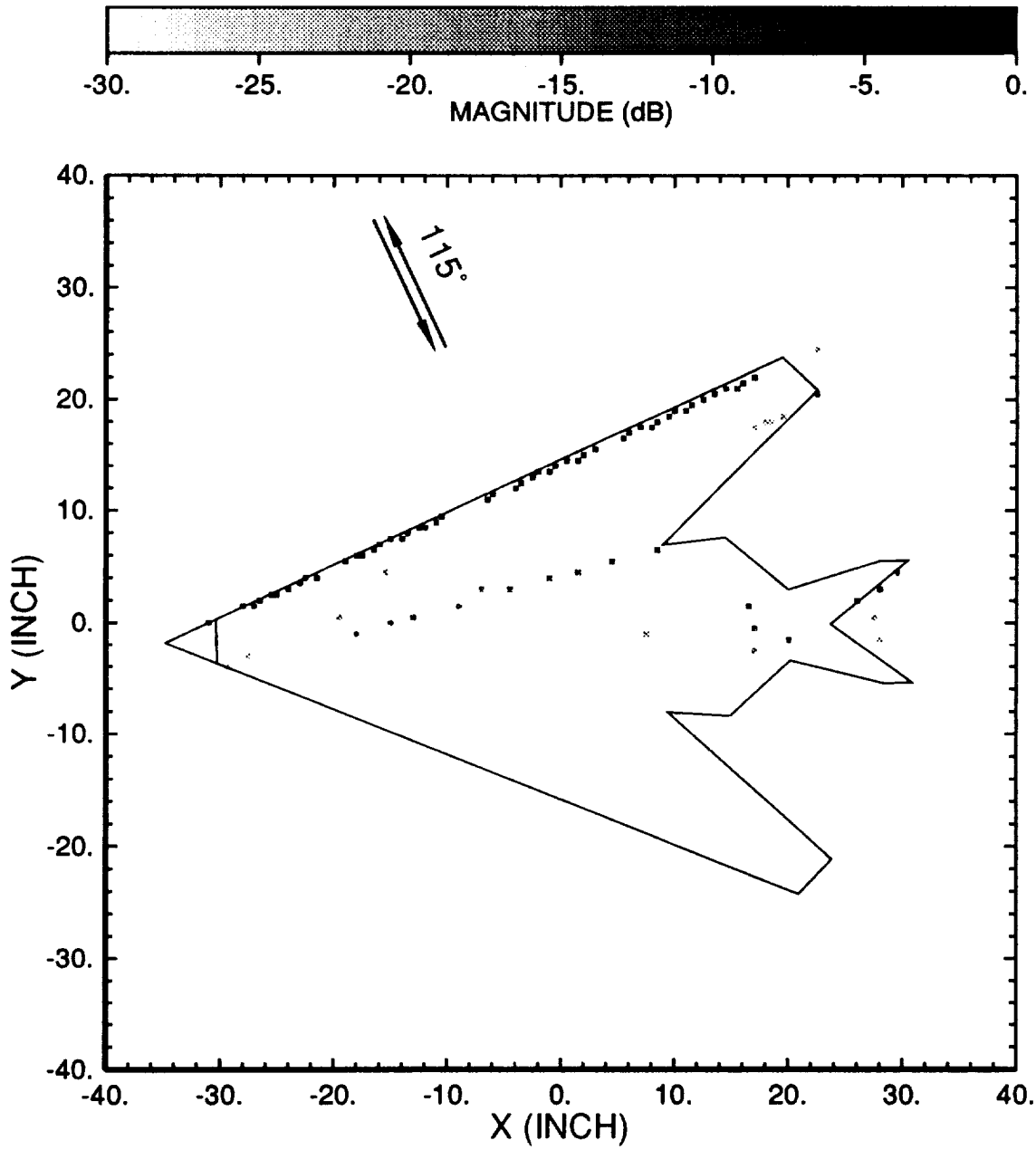

Figure 5.2: Peak positions in the F-117 fighter model ISAR at 115°.

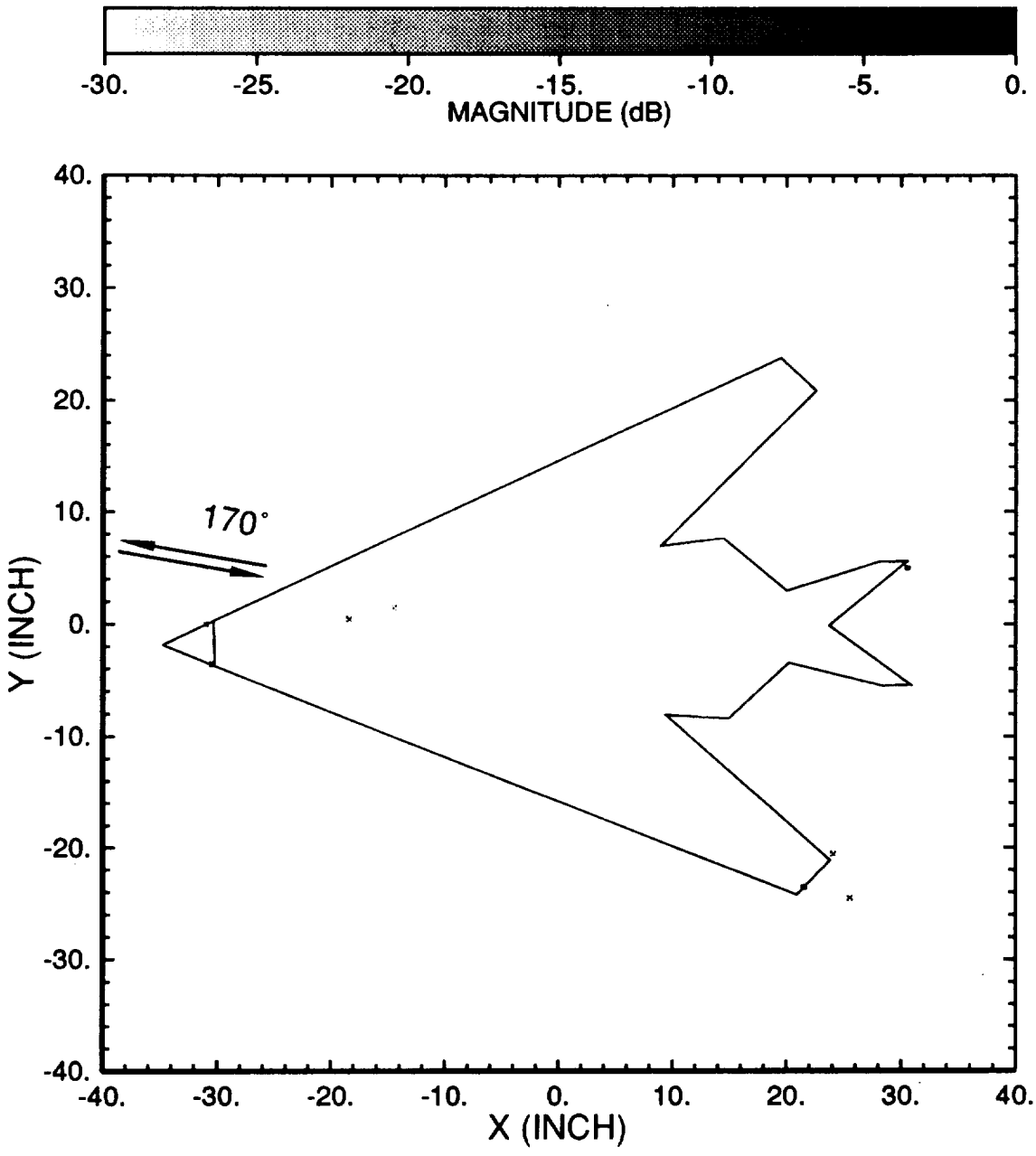

Figure 5.3: Peak positions in the F-117 fighter model ISAR at 170°.

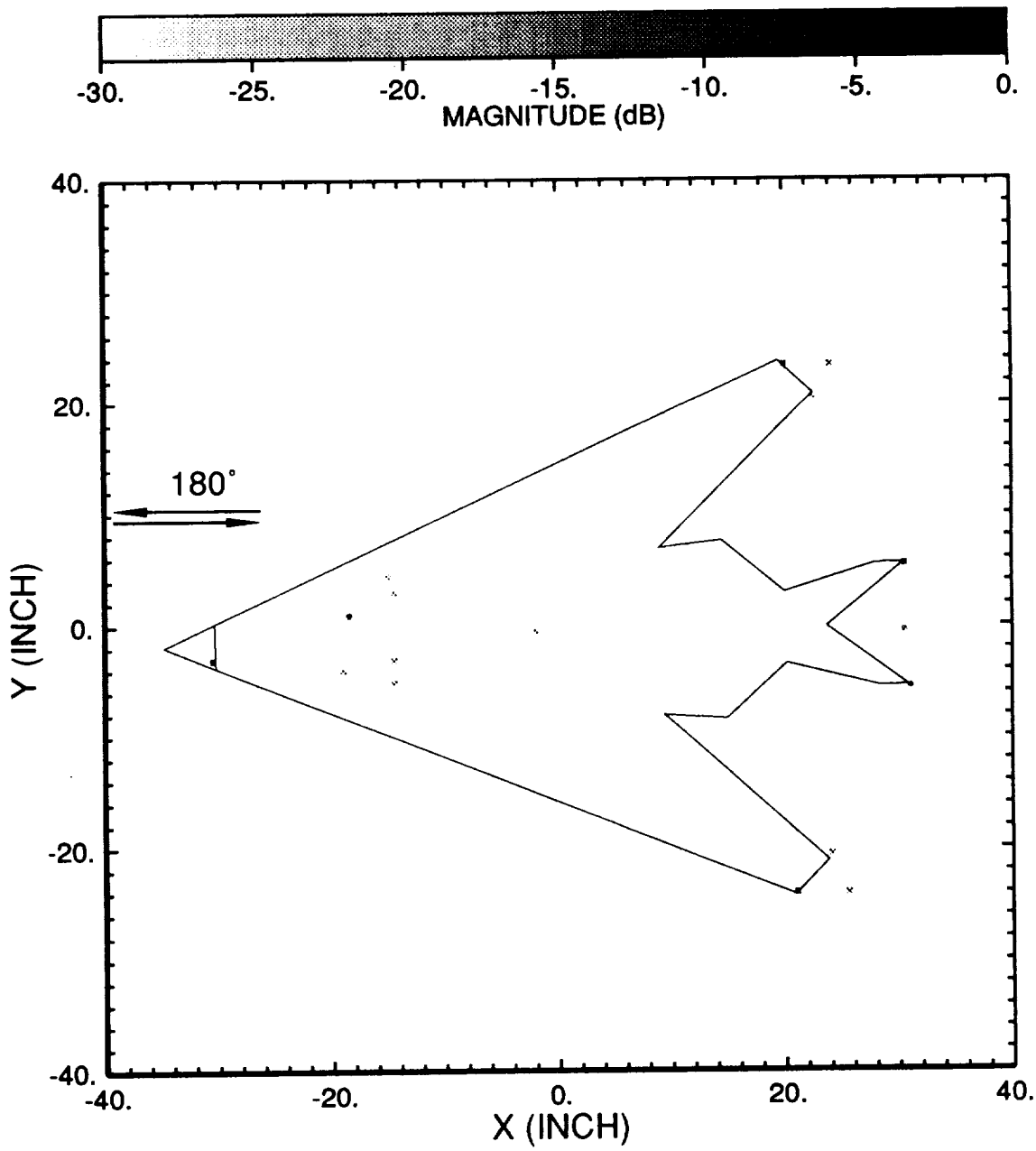

Figure 5.4: Peak positions in the F-117 fighter model ISAR at 180°.

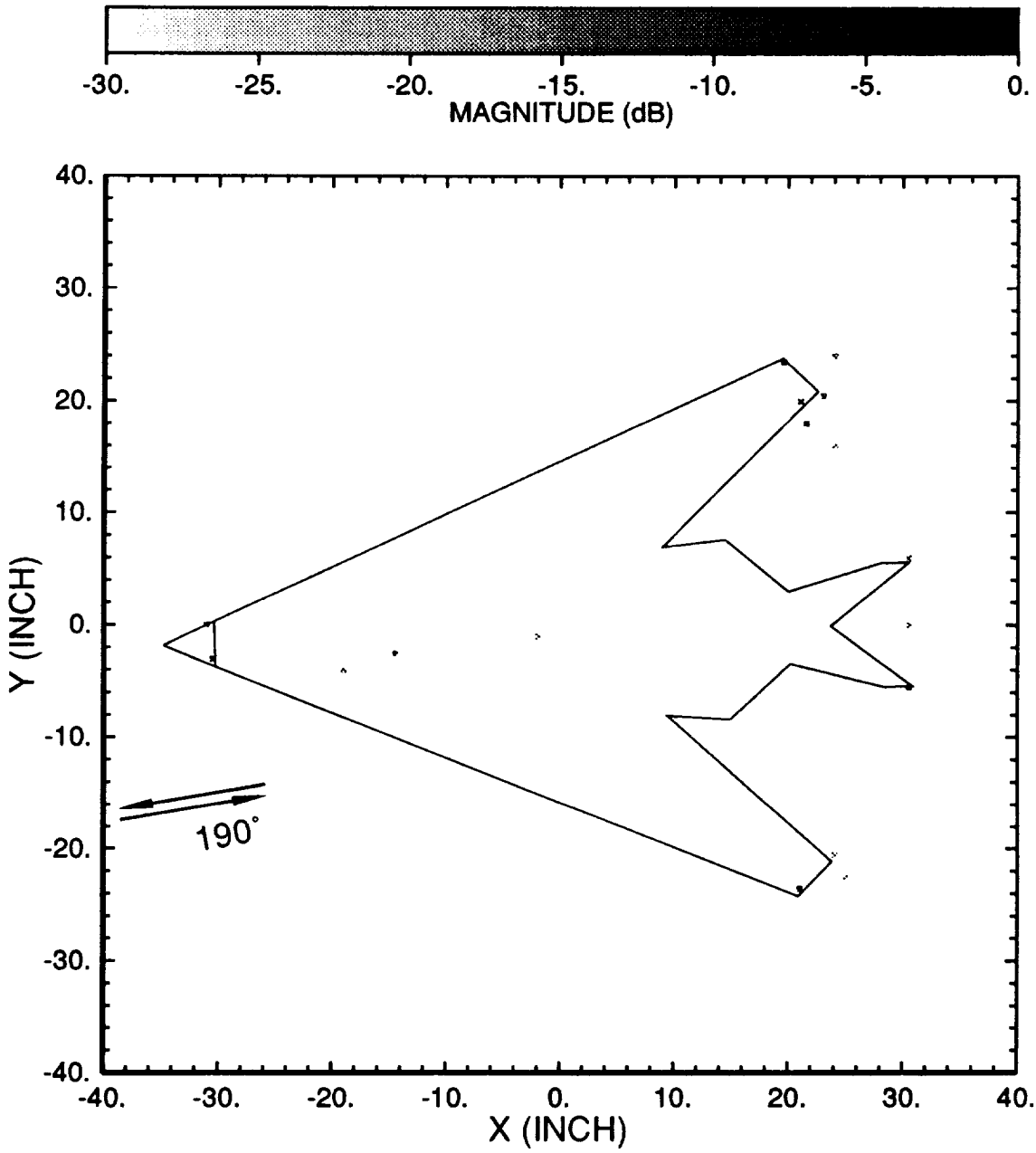

Figure 5.5: Peak positions in the F-117 fighter model ISAR at 190°.

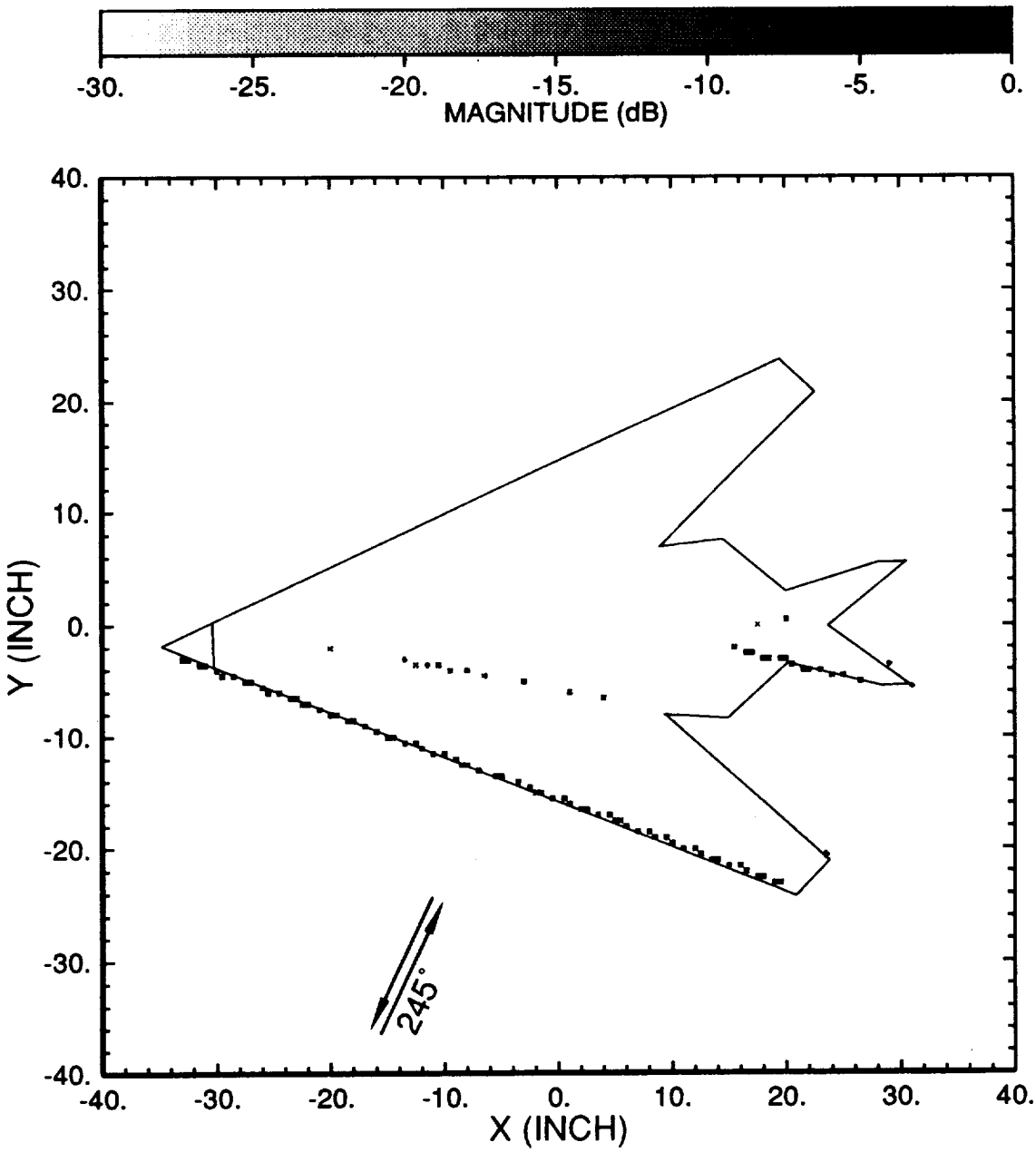

Figure 5.6: Peak positions in the F-117 fighter model ISAR at 245°.

5.2 Data Compression and Reconstruction by Gating

Here the azimuth angle from $\phi = 175°$ to $\phi = 185°$ region is processed. In this region, a typical number of 20 scattering centers are detected in the $\phi = 175°, 180°$ and $185°$ ISAR images. Table 2 shows the magnitudes and positions of some scattering centers in the $\phi = 180°$ ISAR image.

Table 5.1: Positions and magnitudes of dominate scattering centers of the F-117 fighter model in the $180° \pm 10°$ ISAR.

No.	x (inch)	y (inch)	magnitude (dB)	possible spot
# 1	-29.84	-2.31	0	front tip
# 2	21.91	-23.21	-4.56	left wingtip
# 3	20.55	24.08	-5.55	right wingtip
# 4	31.21	6.06	-6.63	right tailtip
# 5	31.50	-4.76	-7.64	left tailtip
# 6	-17.59	1.59	-9.09	cockpit

To extract out individual scattering centers, the 2-D rectangularly-based uniform gate with a down range width of 1 ns and a cross range width of 0.67 ns is again chosen. After the extraction of each scattering center by gating, a reduced database is formed. Figures 5.7–5.9 show the reconstructed frequency responses out of the reduced database for the three look angles $\phi = 175°$, $180°$ and $185°$.

Figures 5.10-5.12 show the angle domain reconstructed data for frequencies of 4 GHz, 10 GHz and 17 GHz, respectively. The errors in the 10 and 17 GHz angle reconstruction cases are greater than expected. Figures 5.13–5.14, which show the reconstructed frequency responses at $182°$ and $183°$, also indicate the linear interpolation every $5°$ in the angle reconstruction is somewhat failing. To analyze this

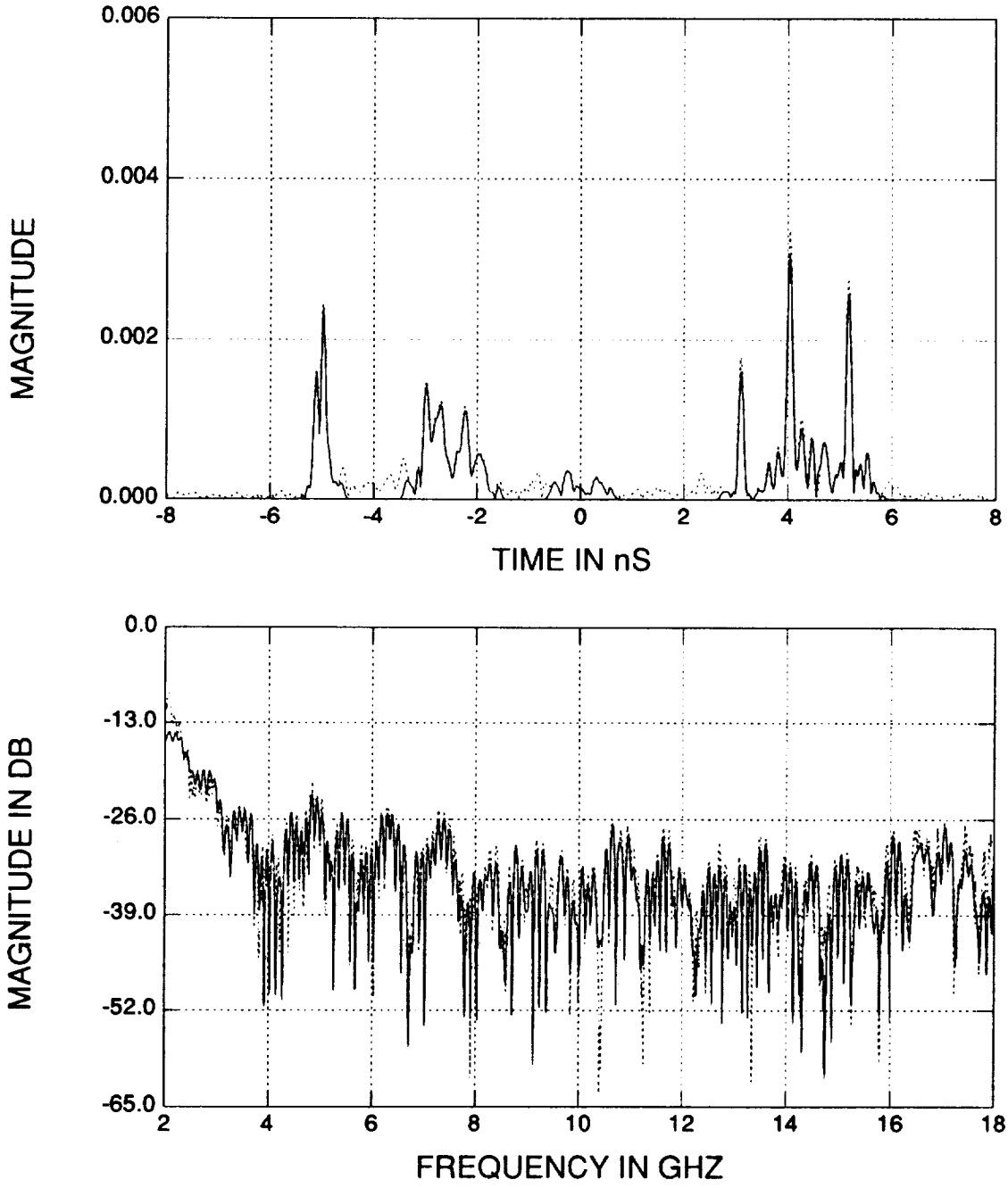

Figure 5.7: Comparison between the reconstructed (solid line) and original (dotted line) frequency responses at 175° for the F-117 model, obtained by gating.

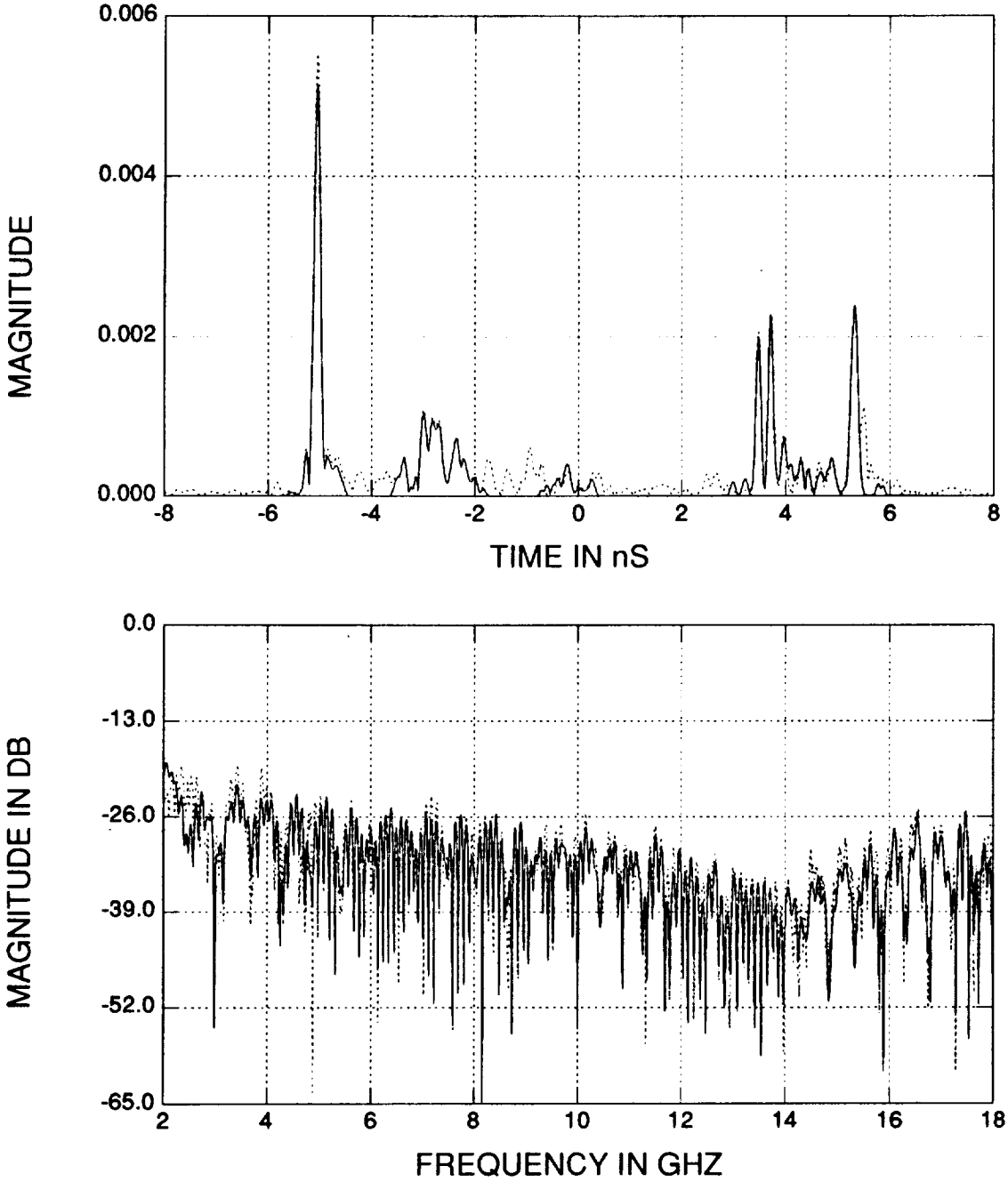

Figure 5.8: Comparison between the reconstructed (solid line) and original (dotted line) frequency responses at 180° for the F-117 model, obtained by gating.

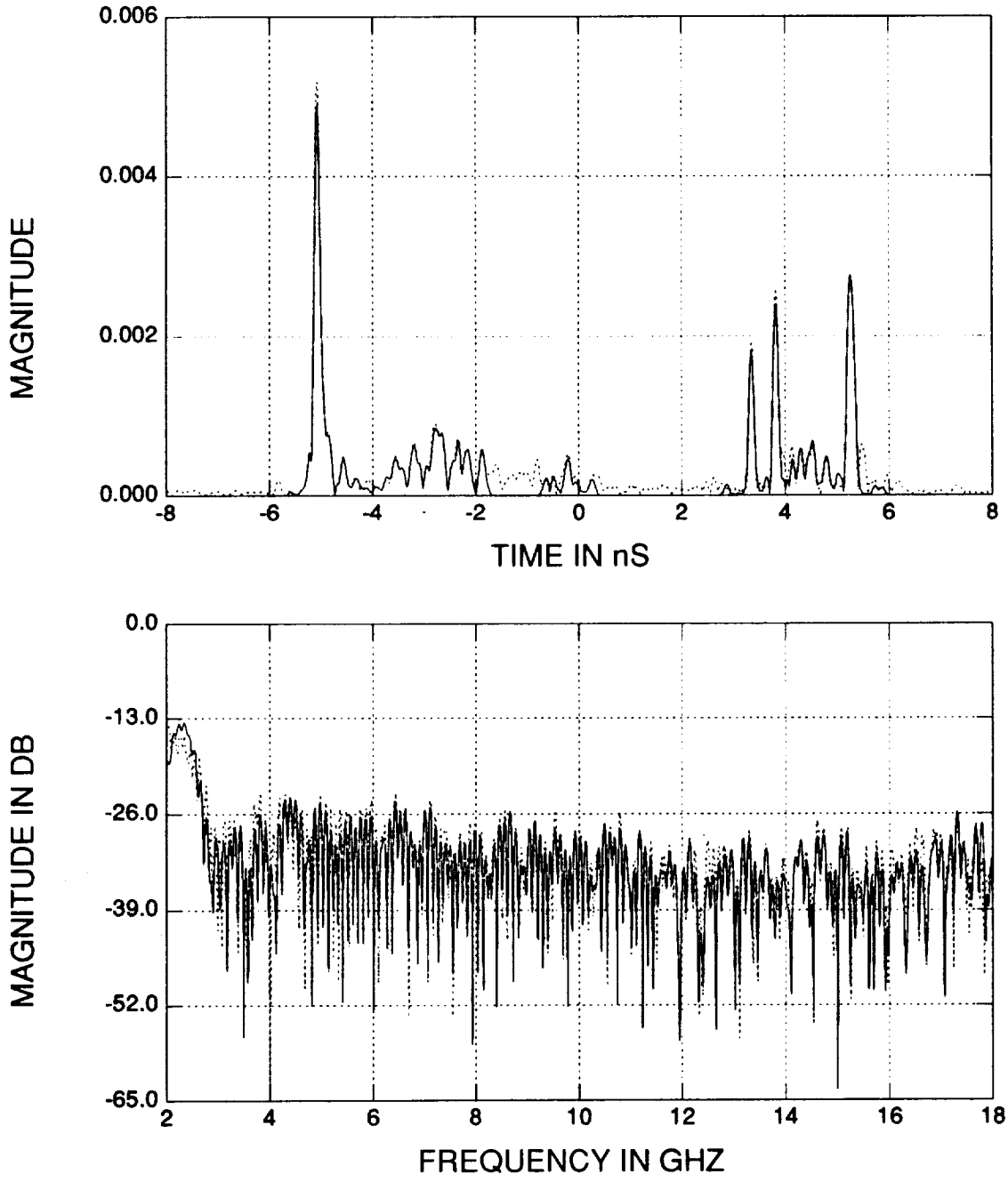

Figure 5.9: Comparison between the reconstructed (solid line) and original (dotted line) frequency responses at 185° for the F-117 model, obtained by gating.

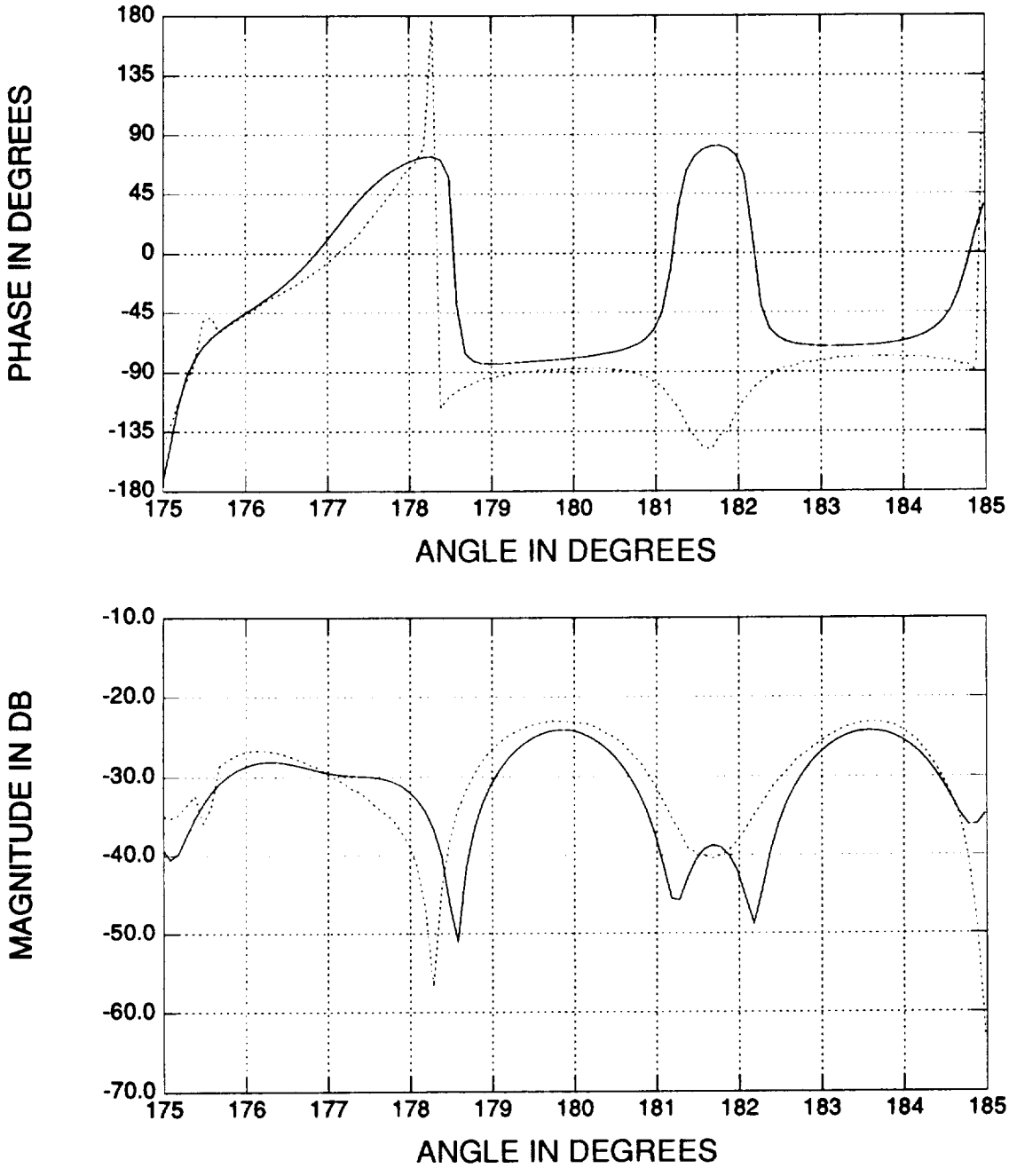

Figure 5.10: Comparison between the reconstructed (solid line) and original (dotted line) azimuth response at 4 GHz for the F-117 model, obtained by gating.

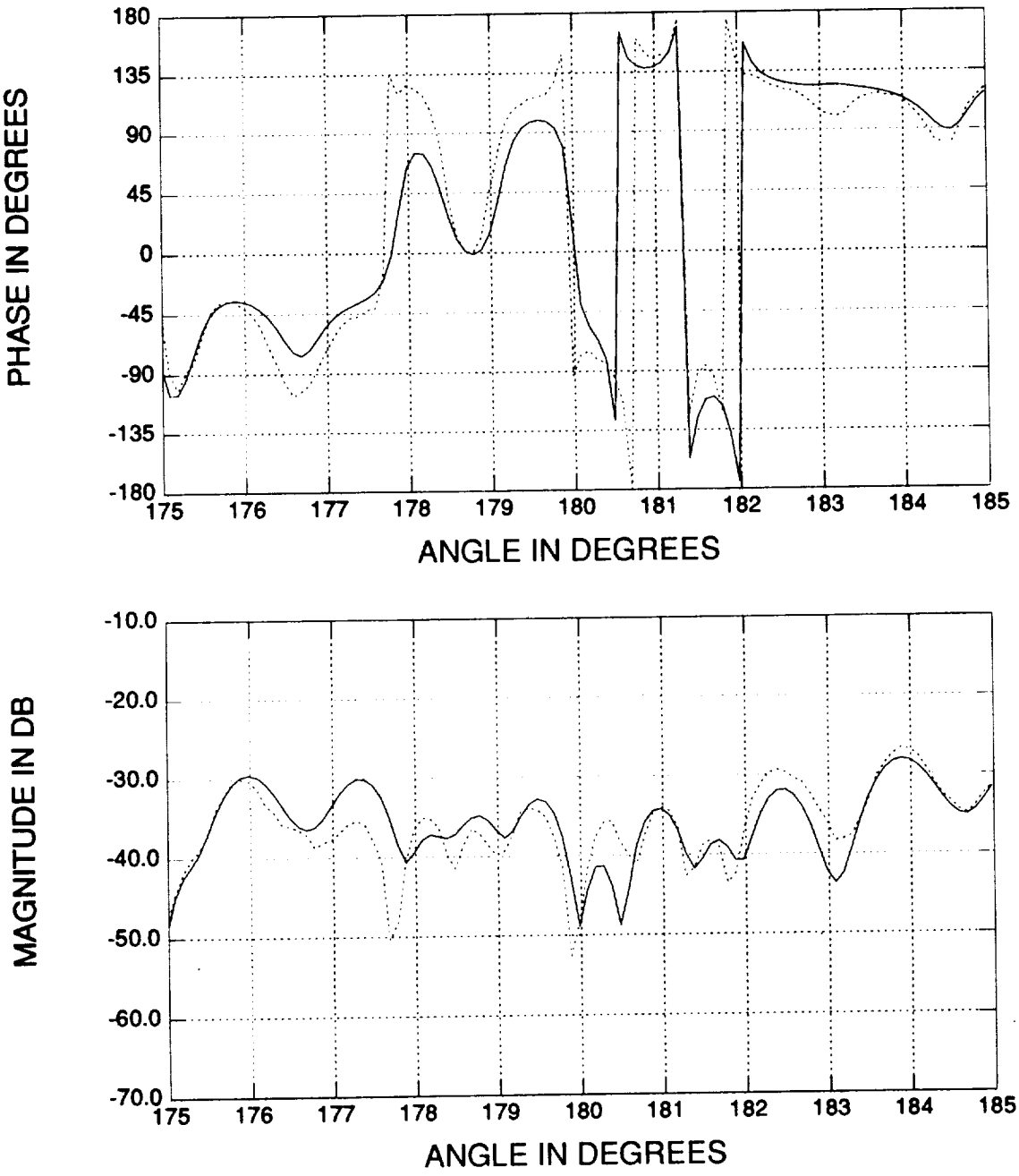

Figure 5.11: Comparison between the reconstructed (solid line) and original (dotted line) azimuth response at 10 GHz for the F-117 model, obtained by gating.

C-2

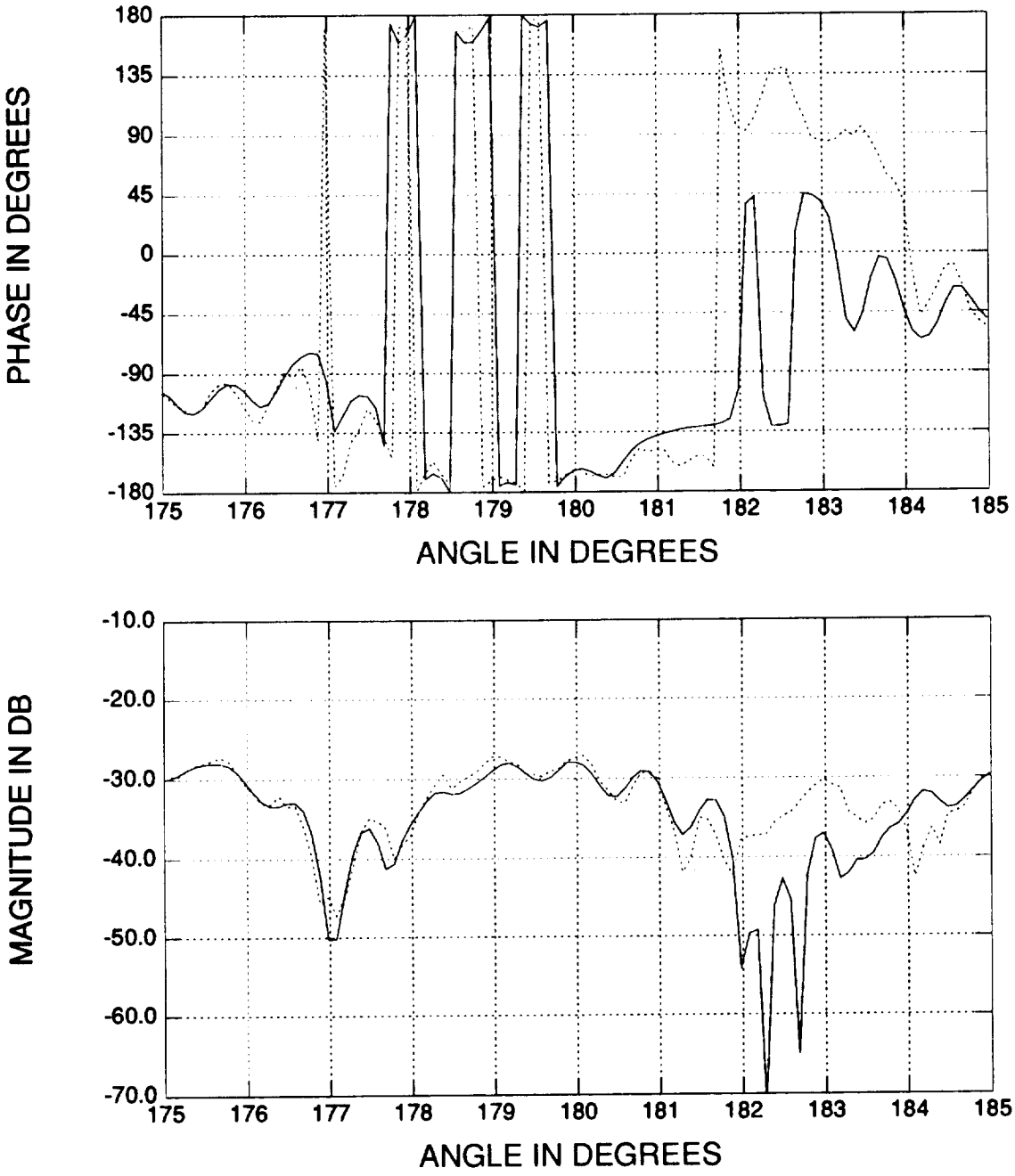

Figure 5.12: Comparison between the reconstructed (solid line) and original (dotted line) azimuth response at 17 GHz for the F-117 model, obtained by gating.

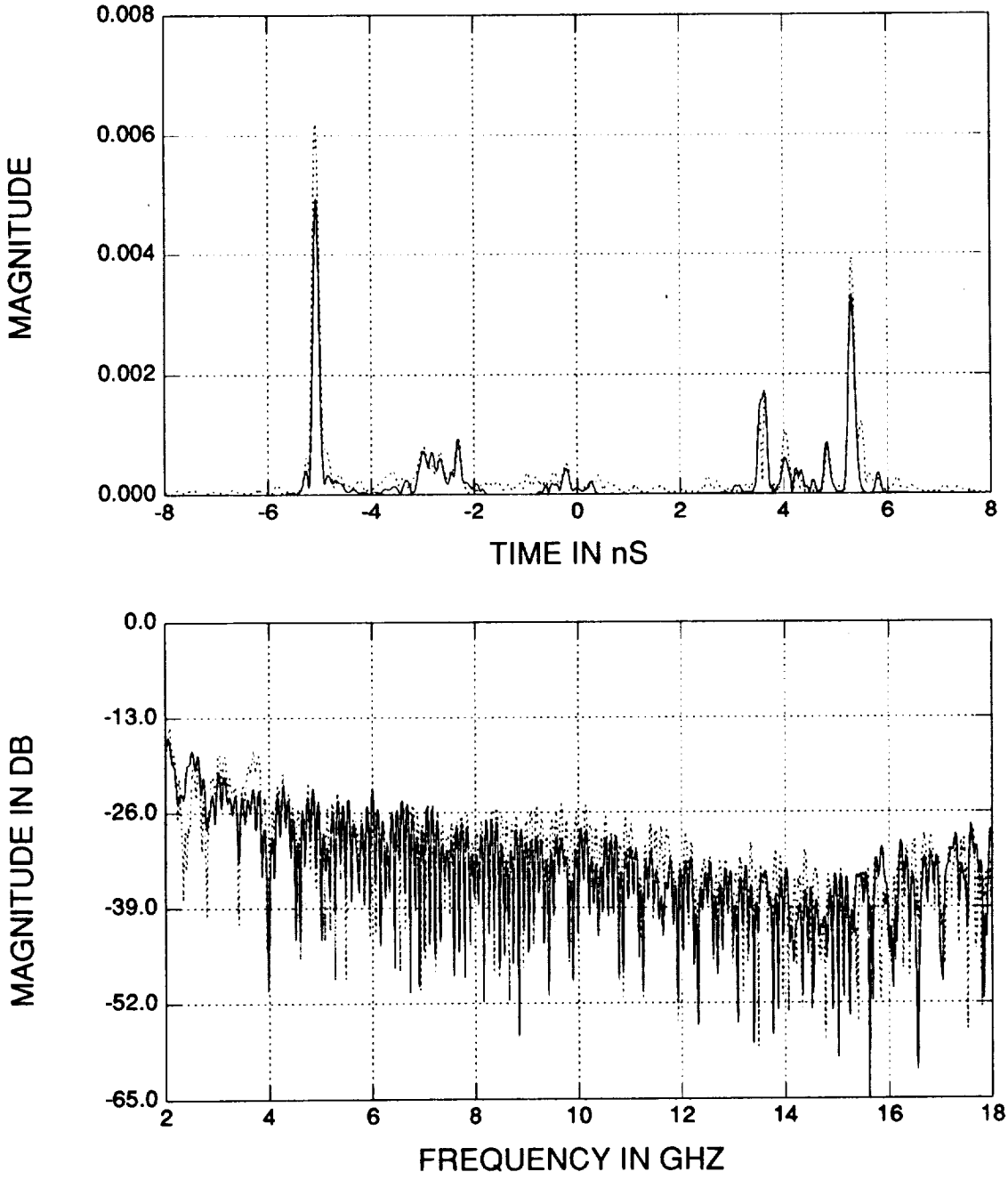

Figure 5.13: Comparison between the reconstructed (solid line) and original (dotted line) frequency responses at 182° for the F-117 model, obtained by gating.

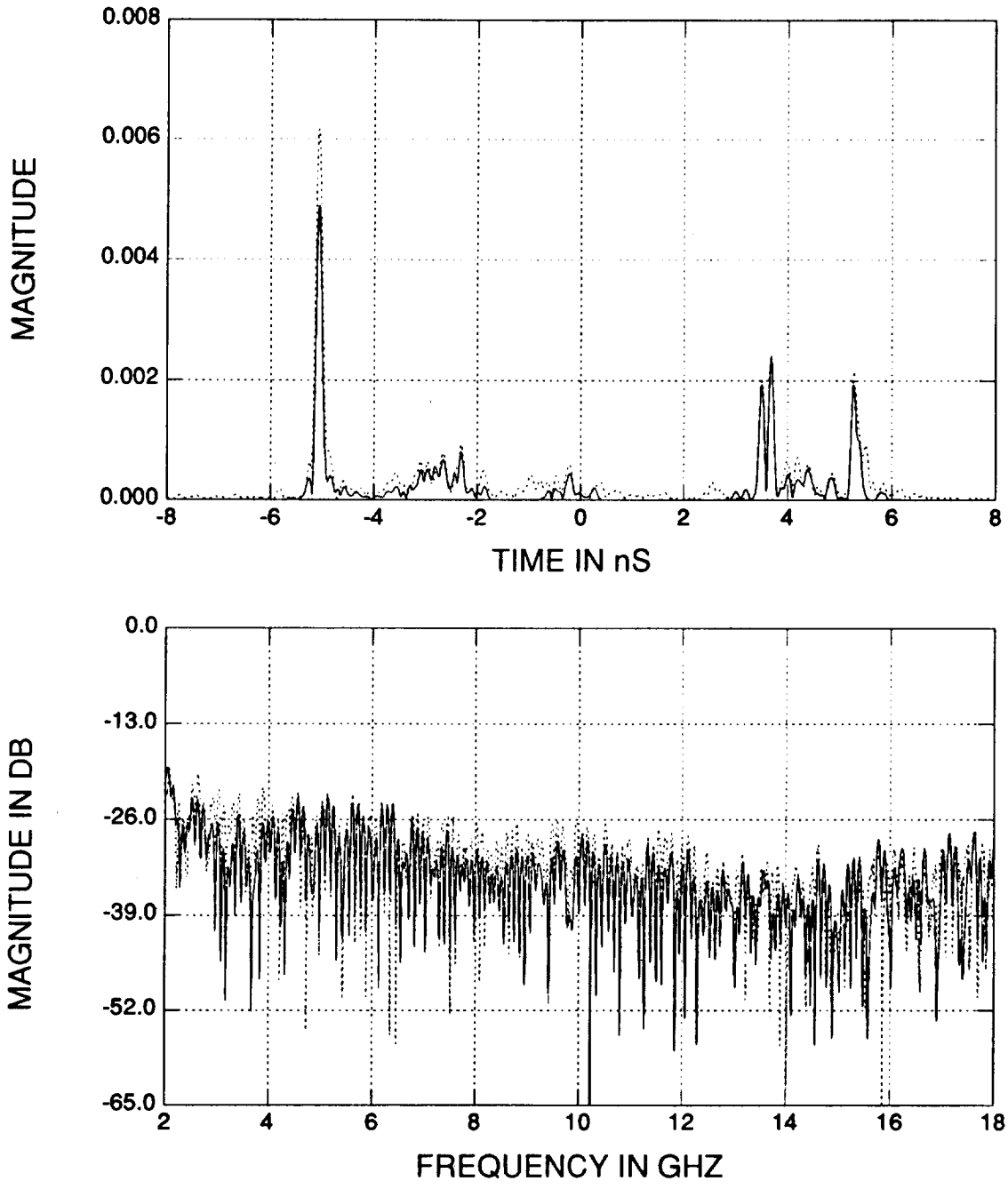

Figure 5.14: Comparison between the reconstructed (solid line) and original (dotted line) frequency responses at 183° for the F-117 model, obtained by gating.

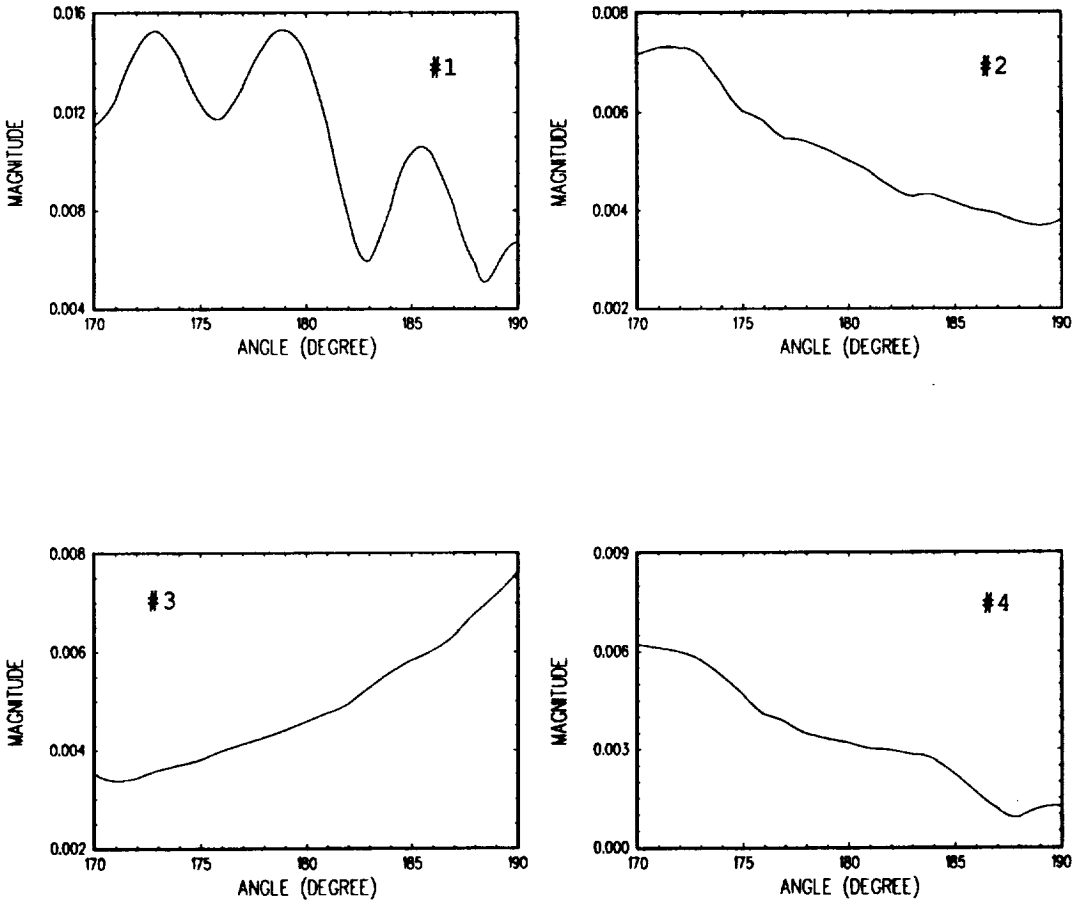

Figure 5.15: Azimuth response for the four dominant scattering centers in the F-117 model at 17 GHz.

problem in detail, let's consider the response of the dominant scattering centers first. Figure 5.15 shows the angle response of the four most dominant scattering centers at 17 GHz obtained using repeated ISAR images every 1° and the gating technique. Note that the #1 scattering center's angle response exhibits an oscillation while the others do not. This phenomenon leads one to postulate that there might be two scattering centers grouped together as one. Note that for a given frequency f_o, the angle response of two equal strength scattering centers separated in the cross range by $2t_d$ is given by

$$E(\phi) = e^{-j2\pi f_o t_d \sin(\phi-\phi_o)} + e^{-j2\pi f_o(-t_d)\sin(\phi-\phi_o)} \tag{5.1}$$

or

$$E(\phi) = 2\cos[2\pi f_o t_d \sin(\phi - \phi_o)] \tag{5.2}$$

where ϕ_o is the central look angle. From Figure 5.15, one can see that the oscillating period for the # 1 scattering center is about 6.5°, if substituted into Equation (5.2), it means there are two scattering centers 0.5 ns (or 3 inches) apart in the cross range direction.

In fact, the nose part of the F-117 model contains a short edge of 3 inches wide or so. The contribution of this short edge can be viewed as two scattering centers which are of the same down range but about 3 inches apart in cross range when this edge is illuminated around the reference angle $\phi = 180°$ (see Figure 5.1). The $\pm 10°$ spanned ISAR images do not have enough resolution to resolve these two scattering centers; hence, they detect only one scattering center somewhere in between. The result is that the two scattering centers are grouped together by the spatial gate and the angle response begins to oscillate as indicated by Equation (5.2). From the # 1 scattering center's case shown in Figure 5.15, one knows that for an angle reconstruction of a high frequency (say 17 GHz), linear interpolation every 5° is not good enough to recover the cosine-shaped curve whose oscillation is about $6.5° \cdot 2 = 13°$ per cycle.

To solve this problem, first a $\pm 15°$ spanned ISAR is re-imaged to resolve the two scattering centers. Then a 1 ns by 0.5 ns gate is positioned around the two scattering

Table 5.2: Positions and magnitudes of dominate scattering centers of the F-117 fighter model in the 180° ± 15° ISAR.

No.	x (inch)	y (inch)	magnitude (dB)	possible spot
# 1*	-29.84	-2.45	0	front edge
# 2	21.91	-23.21	-1.99	left wingtip
# 3	20.55	24.08	-3.41	right wingtip
# 4	31.21	6.06	-5.36	right tailtip
# 5*	-30.20	0.14	-5.57	front edge
# 6	31.50	-4.90	-6.19	left tailtip
# 7	-17.59	1.59	-8.84	cocktip

centers at the front edge one at a time to separate them out. (Others are separated using the previous 1 ns by 0.67 ns gate.) The isolated scattering center positions and strengths are shown in Table 3, and the new reconstructed results are shown in Figures 5.16–5.20. Compared to the previous ones, the newly reconstructed results are much improved.

The above example shows that sampling in the angle domain has to be based on the cross range gate width. Since the employed cross range gate width is 4 inches (0.67 ns), which is the limit of sampling every 5°, if two scattering centers are located within 4 inches in the cross range and hence are gated as one (in which case the sinusoidal behavior occurs in the angle domain), then only sinc interpolation can exactly recover the angle response according to the sampling theorem. But as mentioned in Chapter 3, sinc interpolation is impractical in the angle domain. Therefore, if one still wants to use the linear interpolation in this situation, one has to either separate the two scattering centers or sample the grouped angle response more often; e.g., every 2.5° instead of every 5°.

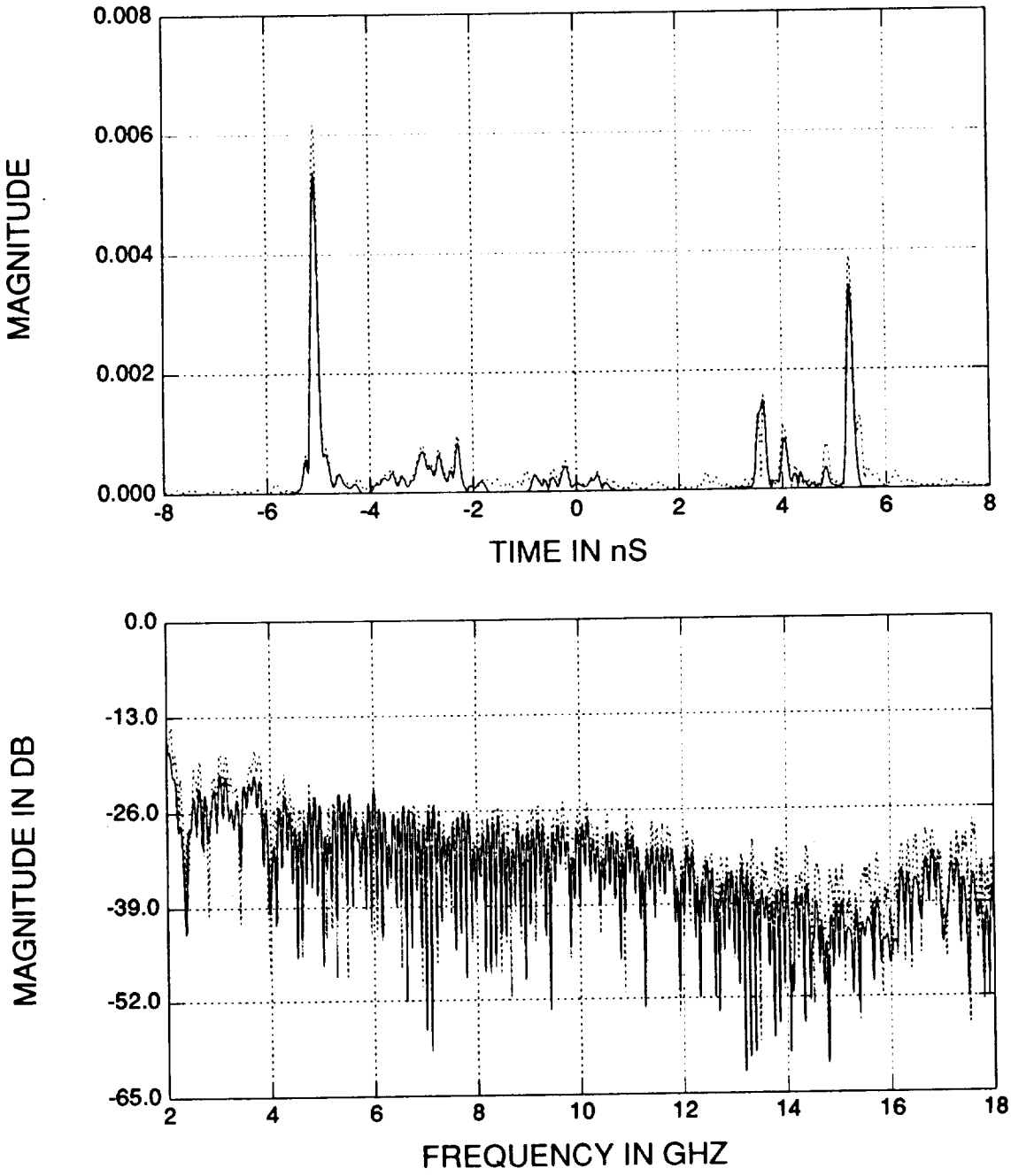

Figure 5.16: Comparison between the reconstructed (solid line) and original (dotted line) frequency responses at 182° for the F-117 model, using 30° spanned ISAR and gating.

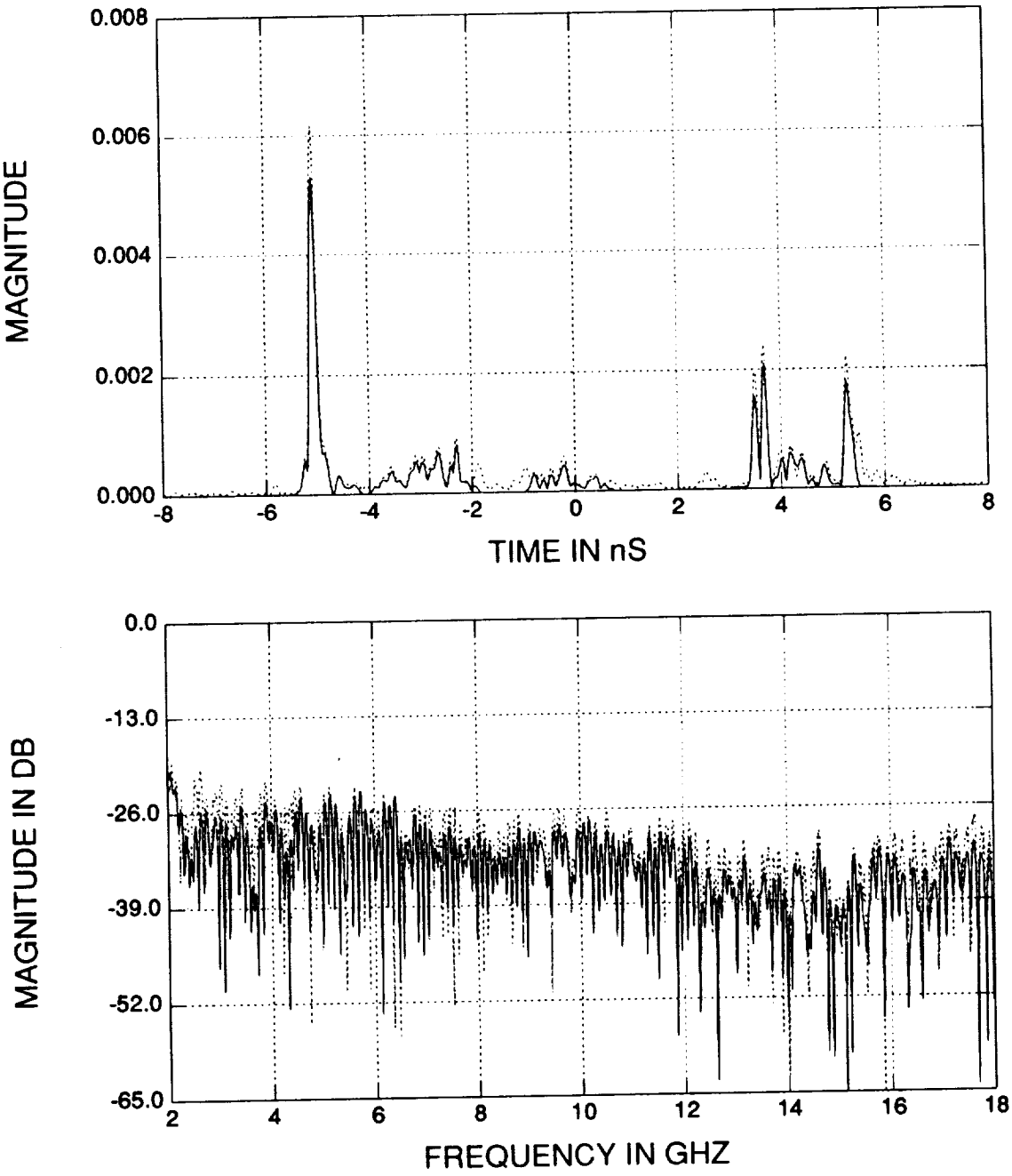

Figure 5.17: Comparison between the reconstructed (solid line) and original (dotted line) frequency responses at 183° for the F-117 model, using 30° spanned ISAR and gating.

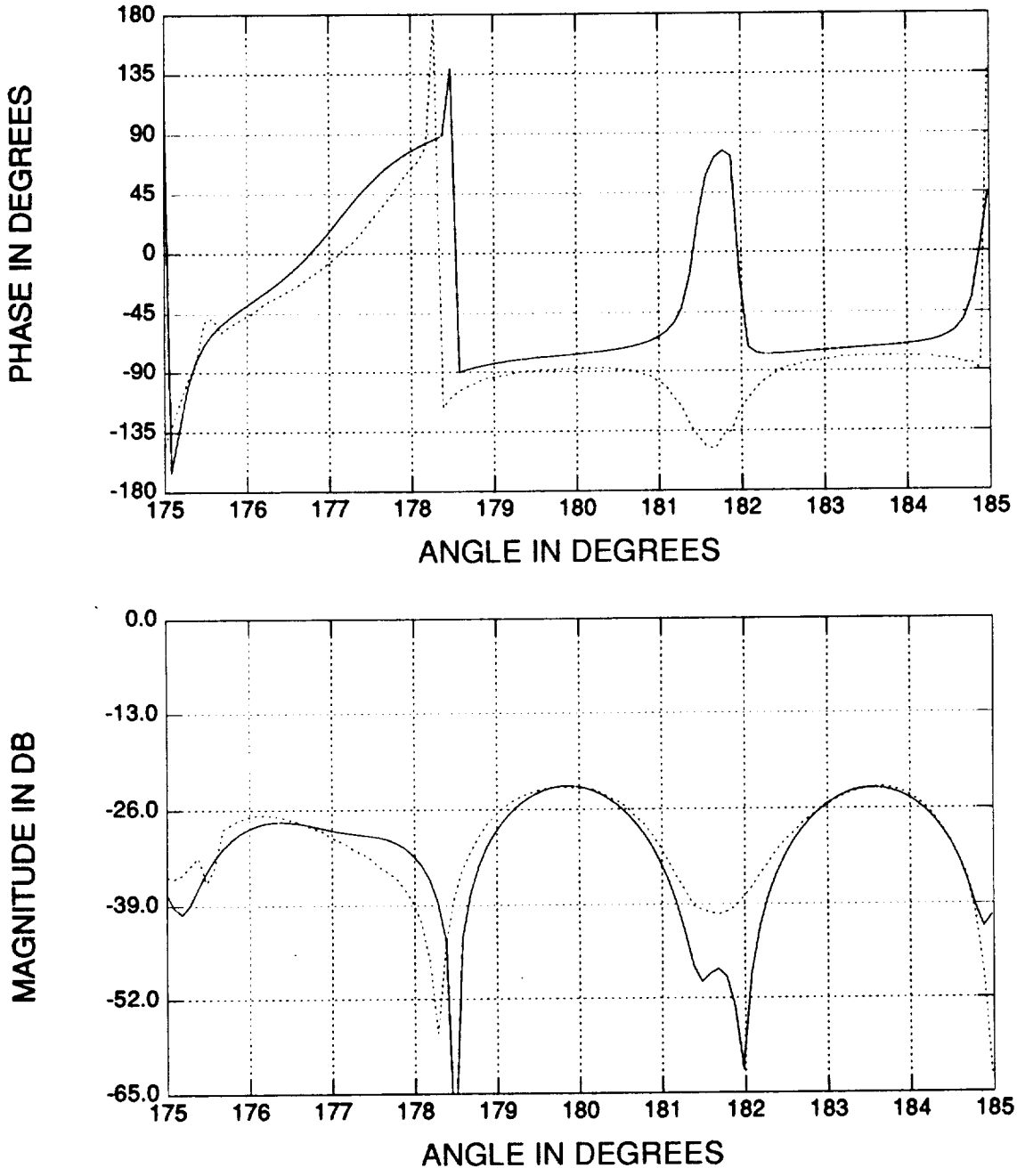

Figure 5.18: Comparison between the reconstructed (solid line) and original (dotted line) azimuth response at 4 GHz for the F-117 model, using 30° spanned ISAR and gating.

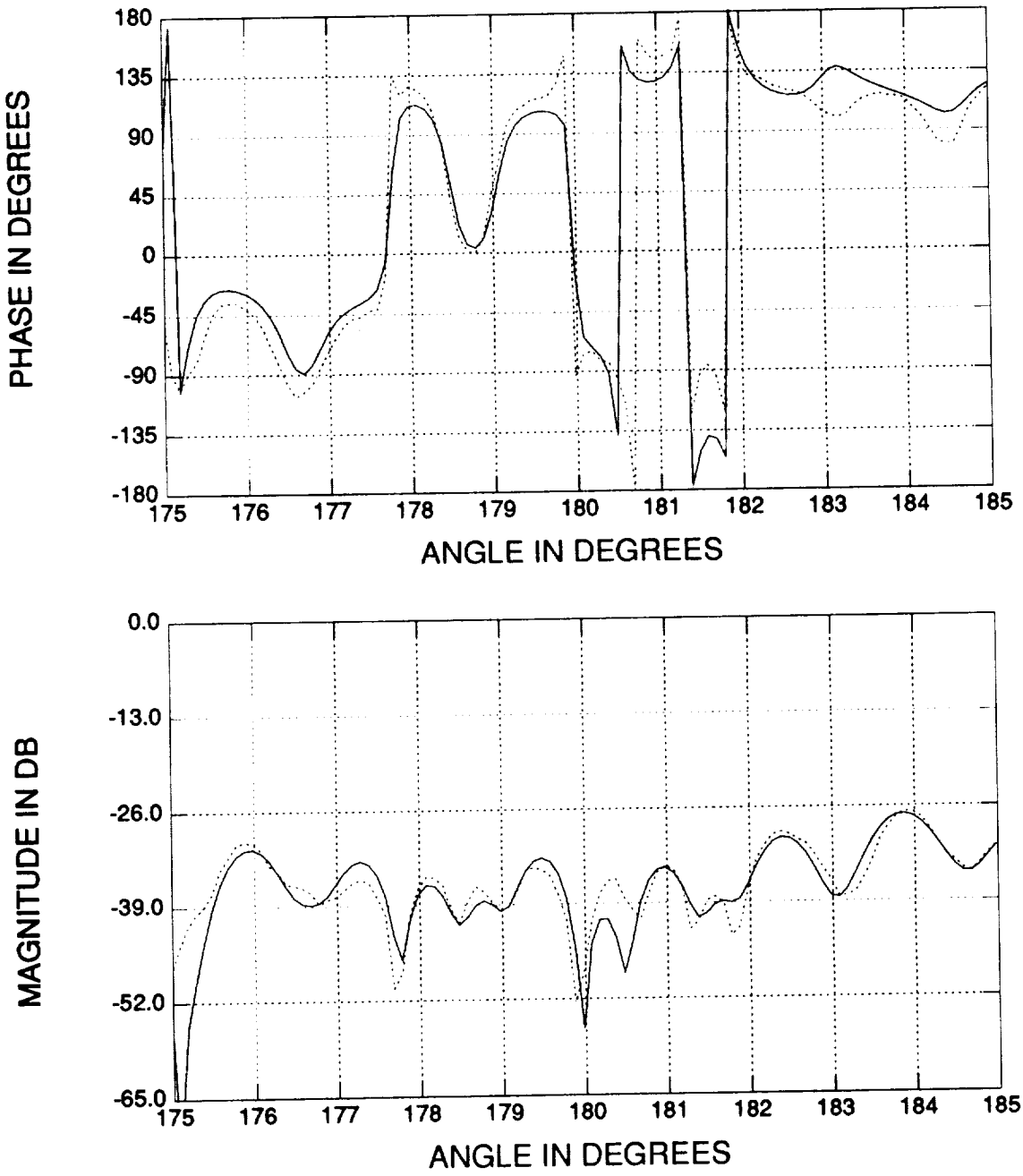

Figure 5.19: Comparison between the reconstructed (solid line) and original (dotted line) azimuth response at 10 GHz for the F-117 model, using 30° spanned ISAR and gating.

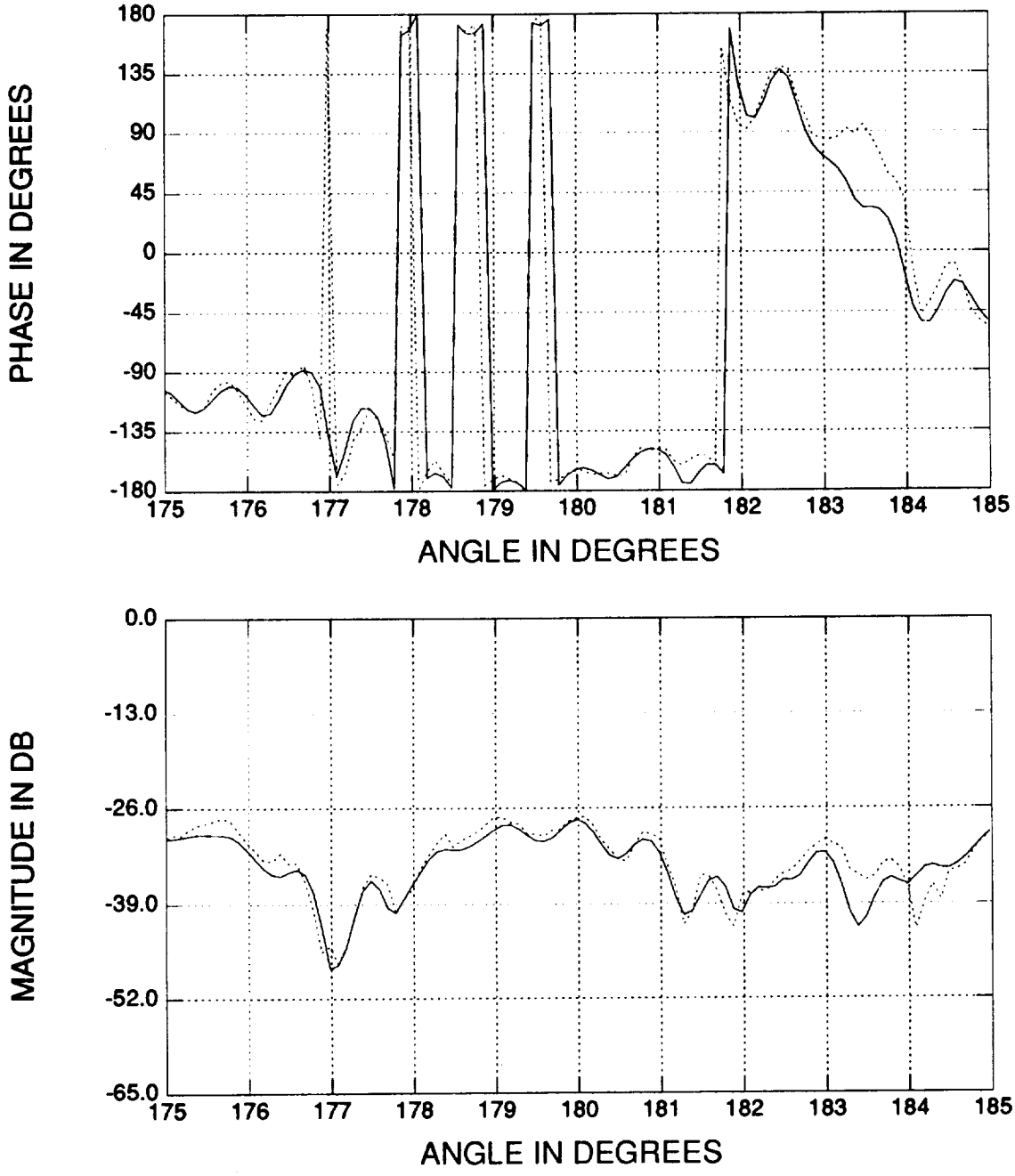

Figure 5.20: Comparison between the reconstructed (solid line) and original (dotted line) azimuth response at 17 GHz for the F-117 model, using 30° spanned ISAR and gating.

5.3 Data Compression and Reconstruction by Smoothing

In the previous section, when the most dominant scattering center was investigated for its angle response (see Figure 5.15), it could be isolated for each different look angle and then tracked manually. But as mentioned in Chapter 4, for a real-world target, the scattering centers can really be moving with respect to the look angle (such as in a metal sphere case), and the numerical inaccuracy in the ISAR processing can also contribute to the positional shift of a given scattering center. These factors make it very difficult to track how these scattering centers move, let alone there may even be different number of scattering centers in different look angles. To solve this problem, a newly reduced database concept is proposed using the smoothing technique.

The new proposal is, for a look angle ϕ (say 175°), the smoothed results of $\phi - 5°$, ϕ and $\phi + 5°$ are to be recorded instead of ϕ alone. Since these three datasets are obtained based on the information from the same ISAR image, there is no need to match scattering centers among them. Therefore, one can easily interpolate the response at, say 177° from these three datasets. Note that by doing so there will be repeated angle regions; e.g., the smoothed results of $\phi = 180°$ will cover 175°, 180° and 185° which can also generate the data at 177°. Hence, the final response at $\phi = 177°$ is a weighted result of the two reconstructed curves which should have already been very close to each other. Also note that since one has three datasets, the interpolating function can be chosen to be a parabolic fit, which is better than the previously used linear fit in a sense that a parabolic fit better represents the sinc interpolation.

Figures 5.21 through 5.25 show the results of the frequency reconstructions for $\phi = 175°, 180°, 182°, 183°$ and 185°. And Figures 5.26 through 5.28 show the results of angle response reconstructions for frequencies of 4 GHz, 10 GHz and 17 GHz, respectively. Again these results are similar to those obtained by gating.

5.4 Data Compression and Reconstruction for a Special Case: the Broadside Scattering

The ISAR image of the F-117 fighter at $\phi = 115°$ is shown in Figure 5.2. As shown in the image, the long straight edge of the wing dominates because around this angle the incident wave illuminates the wing edge in phase, which results in a very strong backscattered field. This scattering obviously is not a point scatterer, but rather a line scatterer. One can employ a GTD model to calculate the frequency and angle response of this line source and store it as a special case in the database, but this would ruin the database structure and complicate the compression and reconstruction schemes. Here a method is offered to represent the line source by many "pseudo" discrete point scatterers whose spacing is decided by the cross range gate width, and then one still use the gating/smoothing technique to achieve data compression and reconstruction.

Figures 5.29 to 5.31 show the frequency reconstructions, and Figures 5.32 to 5.34 show the angle reconstructions around the broadside scattering angle by this method. The results are very good. The reason is that a line source is an integration of point sources, if one continuously gates out the line scatterer according to these pseudo scattering centers, the sum of these segments will approximate the original line source such that total energy is not lost at all.

However, the reconstruction is done at the cost of an increased number of pseudo scattering centers. In our case, each pseudo scattering center is chosen to be about 1.5 inches apart and the typical number of scattering centers is about 40 for a 60 inch long wing. This means the database for this particular angle is larger than normal, and the reconstruction will be a little slower.

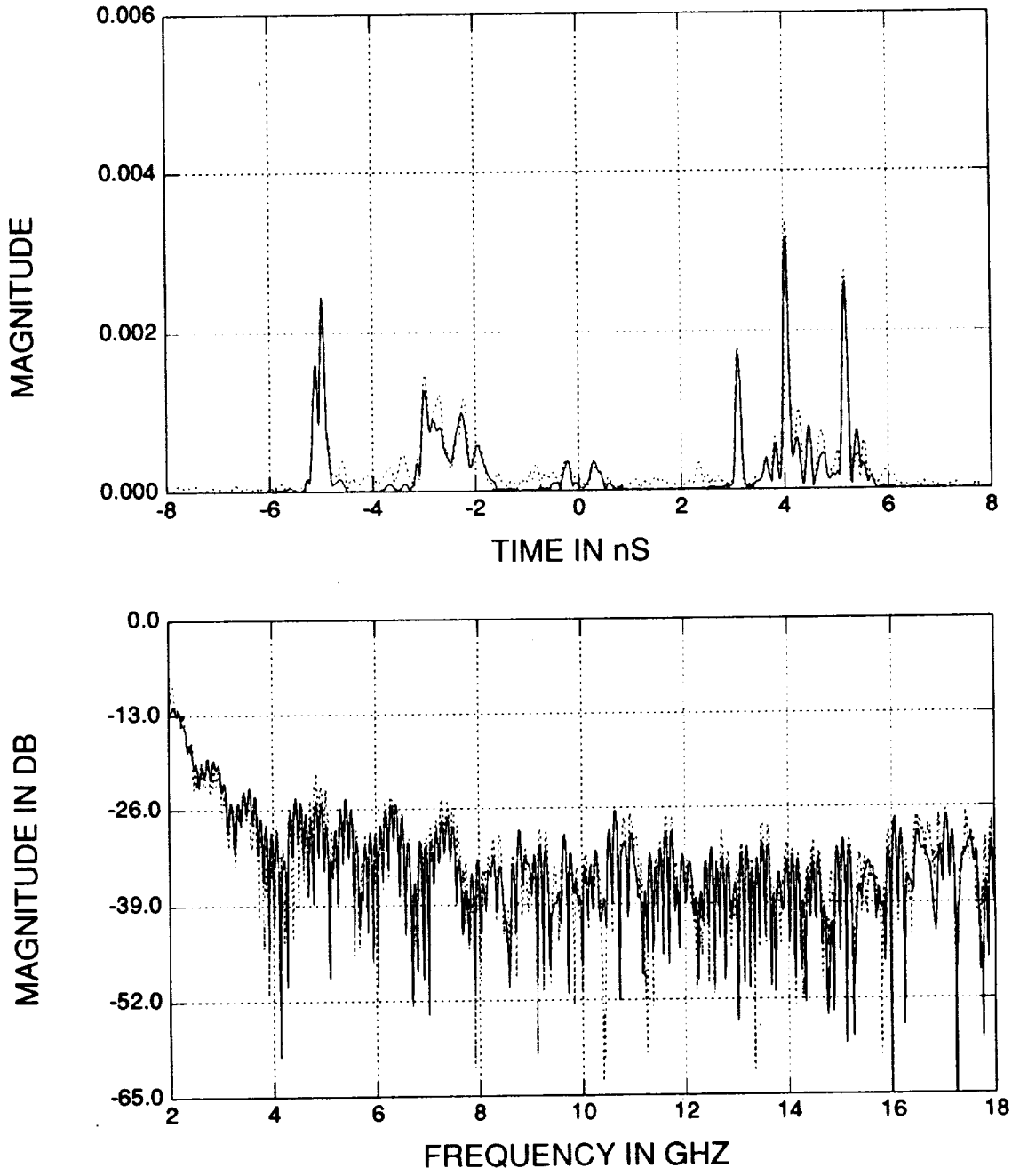

Figure 5.21: Comparison between the reconstructed (solid line) and original (dotted line) frequency responses at 175° for the F-117 model, obtained by smoothing.

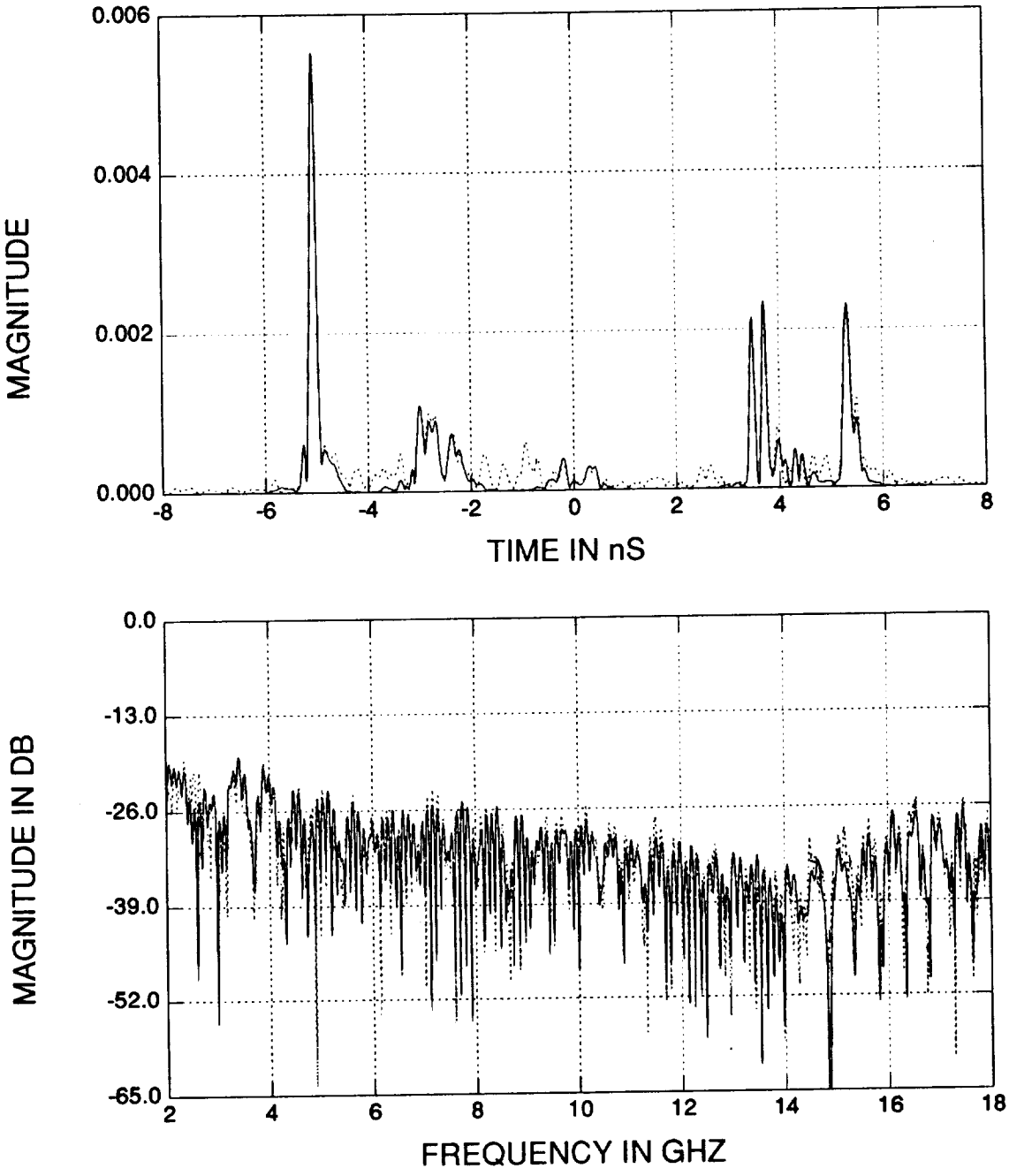

Figure 5.22: Comparison between the reconstructed (solid line) and original (dotted line) frequency responses at 180° for the F-117 model, obtained by smoothing.

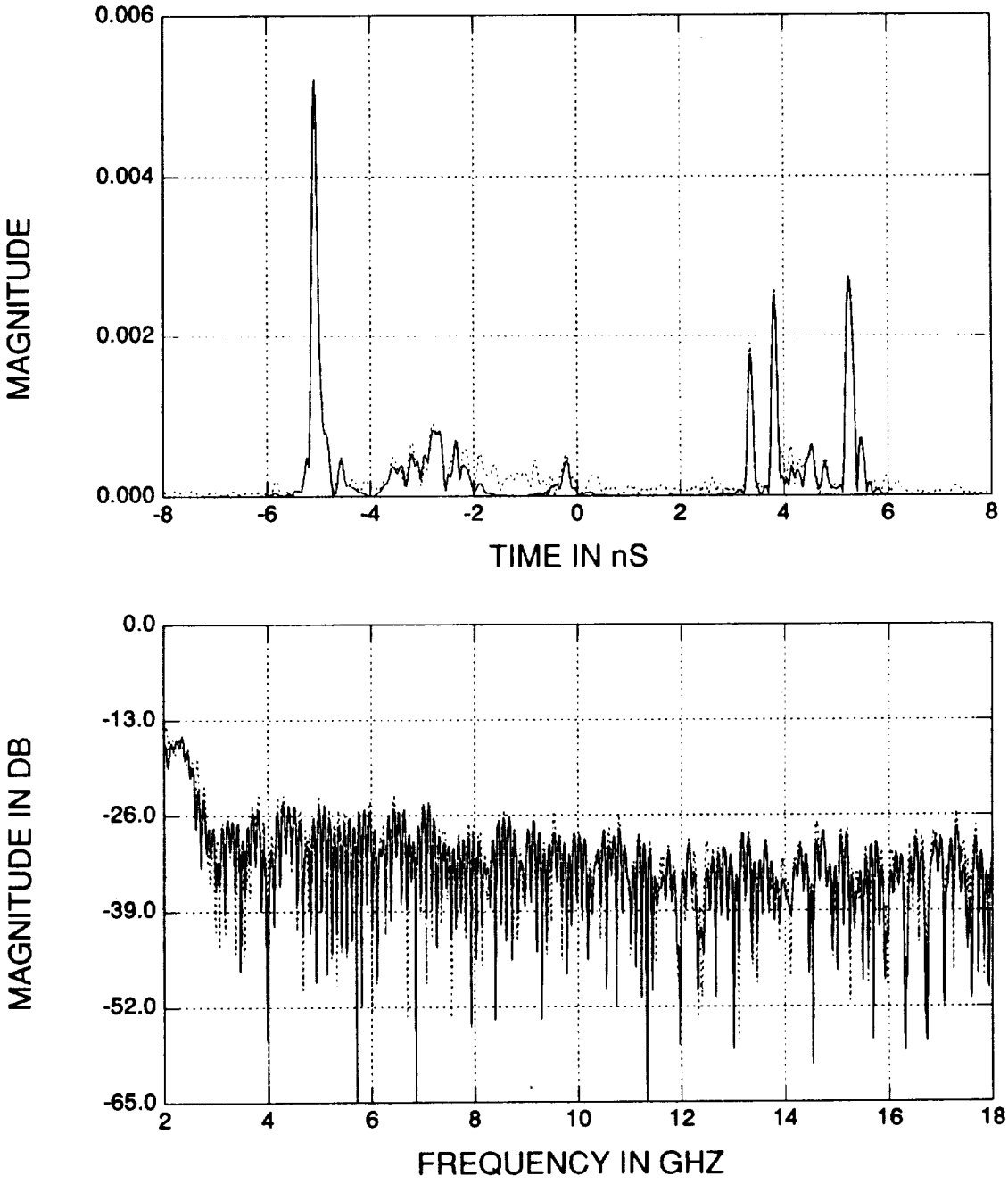

Figure 5.23: Comparison between the reconstructed (solid line) and original (dotted line) frequency responses at 185° for the F-117 model, obtained by smoothing.

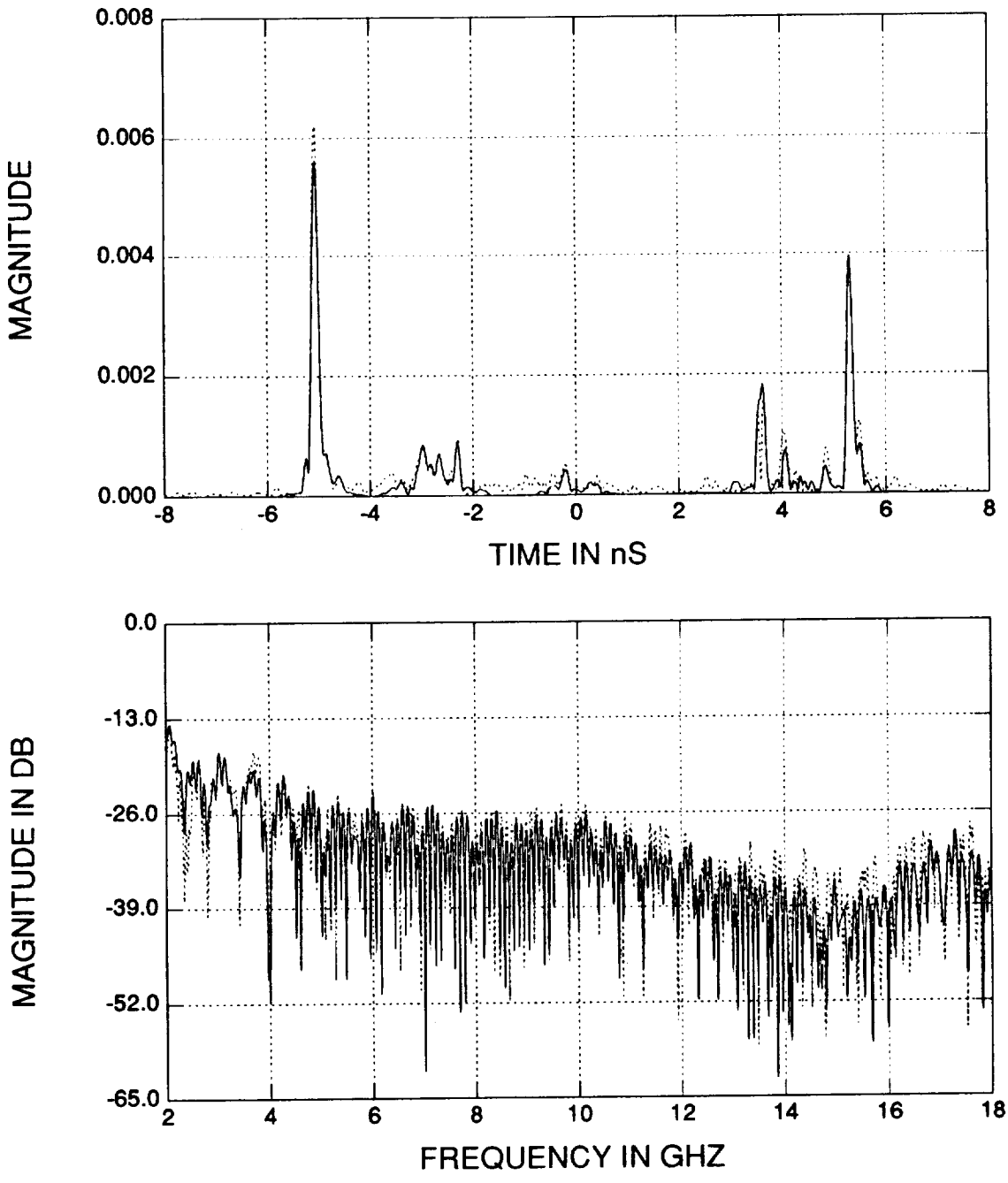

Figure 5.24: Comparison between the reconstructed (solid line) and original (dotted line) frequency responses at 182° for the F-117 model, obtained by smoothing.

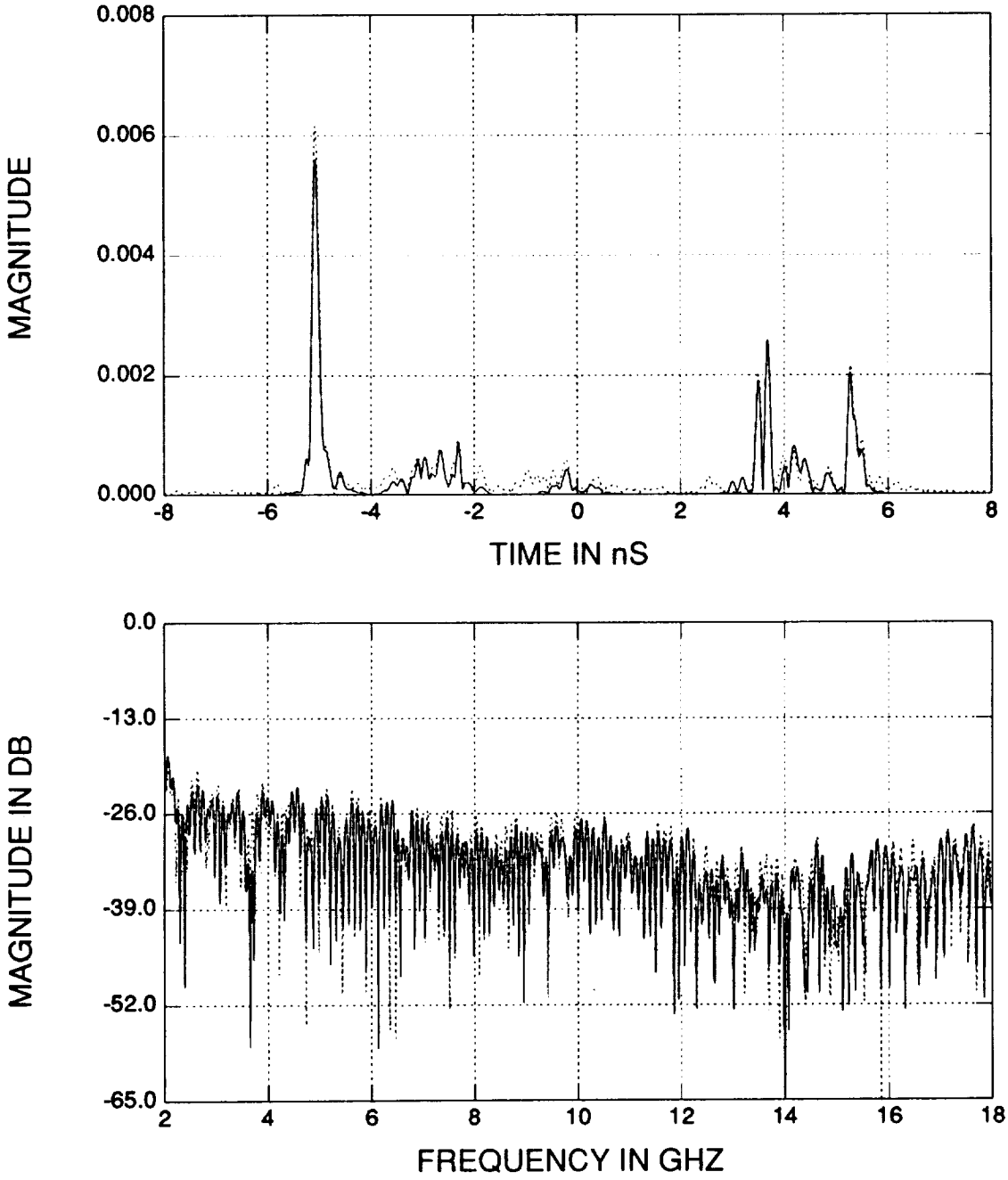

Figure 5.25: Comparison between the reconstructed (solid line) and original (dotted line) frequency responses at 183° for the F-117 model, obtained by smoothing.

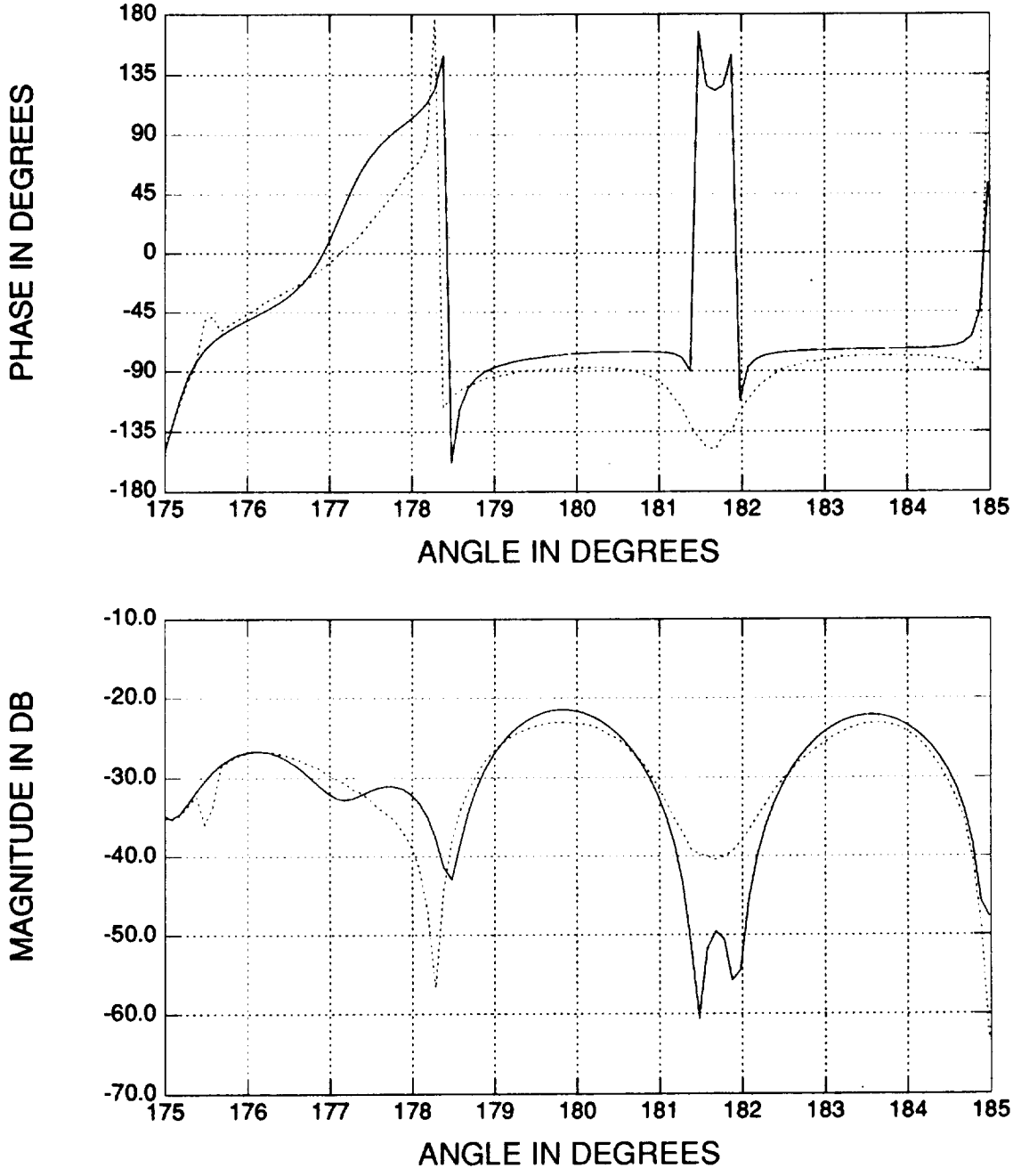

Figure 5.26: Comparison between the reconstructed (solid line) and original (dotted line) azimuth response at 4 GHz for the F-117 model, obtained by smoothing.

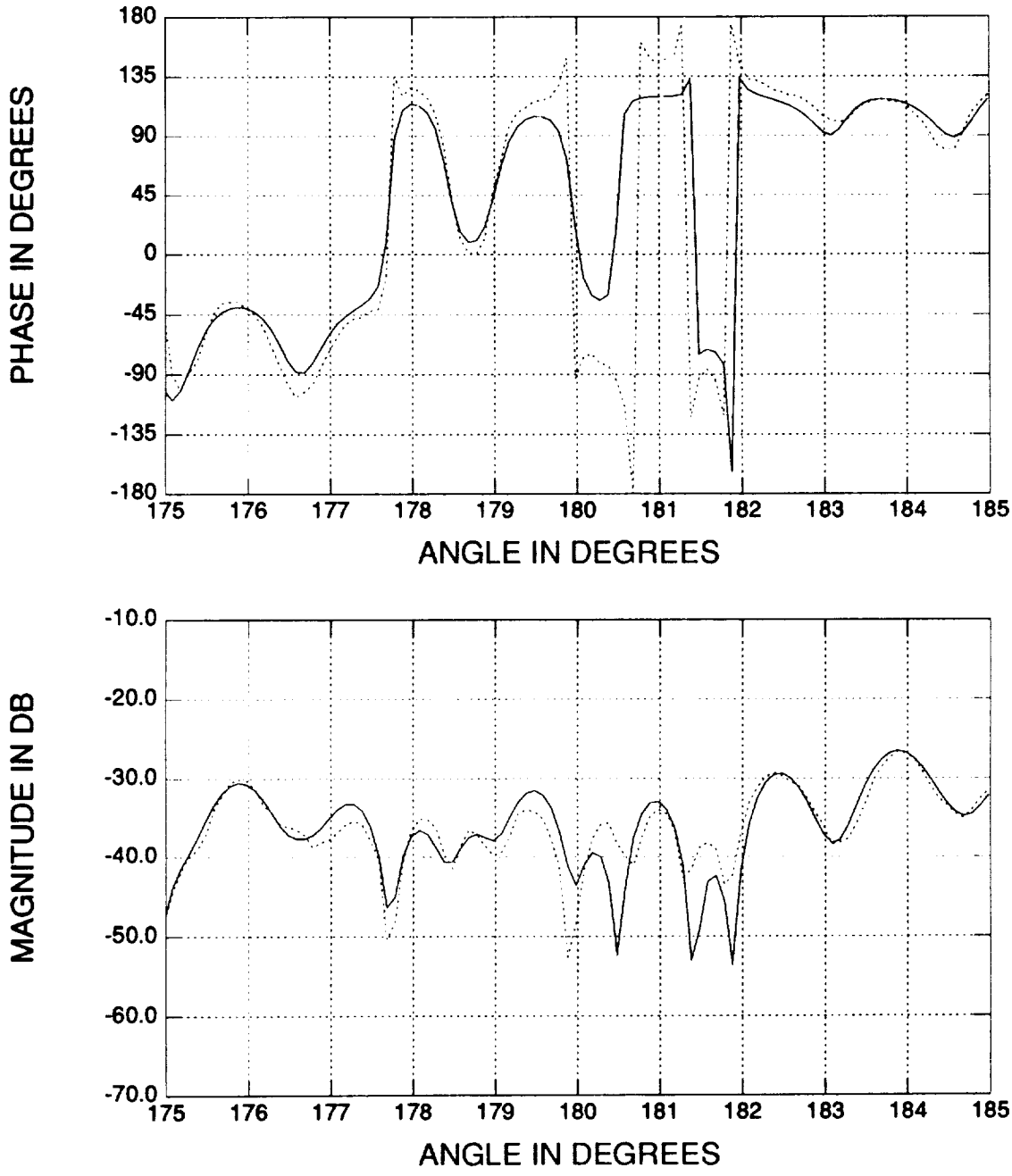

Figure 5.27: Comparison between the reconstructed (solid line) and original (dotted line) azimuth response at 10 GHz for the F-117 model, obtained by smoothing.

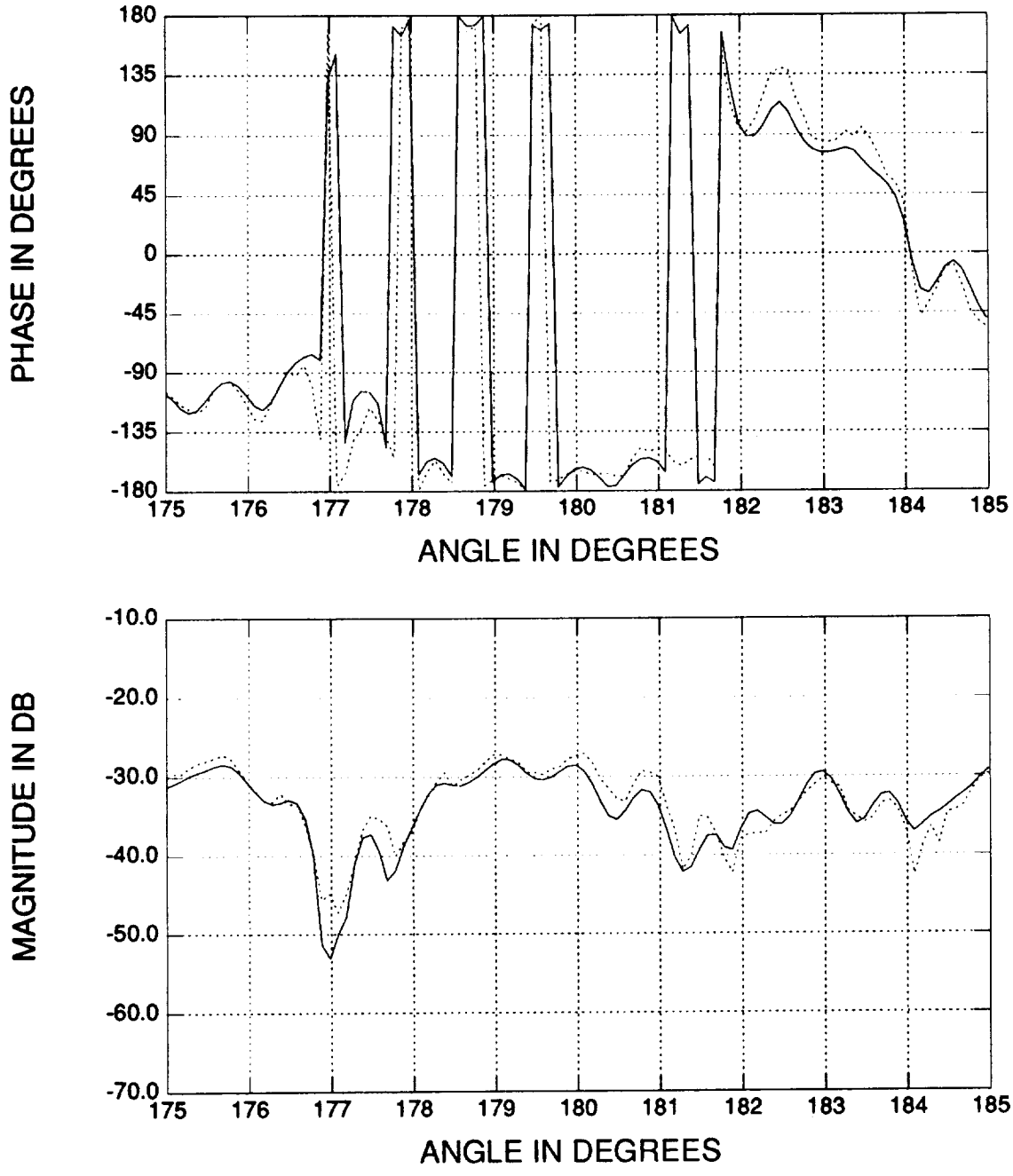

Figure 5.28: Comparison between the reconstructed (solid line) and original (dotted line) azimuth response at 17 GHz for the F-117 model, obtained by smoothing.

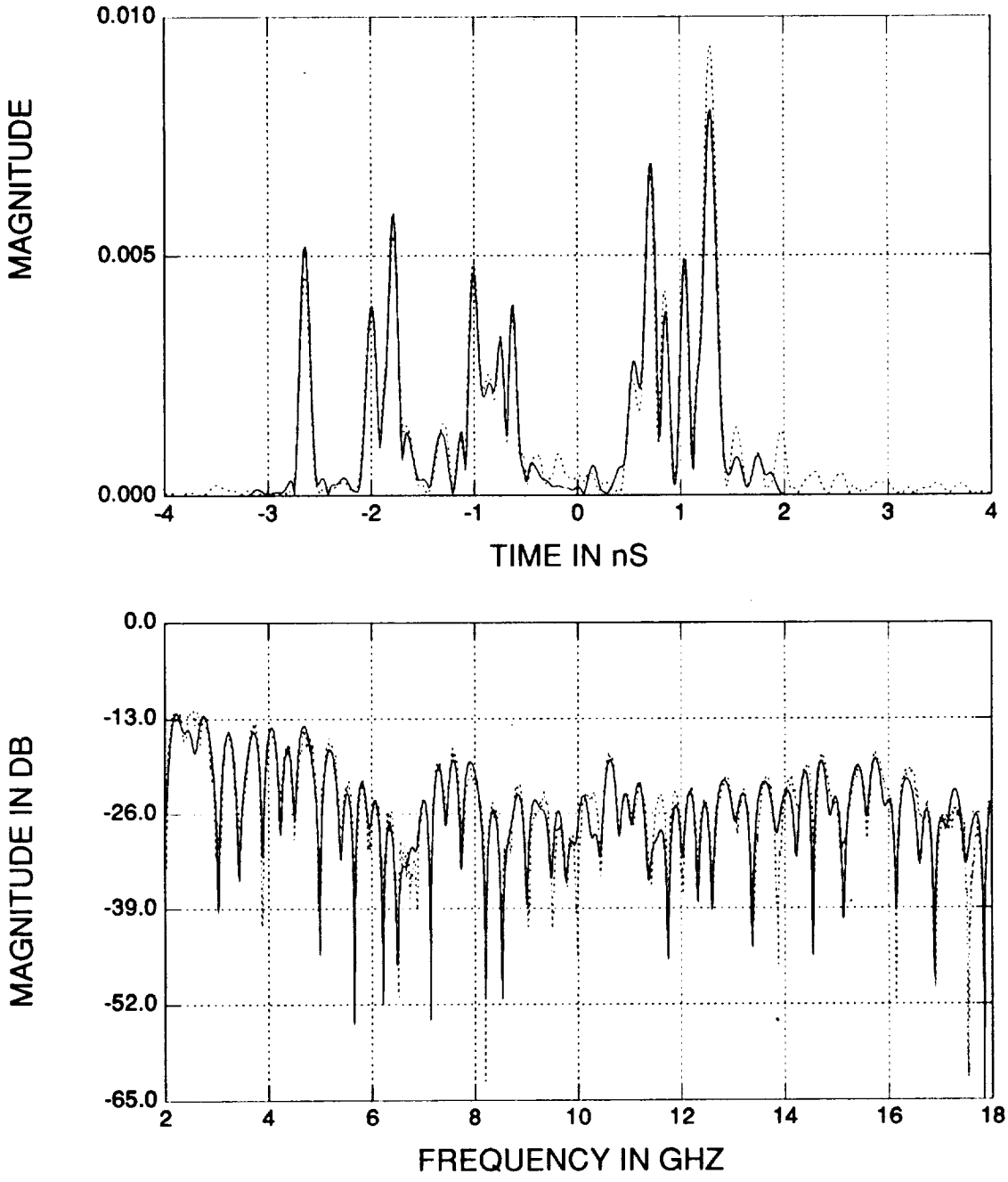

Figure 5.29: Comparison between the reconstructed (solid line) and original (dotted line) frequency responses at 110° for the broadside case.

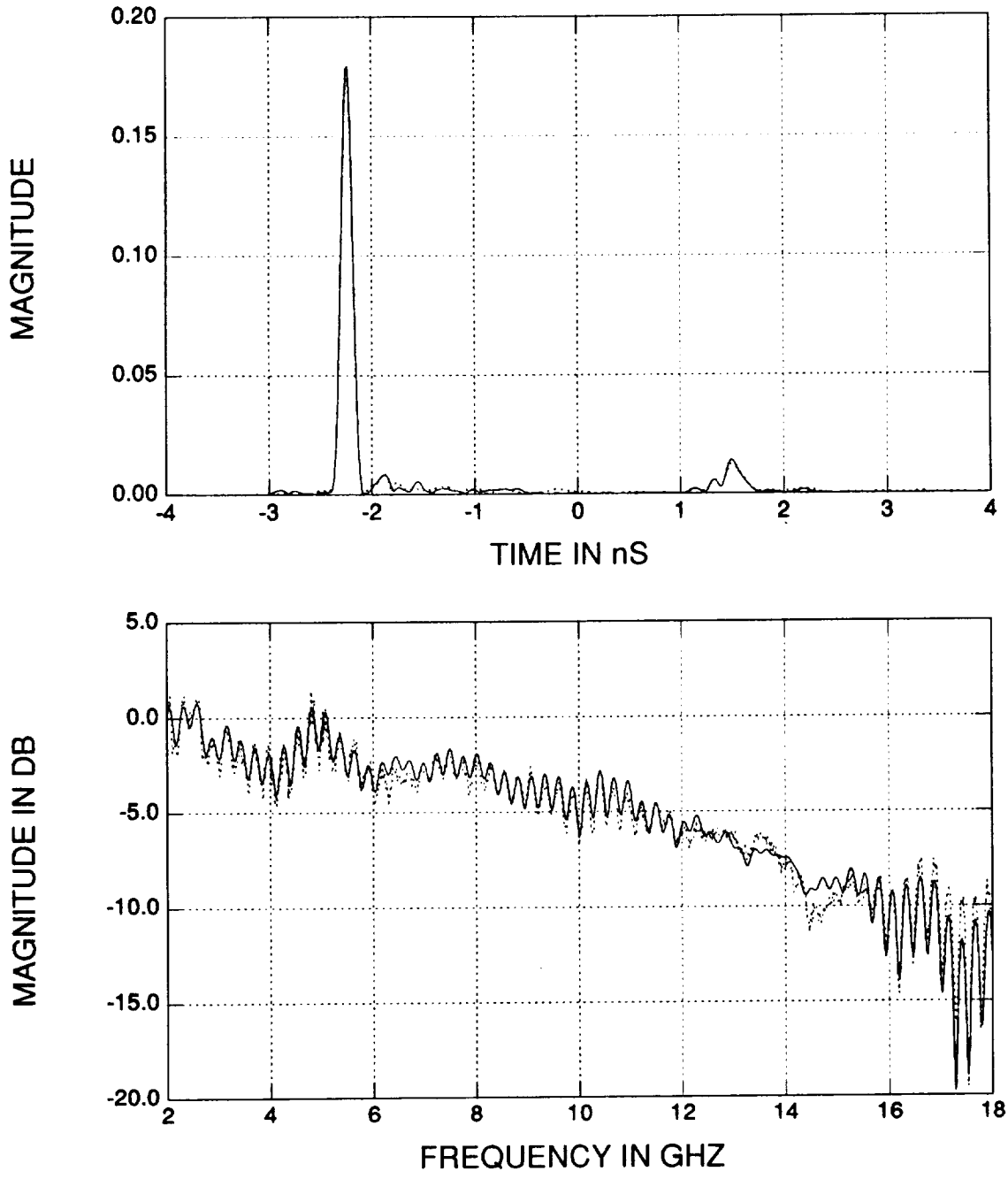

Figure 5.30: Comparison between the reconstructed (solid line) and original (dotted line) frequency responses at 115° for the broadside case.

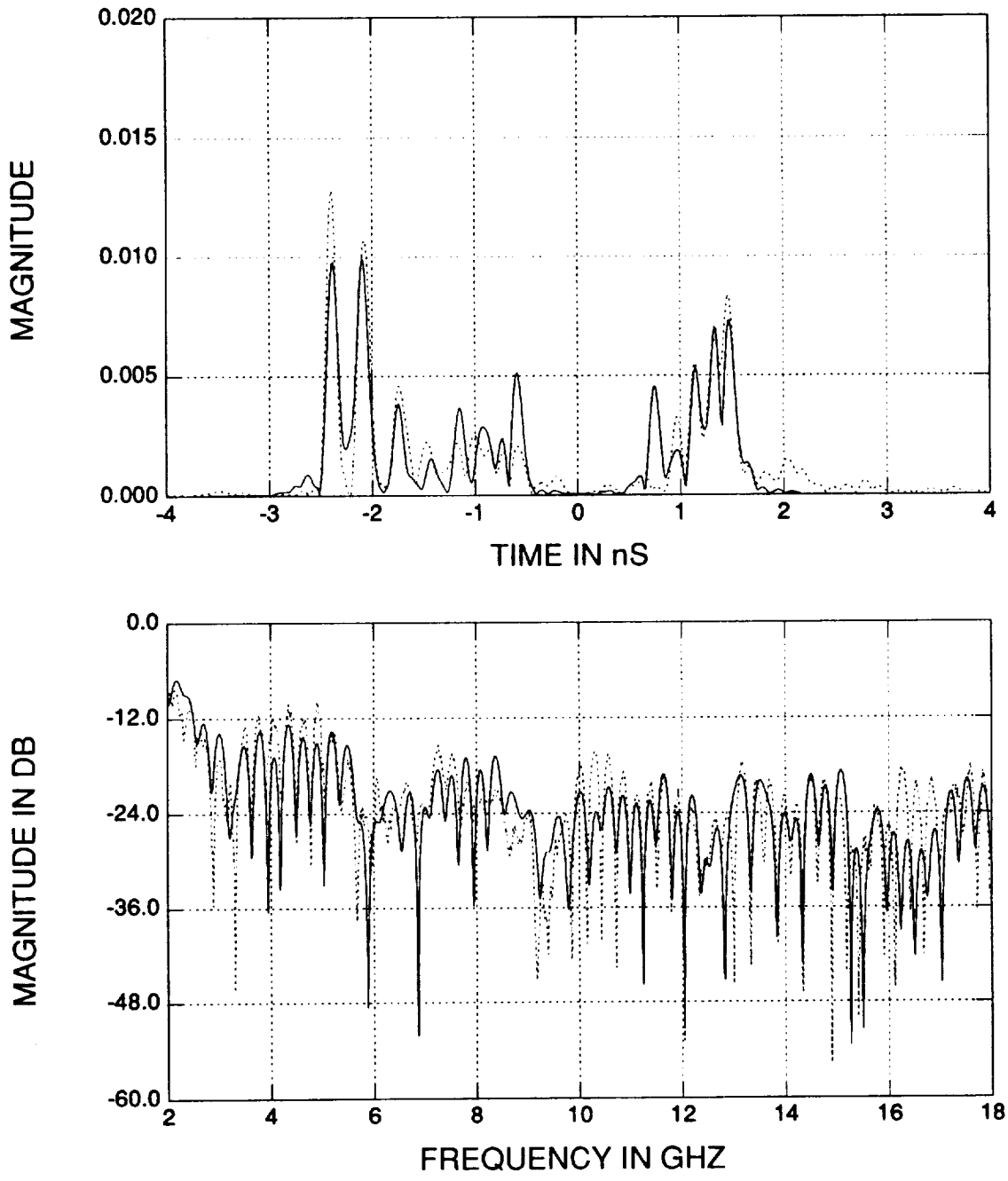

Figure 5.31: Comparison between the reconstructed (solid line) and original (dotted line) frequency responses at 113° for the broadside case.

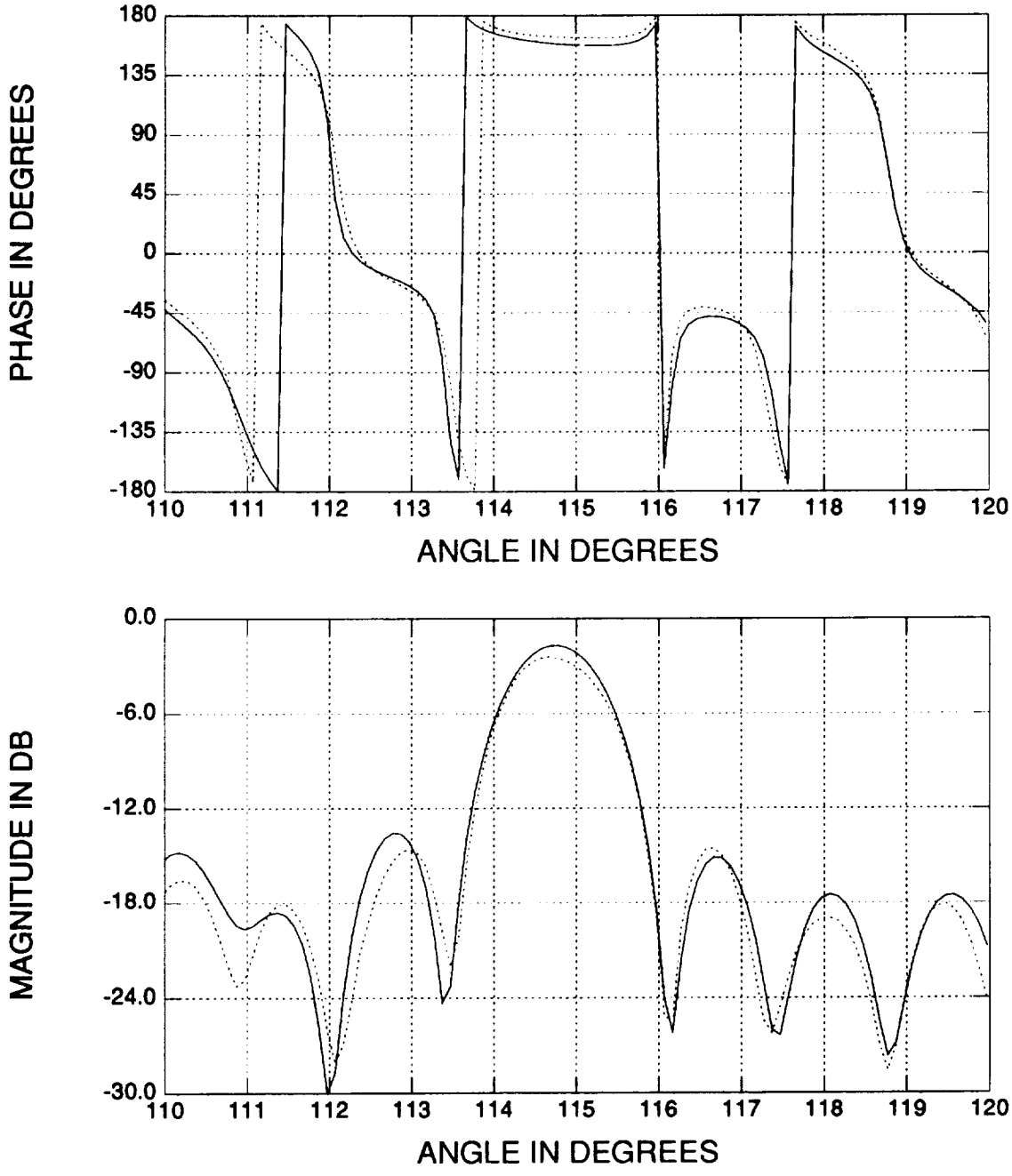

Figure 5.32: Comparison between the reconstructed (solid line) and original (dotted line) azimuth response at 4 GHz for the broadside case.

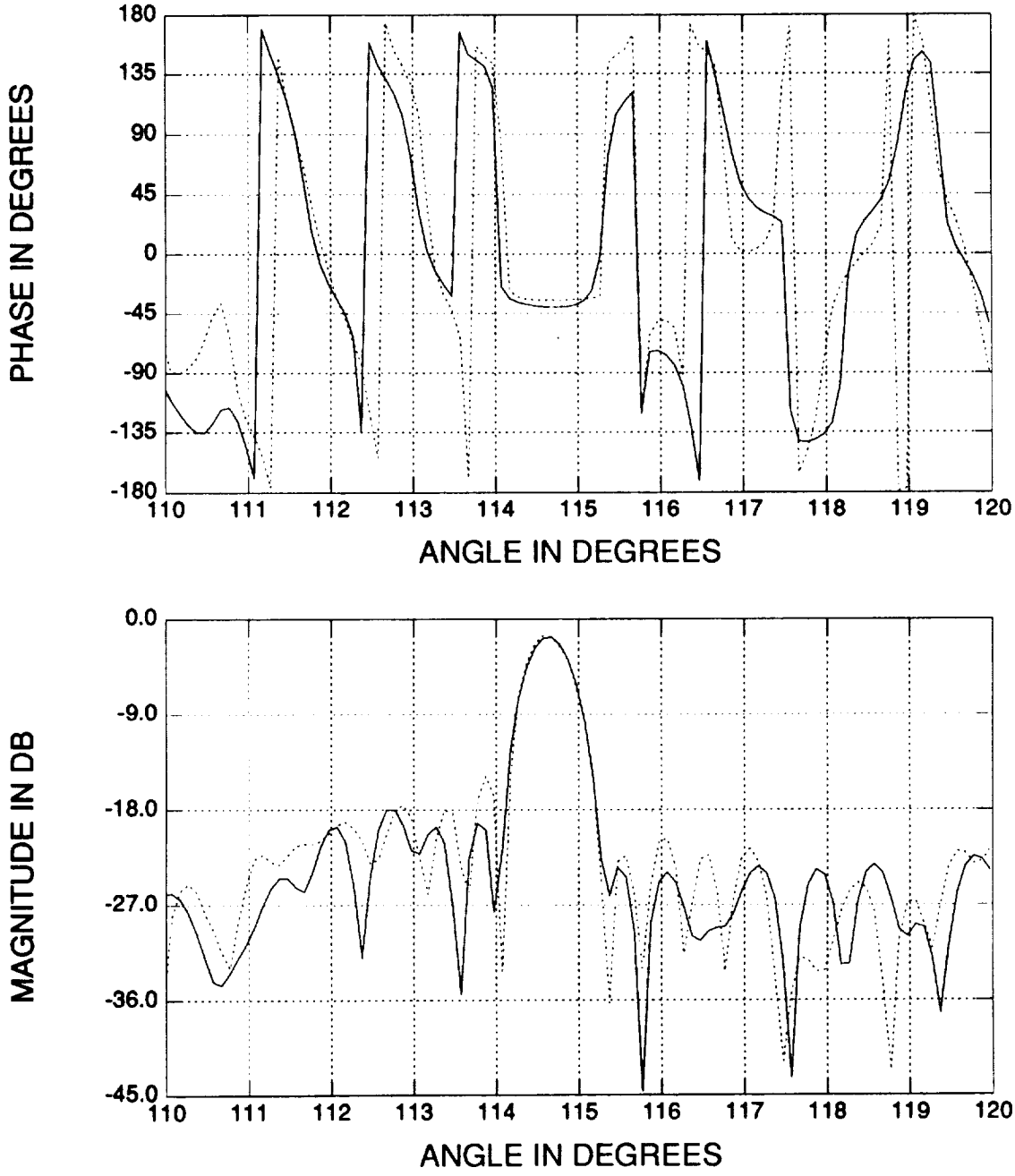

Figure 5.33: Comparison between the reconstructed (solid line) and original (dotted line) azimuth response at 10 GHz for the broadside case.

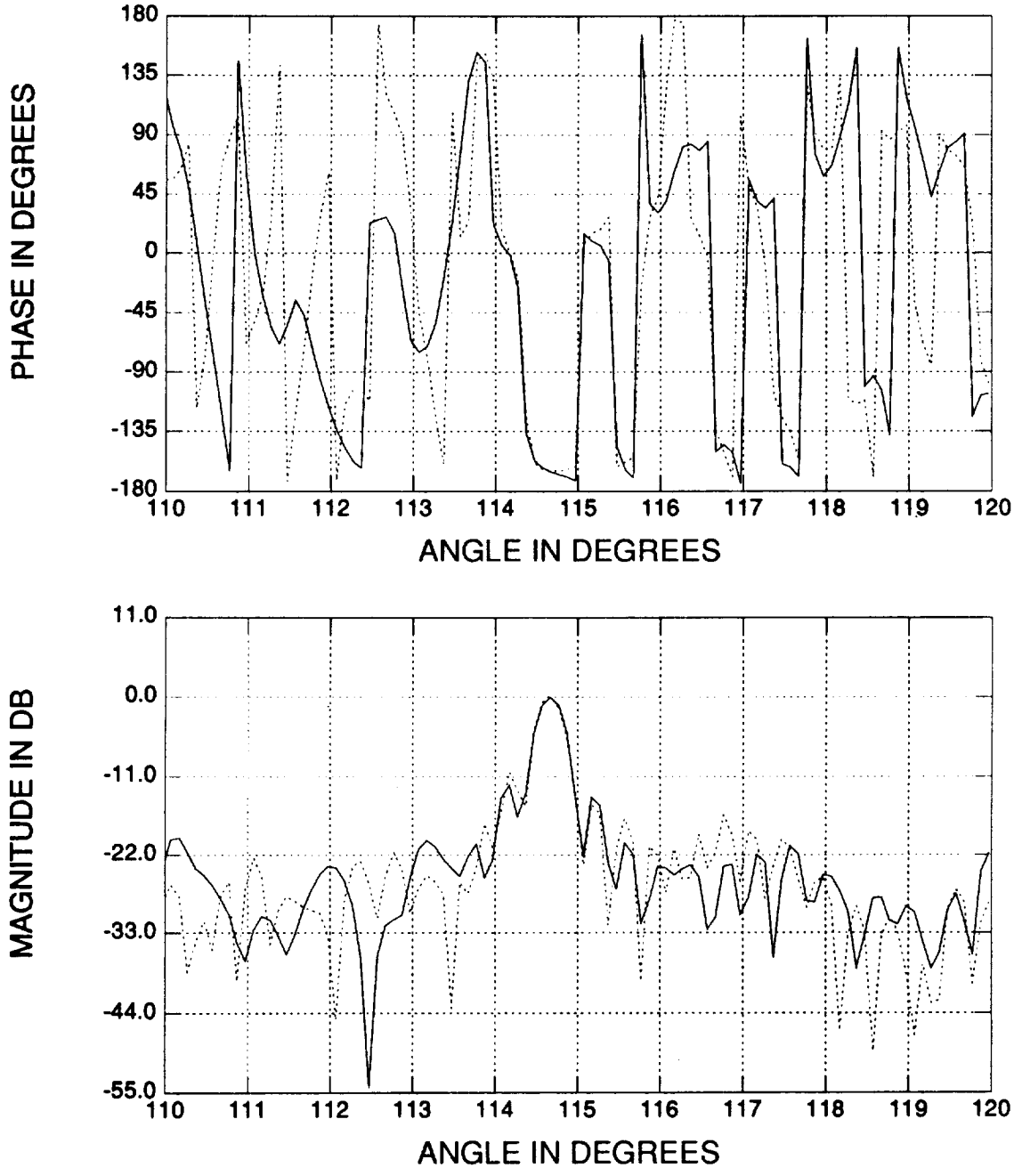

Figure 5.34: Comparison between the reconstructed (solid line) and original (dotted line) azimuth response at 17 GHz for the broadside case.

5.5 Discussion

Though the gating and smoothing techniques operate on different domains, they basically carry the same idea of mechanism extraction and data compression. So here the discussion will concentrate on the gating technique.

As shown before, the gate widths in the image domain dictate the sampling rates in the spectral domain. Since one wants to represent the spectral response of an individual scattering center by the fewest points, he should use as small a spatial gate as possible. But the gate widths cannot be arbitrarily small. The gate one chooses should cover most of a scattering center's energy in the spatial domain. According to the descriptions in Chapter 3, the mainlobe widths of a scattering center in the down range and cross range directions of the ISAR image are mainly decided by the available bandwidth and angle spans. In short, the larger the bandwidth and angle span, the smaller the scattering center's mainlobe widths, and hence the smaller gate one needs. This in turn implies a larger sampling rate in the frequency domain and results in fewer data points to be stored. In our experiments, the available bandwidth was 16 GHz, which gives an ideal scattering center's down range width of 0.75 inches (0.125 ns) or so. A uniform gate which has 1 ns down range width was chosen in this report, which makes the sampling every 1 GHz in the frequency scan possible. (Actually the down range gate width can be safely reduced to 0.5 ns and the sampling period can thus be increased to 2 GHz.)

A larger bandwidth usually means collecting data at higher frequencies. This demands a smaller sampling rate in the angle domain if the cross range gate width is fixed. To compensate for this disadvantage, one can increase the available angle span with which to construct an ISAR image such that the scattering centers will spread out less in cross range and hence the cross range gate width can be reduced. In this report, the angle span was first set to be $\pm 10°$, which gave approximately a cross range mainlobe width of 4 inches and a sampling rate of $5°$ in the angle domain, given the highest frequency of 18 GHz. When the angle span was next

set to be $\pm 15°$, the cross range mainlobe width was roughly reduced by a factor of $\frac{30}{20} = 1.5$, and hence the azimuth sampling rate could have been increased from 5° to 7.5°. Note that $\pm 15°$ is almost the maximum angular range to form a "local" ISAR image; furthermore, a polar region over this range can hardly be approximated by a rectangular region since the relation $\sin\phi \approx \phi$ can no longer be applied.

As one can see, there are a lot of tradeoffs in this algorithm. Therefore, before one applies this algorithm, it is suggested that one first come up with an optimal way to compress the data according to the available bandwidth and limitations of his measurements.

Chapter 6

Conclusions

Complete real-world scattering measurements require enormous data storage. The main goal of this report research is to reduce this massive data amount while still preserving the information contained in the original measurements. A compression and reconstruction technique has been developed in this report to achieve this goal. The results of corner reflectors and the F-117 fighter model in Chapters 4 and 5 showed this technique is very efficient and accurate.

The most important physical phenomenon which supports the idea of compression for the RCS measurement data is that when one illuminates a target by an electromagnetic plane wave with a relatively small wavelength, the majority of scattering mechanisms on the target can be classified as point scatterers. So instead of storing the whole shape of the target in an optical sense, one can reduce the data amount by storing just a few isolated scattering centers. For example, in an ideal case, the true information buried in the measured data will only be the positions and scattered field responses of a few scattering centers. Namely, if these scattering centers' positions along with their frequency and angle dependences are detected, one can represent their total scattered field out of this information.

To achieve this goal of data compression, the proposal in this report was to isolate the scattering centers on a target and store the spectral responses of these isolated scattering centers using the fewest points. Two-dimensional (2-D) gating

and smoothing techniques have been examined to serve this purpose of mechanism isolation and extraction.

The 2-D gating technique is a straightforward method to extract out an individual scattering center in the 2-D ISAR image. And through the gate widths in the down range and cross range directions, one can calculate the sampling rates needed in the frequency and angle scans, respectively. These calculations are based on Fourier analysis and the sampling theorem. In short, the sampling rate in the frequency scan is the reciprocal of the down range gate width; whereas, the sampling rate in the angle scan is inversely proportional to both the cross range gate width and the highest frequency available. In general, the shorter the gate widths, the fewer points one needs to sample in the spectral domain.

The 2-D smoothing technique is an alternative tool to separate individual scattering mechanisms. This technique takes more time in processing, but because it operates directly on the spectral domain data, the smoothing technique minimizes the endband region errors which would otherwise be caused by gating (also known as the Gibbs phenomenon [6]). Besides, in reconstructing the angle scan data, the smoothing technique was refined to solve the problem that scattering centers moved with look angle, and this was done without having to track individual scattering centers from the present angle to the next. The details have been shown in Section 5.3.

After the mechanism extraction by either gating or smoothing, the isolated scattering center's spectral response is smooth and can be sampled much more loosely according to the sampling theorem. These sampled data points form a reduced database for the target under test. From this reduced database, one can generate any response of interest in the 2-D spectral domain. And the reconstruction can be done very fast if the total number of scattering centers is not too large.

The typical compression ratio made by the data compression and reconstruction algorithm in this research can be larger than 50 under the situation that three data

sets are recorded after the processing of one central look angle. This algorithm has been shown to perform very well for both the corner reflectors and the F-117 fighter model. Even for the broadside scattering case as shown in Section 5.4, the result is still very good.

There are several issues that can be pursued following this research. The first one is to extend the 2-D case to a 3-D database compression and reconstruction technique. Younger [12] had proposed two methods which can be used to locate a scattering center on the target in three dimensions. A 3-D gating or smoothing technique should be able to extract the individual scattering centers, such that one could build a 3-D reduced database which is more realistic for real-world targets.

The second issue is how to compress the 2-D data more efficiently. Fourier analysis is a basic tool for image processing, but not necessarily the only one. Other algorithms such as superresolution techniques, Wavelet theory or spatial domain modeling approaches may help one achieve the goal, too.

The third issue is how to improve the situation that the scattering mechanisms are other than point scatterers. The broadside case shown in Section 5.4 is a good example. What is the proper model to represent a non-point scattering mechanism? Does the model help to reduce the database? These questions become important when the pseudo scattering center method proposed in Section 5.4 fails to represent a special geometry. Other issues are also of interest such as how to process the data directly in polar form, or how to deal with moving targets whose speeds and positions are constantly changing.

The most important application of this research may lie in target identification. Recall that the target's scattering over a small angular region can be accurately represented by a linear combination of the data points stored in the reduced database. This should allow one to develop some very unique classification filters to separate out one target from a large number of possibilities.

Bibliography

[1] J. B. Keller, "Geometrical theory of diffraction," *J. Opt. Soc. Am.*, vol. 52, no. 2, pp. 116-139, Feb. 1962.

[2] D. A. Ksienski, "Method of resolving data into two maximally smooth components," *Proc. IEEE,* vol.73, no. 1, pp. 166-168, Jan. 1985.

[3] A. K. Dominek *et al.*, "A time domain technique for mechanism extraction," *IEEE Trans. Antennas Propagat.*, vol. ap-35, no. 3, pp. 305-312, Mar. 1987.

[4] D. L. Mensa, *High Resolution Radar Imaging,* Artech House, Inc., Dedham MA, 1981.

[5] F. J. Harris, "On the use of windows for harmonic analysis with the discrete Fourier transform," *Proc. IEEE,* vol. 66, no. 1, p. 51, Jan. 1978.

[6] A. V. Oppenheim, *Signals and Systems,* Prentice-Hall, Inc., Englewood Cliffs NJ, 1983.

[7] R. C. Gonzalez and P. Wintz, *Digital Image Processing,* Addison-Wesley, Reading MA, 1987.

[8] A. C. Kak and M. Slaney, *Principles of Computerized Tomographic Imaging*, IEEE PRESS, New York NY, 1988.

[9] D. R. Wehner, *High Resolution Radar*, Artech House, Inc., Norwood MA, 1987.

[10] D. L. Mensa *et al.*, "Coherent Doppler tomography for microwave imaging", *Proc. IEEE,* vol. 71, no. 2, pp. 254-261, Feb. 1983.

[11] D. L. Mensa and K. Vaccaro, "Two-dimensional RCS image focusing," *Proc. AMTA*, pp. 164-170, Sep. 1987.

[12] P. R. Younger, "Scattering center identification in three dimensions," MS Thesis, The Ohio State University, Department of Electrical Engineering, Columbus, Ohio, 1990.

722780-4, "A Very Efficient RCS Data Compression and Reconstruction Technique", Tseng & Burnside, 11/92